

UNIVERSITY OF THE WITWATERSRAND

PhD IN ENGINEERING DEGREE

**Reducing Water Absorption Characteristics of Kraft Paper  
Reinforced with Modified Nanoparticles**

*Author:*

Mohammed Mahmood Katun

*Supervisor:* Prof. Chandima Gomes

*Co-Supervisor:* Prof. Cuthbert Nyamupangedengu

*A Thesis Submitted to the Faculty of Engineering and Built Environment, University of the  
Witwatersrand, in partial fulfilment of the requirements for the PhD degree in  
Engineering.*

March 2023



UNIVERSITY OF THE  
WITWATERSRAND,  
JOHANNESBURG

## Declaration

I, **Mohammed Mahmood Katun**, declare that this thesis titled “**Reducing Water Absorption Characteristics of Kraft Paper Reinforced with Modified Nanoparticles**” and the contents presented in it are my unaided work. I confirm that this work was done primarily while I was a candidate for a research degree at the University of the Witwatersrand, Johannesburg. I declare that this thesis is being submitted for the PhD degree in Engineering of this University. It has not been presented before for any degree or examination at any other University.



Signature: \_\_\_\_\_

Date: 15/03/2023

## Abstract

The inherent hydrophilic characteristics of cellulose wood fibre compromise the dielectric properties of kraft paper insulation that is used mainly in oil-insulated power transformers. This thesis, therefore, presents a novel material design model of nanocomposite kraft paper with improved hydrophobic properties for power transformer insulation applications. The concept of nanodielectric kraft paper design was used. Rutile-titanium dioxide nanoparticles (rutile-TiO<sub>2</sub> NPs) were selected as the nanofiller. Compared with other metal-oxides, rutile-TiO<sub>2</sub> NPs are stable in chemical reactions, have good thermal stability and also have high electrical resistivity. Rutile-TiO<sub>2</sub> of 19.72 nm diameter were fabricated using the sol-gel method and then used in reinforcing the kraft paper to produce a nanocomposite kraft paper with improved dielectric properties. Since the nanoparticles are inherently hydrophilic, and the intention is to produce a hydrophilic nanocomposite kraft paper, a technique was devised to make the NPs hydrophobic. The rutile-TiO<sub>2</sub> NPs were surface conditioned with two alternative surfactants; Alkyl ketene dimer (AKD) and alkenyl succinic anhydride (ASA). Various quantities of the two surfactants were investigated to determine the optimal amount. The resultant surface-modified rutile-TiO<sub>2</sub> NPs were studied to understand their hydrophilicity and thermal stability properties. It was found that the unmodified rutile-TiO<sub>2</sub> NPs absorbed more moisture, compared with the surface-modified nanofiller, the mass increased by about 4% due to moisture absorption. The surface-modified rutile-TiO<sub>2</sub> NPs with 5% AKD had 45% more thermal resilience than the unmodified rutile-TiO<sub>2</sub> NPs surface and this is a significant knowledge contribution of this thesis. Using an unbleached kraft pulp, nanocomposite kraft paper specimens were fabricated with nanoparticles having varying surfactant loading. The specimens were then characterized to reveal various critical properties such as hydrophobicity, thermal, dielectric losses and dielectric strength. The version of the nanocomposite kraft paper that gave the most improved water and moisture absorption properties was that with 5vol/vol% ASA surface-modified NPs. The moisture absorption rate dropped by 74% compared to the unfilled kraft paper, and the water vapor transmission rate decreased by 30%. The contact angle of water droplets improved by 12%, and water absorption rate improved by being 4 times slower. The dielectric loss measurements showed that the nanocomposite kraft paper containing rutile-TiO<sub>2</sub> NPs (5 vol/vol% ASA) also had 40% lower dielectric losses than the reference (unfilled) samples. The breakdown voltage of the nanocomposite kraft paper increased by about 15% while thermal withstand was improved by 5.4%. This research, therefore, has successfully improved the hydrophobic properties of kraft paper by filling it with surface-modified rutile-TiO<sub>2</sub> NP. It can be argued from the results that for power transformer application, the novel nanocomposite kraft paper developed in this thesis will improve power transformer insulation reliability design by mitigating the main agents of insulation degradation which are water and thermal stress.

## **Dedication**

*This research work is dedicated to my father, BABAIYA.*

## Acknowledgements

I would like to express my profound appreciation to my supervisor Prof. Chandima Gomes for accepting to supervise me. His guidance and words of encouragement kept me going throughout this journey. Working under his supervision has sincerely improved my academic and personal life.

I would like to also thank Prof. Nyamupangedengu for accepting to co-supervise me. His experience and guidance navigate my path towards achieving the set objectives throughout the research work.

I acknowledge the Tertiary Education Trust Fund (TetFund) for funding my study and Eskom Centre in HV Eng. Research at Wits University for their support too. Also, I would like to identify with the management of Federal Polytechnic Bida for allowing me to embark on this historical journey of my life.

My sincere appreciation goes to Prof. Nosipho and Dr Rudo from the Molecular Science Institute, School of Chemistry, Wits University, for their guidance all through the period of synthesizing, the surface modification and characterizing the rutile-TiO<sub>2</sub> nanoparticles. Special thanks to Mr Ashley of Sappi Technology Laboratory for his experience and guidance while fabricating the nanocomposite kraft paper insulation. I would also like to thank Mr Motlatsi of Chemical Engineering, Wits University, for always being there for my needs. For the staff of Electrical and Information Engineering, Faculty of Engineering and Built Environment, Wits University, I am proud to associate with you all. Thank you Dr Adamu Gati, Abubakar (stakeholder), Dr Hassan, Dr Sadiq, Kayode, Moses, Mr Rembiluwani Philip, Didace, Aunty Claudette, Mabontsi and endless is the list, for all the love.

I want to acknowledge my mother for her unrelenting prayers; thank you Atadee. My appreciation goes to my sisters Aunty Fati, Hassana, Fati and Yaka. And also to my brothers Yakatubante, Yakatuntetengi, Yantene, Nmalaji, Yaman police, Abdul, Aliyu, and my uncle Nmadaisa and Ndaginako (Kwaran Nupe). My sincere gratitude goes to my friends Ibrahim Tako, Kazeem, Baba Abdullahi, Salihu (Prof), Mal. Abubakar and Aliyu Ndakutso. Thank you all for your prayers and support.

I want to acknowledge my uncle, His Royal Highness Alhaji (Dr.) Yahaya Abubakar (CFR). His support and encouragement towards my academic journey cannot be overstressed.

No, I will not forget! Thank you Zainab, thank you Ajanna and thank you Baba for enduring. God bless you all.

Finally, and most importantly, **ALHAMDULILLAH** for the opportunity and privilege to pursue my PhD degree.

## List of research articles published in the cause of the thesis work

1. M. Mahmood Katun, R. Kadzutu-Sithole, N. Moloto, C. Nyamupangedengu, and C. Gomes, "Improving Thermal Stability and Hydrophobicity of Rutile-TiO<sub>2</sub> Nanoparticles for Oil-Impregnated Paper Application," *Energies*, vol. 14, no. 23, p. 7964, Nov. 2021, doi: 10.3390/en14237964.
2. M. M. Katun, A. Smith, R. Kadzutu-Sithole, C. Gomes, C. Nynamupangedengu, and N. Moloto, "Impact of fibres and reinforced nanoparticles on tensile strength of transformer oil-impregnated paper," *2022 30th Southern African Universities Power Engineering Conference (SAUPEC)*, Jan. 2022, pp. 1–6. doi: 10.1109/SAUPEC55179.2022.9730720.
3. M. K. Mahmood, C. Nyamupangedengu, C. Gomes and A. Smith, "Reducing Hydrophilic Characteristics of Kraft Paper Insulation by Reinforcing With Surface Modified Rutile-TiO<sub>2</sub> Nanoparticles," in *IEEE Access*, vol. 10, pp. 102237-102246, 2022, doi: 10.1109/ACCESS.2022.3208596.
4. M. M. Katun, C. Gomes and C. Nynamupangedengu, "Significance of Nanoparticles on Electrical Breakdown Strength of Oil-Impregnated Paper Reinforced with Rutile-TiO<sub>2</sub>," *2023 31st Southern African Universities Power Engineering Conference (SAUPEC)*, Johannesburg, South Africa, 2023, pp. 1-4, doi: 10.1109/SAUPEC57889.2023.10057888.

# Table of Contents

Declaration.....	i
Abstract.....	ii
Dedication.....	iii
Acknowledgements.....	iv
List of research publications.....	v
Table of Contents.....	vi
List of Figures.....	ix
List of Table.....	xii
Acronyms and Abbreviations.....	xiii
Chapter 1: Introduction.....	1
1.1    Research Background.....	1
1.2    Problem Statement.....	4
1.3    The Research Questions.....	5
1.4    The Research Objectives.....	5
1.5    The Research Road Map.....	5
1.6    Thesis Structure.....	7
Chapter 2: Kraft Paper Insulation Technology; a Critical Review.....	8
2.1    Introduction.....	8
2.2    Kraft Paper Raw Material.....	8
2.3    Overview of Kraft Paper Insulation.....	8
2.4    Moisture Absorption in Paper Insulation.....	11
2.5    The Problem Associated with wet Kraft Paper Insulation.....	12
2.5.1    Moisture Content Diagnostic Methods on Kraft paper Insulation... 13	
2.6    Influence of Moisture on the Ageing and Degradation Mechanism of Kraft Paper Insulation in power transformer.....	14
2.7    Chapter Conclusion.....	17
Chapter 3: Nanocomposite Kraft Paper Technology: a critical review.....	19
3.1    Introduction.....	19
3.2    The Concept of Nanotechnology.....	19
3.2.1    Structure of Nanoparticles.....	21
3.3    Nanocomposites Material.....	22
3.4    Modification of Kraft Paper Insulation with Nanoparticles.....	23
3.4.1    Selection of most suitable Nanoparticles for Modification of Kraft Paper Insulation for Power Transformer Application.....	25

3.4.2	Titanium Dioxide (TiO <sub>2</sub> ) NPs fillers in Kraft Paper Insulation.....	25
3.5	Chapter Conclusion.....	28
Chapter 4: Synthesis, Surface Modification and Characterization of Rutile-TiO <sub>2</sub>		
Nanoparticles for use in Transformer Kraft Paper.....		
4.1	Introduction.....	29
4.2	Synthesis of TiO <sub>2</sub> Nanoparticles.....	29
4.3	The Overview Process of Synthesizing Rutile-TiO <sub>2</sub> Nanoparticles using the Sol-gel Method.....	32
4.3.1	The Designed and Implemented Process of Fabricating Rutile-TiO <sub>2</sub> NPs Specific Size (19.72nm).....	33
4.3.2	Characterization of the obtained Rutile-TiO <sub>2</sub> Nanoparticles	35
4.3.2.1	Phase Identification of the obtained Nanoparticles using X-ray Diffraction Spectrometry.....	35
4.3.2.2	Raman Spectrometry of the obtained Nanoparticles.....	36
4.3.2.3	Average Crystallite Size and Phase Composition of the obtained Rutile-TiO <sub>2</sub> Nanoparticles.....	37
4.3.2.4	Fourier Transform Infrared (FT-IR) Spectroscopy of the obtained Rutile-TiO <sub>2</sub> Nanoparticles.....	39
4.3.2.5	Transmission Electron Microscopy (TEM) of the obtained Rutile-TiO <sub>2</sub> Nanoparticles Mophology.....	40
4.4	Surface Modification of the obtained Rutile-TiO <sub>2</sub> Nanoparticles.....	41
4.5	The Theoretical Concept Surface Modification of the Rutile-TiO <sub>2</sub> Nanoparticles.....	43
4.5.1	The Practical Procedure Implemented in Surface Modification of Rutile-TiO <sub>2</sub> Nanoparticles.....	46
4.5.1.1	Fourier Transform Infrared Spectroscopy (FT-IR) of the Surface Modified Rutile-TiO <sub>2</sub> Nanoparticles.....	47
4.5.1.2	Moisture Absorption Characteristics of the Surface Modified Rutile-TiO <sub>2</sub> Nanoparticles.....	49
4.5.1.3	Thermal Stress Induced Weight Loss of Surface Modified rutile-TiO <sub>2</sub> Nanoparticles.....	49
4.5.1.4	Thermogravimetric Analysis (TGA) of the Surface-Modified Rutile-TiO <sub>2</sub> Nanoparticles.....	50
4.6	Chapter Conclusion.....	53
Chapter 5: Fabrication and Characterization of Rutile-TiO <sub>2</sub> Nanocomposite Kraft Paper for Power Transformer Application.....		
54		

5.1	Introduction.....	54
5.2	Papermaking.....	54
5.3	Bonding and Structural Mechanism of the Fabricated Nanocomposites Kraft Paper Insulation.....	55
5.4	Procedure for the Fabrication of the Kraft Paper Insulation.....	57
5.4.1	Materials and Chemicals used to Fabricate the Kraft Paper Insulation.....	58
5.4.2	Experimental Procedure for Fabricating the Kraft Paper Insulation.....	58
5.5	Fibre Characterization and Scanning Electron Microscope (SEM) of the Fabricated Kraft Paper Insulation.....	59
5.5.1	Fibre Analysis of the Fabricated Kraft Paper Insulation.....	59
5.5.2	Scanning Electron Microscope (SEM) Analysis of the Fabricated Kraft Paper Insulation.....	62
5.5.3	Percentage of Filler Retention (Rutile-TiO <sub>2</sub> NPs) in the Nanocomposite Kraft Paper.....	63
5.5.4	Tensile Strength of the Fabricated Kraft Paper Insulation.....	64
5.5.5	Thermal Stability of the Fabricated Kraft Paper Insulation.....	66
5.5.6	Hydrophilicity Test on the Fabricated Kraft Paper Specimens.....	70
5.6	Chapter Conclusion.....	78
Chapter 6: Dielectric Characteristics of the Fabricated Kraft Paper Insulation.....		79
6.1	Introduction.....	79
6.2	Dielectric Dissipation Factor (Tan Delta) of the Fabricated Kraft Paper Insulation.....	79
6.3	Electrical Breakdown Strength of the Fabricated Kraft Paper Insulation.....	83
6.4	Chapter Conclusion.....	85
Chapter 7: Conclusion and Future Research Work.....		88
7.1	Introduction.....	88
7.2	Summary of Major Findings and Knowledge Contribution.....	88
7.3	Contributions and Limitations.....	90
7.3.1	Contributions.....	90
7.3.2	Limitations.....	90
7.4	Recommendations for Future Work.....	91
Reference.....		93
Appendices.....		107

## List of Figures

<b>Figure 1.1:</b> A cut-out view of power transformer.....	2
<b>Figure 1.2:</b> Causes of transformer failure.....	3
<b>Figure 1.3:</b> Block illustration of the research path.....	6
<b>Figure 2.1:</b> Glucose molecule and cellulose polymer.....	9
<b>Figure 2.2:</b> Hydrogen bond formation.....	10
<b>Figure 2.3:</b> Demonstration of the hydrogen bonding that allows the parallel arrangement of the cellulose polymer chains.....	10
<b>Figure 2.4:</b> Attraction of water molecules to hydroxyl groups on the cellulose surface.....	12
<b>Figure 2.5:</b> Hydrolytic degradation reaction of cellulose.....	15
<b>Figure 2.6:</b> Oxidation degradation of cellulose.....	16
<b>Figure 2.7:</b> Thermal degradation of cellulose.....	17
<b>Figure 3.1:</b> Nanoparticles Classification.....	20
<b>Figure 3.2:</b> Typical dimensional shapes of the nanoparticles.....	21
<b>Figure 3.3:</b> Nanoparticles Structure.....	22
<b>Figure 3.4:</b> Structures of TiO <sub>2</sub> phases.....	27
<b>Figure 3.5:</b> Surficial Ti interaction with water molecules.....	27
<b>Figure 4.1:</b> Bottom-up and Top-down approaches to synthesizing TiO <sub>2</sub> nanoparticles.....	30
<b>Figure 4.2:</b> Steps involved in synthesizing TiO <sub>2</sub> NPs via the sol gel.....	32
<b>Figure 4.3:</b> Sequence of synthesizing rutile-TiO <sub>2</sub> NPs.....	34
<b>Figure 4.4:</b> Images of various stages of the synthesis.....	34
<b>Figure 4.5:</b> XRD pattern (signature) of the obtained rutile-TiO <sub>2</sub> nanoparticles.....	36
<b>Figure 4.6:</b> Raman peak shifts of the obtained rutile-TiO <sub>2</sub> NPs.....	37
<b>Figure 4.7:</b> FT-IR spectrum of the obtained rutile-TiO <sub>2</sub> NPs.....	39
<b>Figure 4.8:</b> TEM images of the obtained rutile-TiO <sub>2</sub> NPs.....	40
<b>Figure 4.9:</b> Sizing agent and mechanism of sizing orientation.....	41
<b>Figure 4.10:</b> ASA Structure.....	42
<b>Figure 4.11:</b> AKD Structure.....	43
<b>Figure 4.12:</b> Silane interface bond between organic and inorganic material.....	44
<b>Figure 4.13:</b> Illustration of surface modification of rutile-TiO <sub>2</sub> NPs.....	44
<b>Figure 4.14a:</b> Reaction model of surface-modified rutile-TiO <sub>2</sub> NPs/AKD.....	45
<b>Figure 4.14b:</b> Reaction model of surface-modified rutile-TiO <sub>2</sub> NPs/ASA.....	45

<b>Figure 4.15:</b> Schematic illustration of surface modification of rutile-TiO <sub>2</sub> NPs.....	46
<b>Figure 4.16:</b> FT- IR Spectra; (a) pure AKD (b) AKD surface-modified rutile-TiO <sub>2</sub> NPs (c) pure ASA (d) ASA surface-modified rutile-TiO <sub>2</sub> NPs.....	48
<b>Figure 4.17:</b> Thermogravimetric Analysis of the nanoparticles (a) pure TiO <sub>2</sub> NPs (b) 5% AKD/TiO <sub>2</sub> NPs (c) 3% AKD/TiO <sub>2</sub> NPs (d) 1% AKD/TiO <sub>2</sub> NPs (e) 5% ASA/TiO <sub>2</sub> NPs (f) 3% ASA/TiO <sub>2</sub> NPs (g) 1% ASA/TiO <sub>2</sub> NPs.....	52
<b>Figure 5.1a:</b> Interaction mechanism of cellulose kraft paper with unmodified rutile-TiO <sub>2</sub> NPs.....	56
<b>Figure 5.1b:</b> Interaction mechanism of cellulose kraft paper with surface modified rutile-TiO <sub>2</sub> NPs having ASA.....	56
<b>Figure 5.1c:</b> Interaction mechanism of cellulose kraft paper with surface-modified TiO <sub>2</sub> NPs having AKD.....	57
<b>Figure 5.2:</b> Steps involved in fabricating the kraft paper insulation.....	59
<b>Figure 5.3:</b> Graphical representation of the fibre length constituents in the various specimens .....	60
<b>Figure 5.4:</b> A graph representing fines in different test specimens of the kraft paper .....	61
<b>Figure 5.5:</b> A graph representing coarseness, fibre content and the wall thickness of the kraft paper developed in this thesis work.....	62
<b>Figure 5.6:</b> Surface morphology of the handsheets (a) without nanofiller (b) with nanofiller uniformly distributed with trace of agglomerated nanoparticles.....	63
<b>Figure 5.7:</b> Percentage of nanofiller particles retention in the rutile-TiO <sub>2</sub> nanocomposite kraft paper .....	64
<b>Figure 5.8:</b> Image of mechanically failed sample strip.....	65
<b>Figure 5.9:</b> Tensile strength of the fabricated kraft paper samples.....	65
<b>Figure 5.10:</b> TGA of the sample (a) control sample (b) kraft paper with unmodified NPs (c) kraft paper filled with rutile-TiO <sub>2</sub> /AKD1% (d) kraft paper filled with rutile-TiO <sub>2</sub> /AKD3% (e) kraft paper filled with rutile-TiO <sub>2</sub> /AKD5% (f) kraft paper filled with rutile-TiO <sub>2</sub> /ASA1% (g) kraft paper filled with rutile-TiO <sub>2</sub> /ASA3% (h) kraft paper filled with rutile-TiO <sub>2</sub> /ASA5%.....	68
<b>Figure 5.11:</b> Percentage increase in mass due to absorbed moisture of the fabricated kraft paper samples .....	70
<b>Figure 5.12:</b> Experimental setup and process of the water vapor transmission rate test .....	71
<b>Figure 5.13:</b> Water vapor transmission rate (WVTR) of the fabricated kraft paper samples .....	72
<b>Figure 5.14:</b> Image of the water Cobb test setup.....	73

<b>Figure 5.15:</b> Graphical representation of Cobb test of fabricated kraft paper samples.....	74
<b>Figure 5.16:</b> Contact angle illustration of a water droplet.....	75
<b>Figure 5.17:</b> Interaction of sized nanocomposite kraft paper with surrounding moisture.....	77
<b>Figure 6.1:</b> Experimental setup of measuring dissipation factor using DIRANA.....	80
<b>Figure 6.2:</b> Absolute values of tan delta measured after 72 hours at 50 Hertz.....	81
<b>Figure 6.3:</b> Absolute values of tan delta measured after curing at 50 Hertz.....	81
<b>Figure 6.4:</b> (a) $\tan\delta$ graph of kraft paper/T-AKD after curing, (b) $\tan\delta$ graph of kraft paper/T-ASA after curing (c) combined $\tan\delta$ graph of kraft paper/T-AKD and ASA after curing (d) $\tan\delta$ graph of kraft paper/T-AKD after 72 hours (e) $\tan\delta$ graph of kraft paper/T-ASA after 72 hours (f) combined $\tan\delta$ graph of kraft paper/T-AKD after curing and 72 hours later (g) combined $\tan\delta$ graph of kraft paper/T-ASA after curing and 72 hours later (h) combined $\tan\delta$ graph of kraft paper/T-AKD and ASA after 72 hours.....	82
<b>Figure 6.5:</b> Breakdown test setup.....	84
<b>Figure 6.6:</b> Breakdown voltage of the fabricated kraft paper.....	85
<b>Figure 6.7:</b> interaction zone in nanocomposite kraft paper.....	86

## List of Tables

<b>Table 3.1:</b> Improvements recorded with the application of different nanoparticles on kraft paper insulation.....	24
<b>Table 4.1:</b> Merit and demerits of different methods of synthesizing TiO <sub>2</sub> NPs.....	30
<b>Table 4.2:</b> Summary of characterization techniques.....	35
<b>Table 4.3:</b> Particle size of the synthesized rutile-TiO <sub>2</sub> NPs.....	38
<b>Table 4.4:</b> Change in mass due to absorbed moisture.....	49
<b>Table 4.5:</b> Weight loss analysis of surface-modified rutile-TiO <sub>2</sub> NPs under thermal stress.....	50
<b>Table 4.6:</b> Effects of surfactant content and type on thermal stability.....	53
<b>Table 5.1:</b> Thermal stability of the fabricated kraft paper samples.....	69
<b>Table 5.2:</b> Contact angle and time taken to absorb water.....	76
<b>Table 7.1:</b> Resultant properties of the fabricated kraft paper and implication on insulation design for the power transformer.....	89

## Acronyms and abbreviations

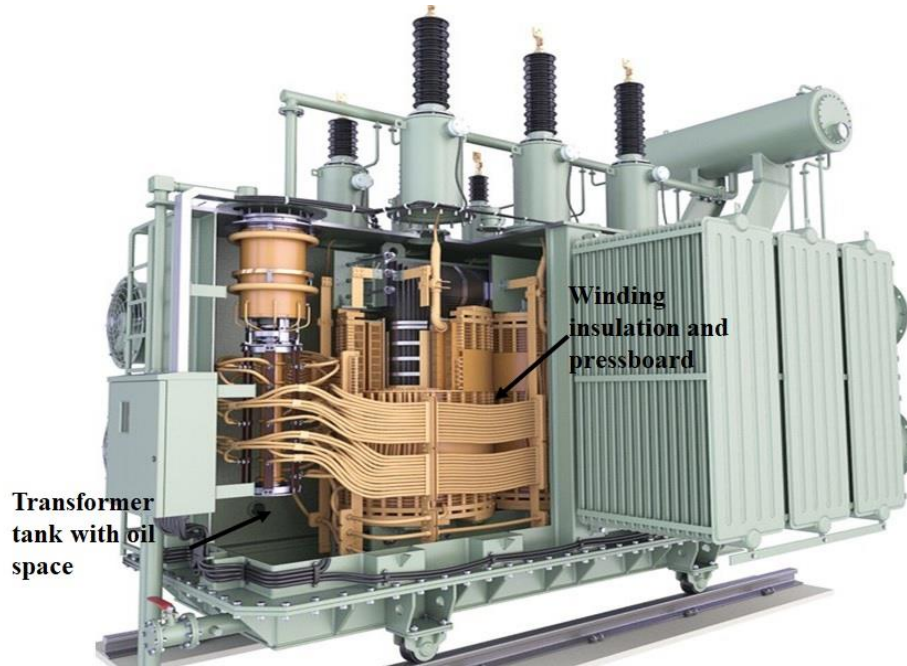
ASA	Alkenyl Succinic Anhydride
AKD	Alkyl Ketene Dimer
DIRANA	Dielectric Response Analyzer
DP	Degree of Polymerization
FT-IR	Fourier Transform Infrared Spectroscopy
KP	Kraft Paper
NPs	Nanoparticles
SEM	Scanning electron microscopy
TEM	Transmission electron microscopy
TGA	Thermogravimetric analysis
TiO <sub>2</sub>	Titanium Dioxide
T-ASA	Rutile-TiO <sub>2</sub> NPs Modified with ASA
T-AKD	Rutile-TiO <sub>2</sub> NPs Modified with AKD
T-Pure	Unmodified Rutile-TiO <sub>2</sub> NPs
vol/vol%	Percentage by volume
wt%	Weight percentage
XRD	X-ray diffraction

# Chapter 1: Introduction

In power systems, a power transformer is a critical equipment. It is critical in voltage transformation; used at the point of transmission, the sub-transmission station, and the distribution end for consumer application [1], [2]. The power transformer comprises components such as the current carrying conductor, insulation system (solid and liquid), magnetic system, cooling system, bushings, tap changer and the tank [3]. The work of this thesis focuses on the power transformer's solid dielectric (kraft paper winding insulation), which is a critical component of the insulation system.

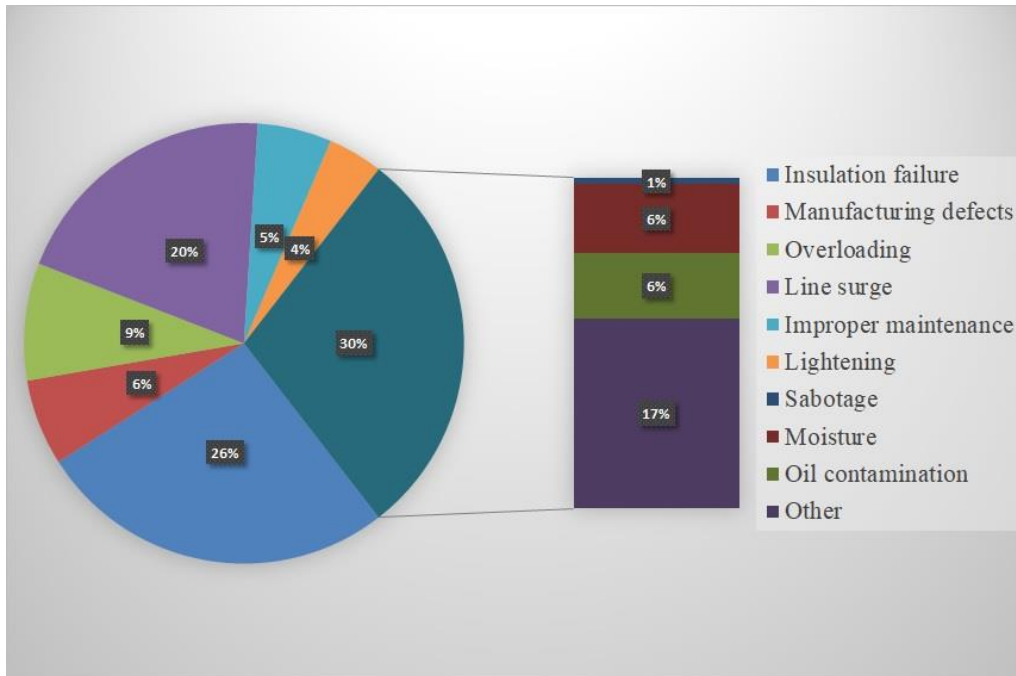
## 1.1 The Background

Historically, it is nearly impossible to single out the period when cellulose wood fibre was discovered as raw material for kraft paper. However, it is known that kraft paper was the insulating material in capacitors and cables before introducing it as winding insulation in power transformers [4]. Kraft paper and pressboard are the two major solid dielectrics in power transformers. The transformer winding insulation around the conductor is the kraft paper which confines the alternating current in the desired path [5]. The pressboard is insulation material placed between the low and high voltage winding to provide high mechanical strength, stability and further insulation around the windings [6]. In a power transformer, the combination of liquid and solid insulation began around the 1930s [4]; the liquid dielectric (oil) in the transformer provides improved dielectric strength between the windings; by filling the pores of the void within the kraft paper winding insulation and the pressboard. The oil also serves as a heat-dissipating medium in the power transformer cooling system [4], [5], [7], [8]. Figure 1.1 of page 2 shows a cut-out view of a power transformer with winding insulation, pressboard and oil insulation space.



**Figure 1.1:** A cut-out view of power transformer.

Each component that makes up the power transformer contributes to its reliability. Therefore, abnormality or fault on any of these components threatens the reliability of the power transformer [9], [10]. Insulation degradation, defective insulation and short circuit are the common causes of transformer failure [5]. Dielectric breakdown in power transformers is a common cause of power transformer failures compared to others as depicted in Figure 1.2 (page 3). The conditions resulting in dielectric insulation failure are most concerned with solid insulation and this include moisture ingress, oxidation, pyrolysis and hydrolysis. Consequently, failure due to solid insulation (kraft paper) is more frequent in insulation breakdown [8]–[19].



**Figure 1.2:** Causes of transformer failure [9].

Over the years, the efforts to improve kraft paper technology to produce quality and reliable insulation have been a consistent research focus. Around the 1950s to 1960s [4], synthetic fibres through chemical and physical methods were used for the first time to improve the thermal property of the dielectric insulation. Cyanide ethylation and Amine compounds are chemicals often used to improve the thermal withstand of electrical grade unbleached kraft paper insulation. The modified papers are referred to as the thermally upgraded oil-impregnated paper insulation. This reduces the effect of pyrolysis on the kraft paper insulation by replacing the hydroxyl group with a stable functional group having enduring thermal withstand [4], [20].

It is notable that among insulation technological development, the application of nanoscience and nanotechnology to improve dielectric properties of cellulose kraft paper for power transformer application is one of the most progressive achievements in recent times [7]. The performance limitation exhibited by the conventional raw materials triggered the quest for this alternative technology. In the area of kraft paper insulation, nanotechnology has presented potential for better insulation properties and performance compared with kraft

paper made purely from traditional raw material. The electrical, thermal and mechanical properties of kraft paper modified with nanoparticles (NPs) can be greatly improved [7].

The synthetic fibres and kraft paper modified with nanoparticles have changed the old narratives of kraft paper technology for power transformer application. However, the toxic byproduct associated with thermally upgraded kraft paper and the hydrophilic nature of the cellulosic fibre (kraft paper insulation) and nanocomposite kraft paper insulation is a significant challenge to the improvements recorded so far [20]–[22]. Research for solutions to the setback associated with nanocomposite kraft paper insulation is the main focus of this thesis.

## **1.2 Problem Statement**

Recent efforts in using nanotechnology on kraft paper insulation have availed a new method for improving the properties of kraft paper insulation. Nano-metal oxides such as ZnO, SiO<sub>2</sub>, MgO and TiO<sub>2</sub> nanoparticles have been reinforced in kraft paper to enhance their dielectric properties. Also, it is on record that modifying cellulose paper with sizing chemicals (Alkenyl Succinic Anhydride (ASA) and Alkyl Ketene Dimer (AKD)) or nanoparticles with AKD increases the resistance of the material to water absorption. Sizing agents are water resistive chemicals that reduce the surface energy of a material [7], [20]. However, a significant knowledge gap exists on the hydrophilicity of the modified kraft paper. Kraft paper being cellulosic material is inherently hygroscopic [23]–[26] and the surface oxygen vacancies associated with metal oxides NPs (nanofiller) acts as active sites in the dissociative absorption of water [27]–[30].

Water/moisture in kraft paper speeds up its structural decomposition. Consequences include; increased dielectric loss (loss factor) due to absorbed moisture, increased susceptibility to partial discharge degradation, and loss of thermal and mechanical properties. In power transformers, the degraded kraft paper eventually results in complete failure of the equipment [20], [31], [32]. So far there are no significant attempts that have been made to address the hydrophilic limitation of nanocomposite kraft paper successfully.

Therefore, this thesis sought for possibilities of nanocomposite kraft paper material designed for improved hydrophobicity.

### **1.3 The Research Questions**

1. To what extent can the hydrophilicity of nanocomposite kraft paper be improved?
2. To what extent does the modification influence other important dielectric properties of the modified kraft paper?

### **1.4 The Research Objectives**

The following milestones characterized the work of this thesis;

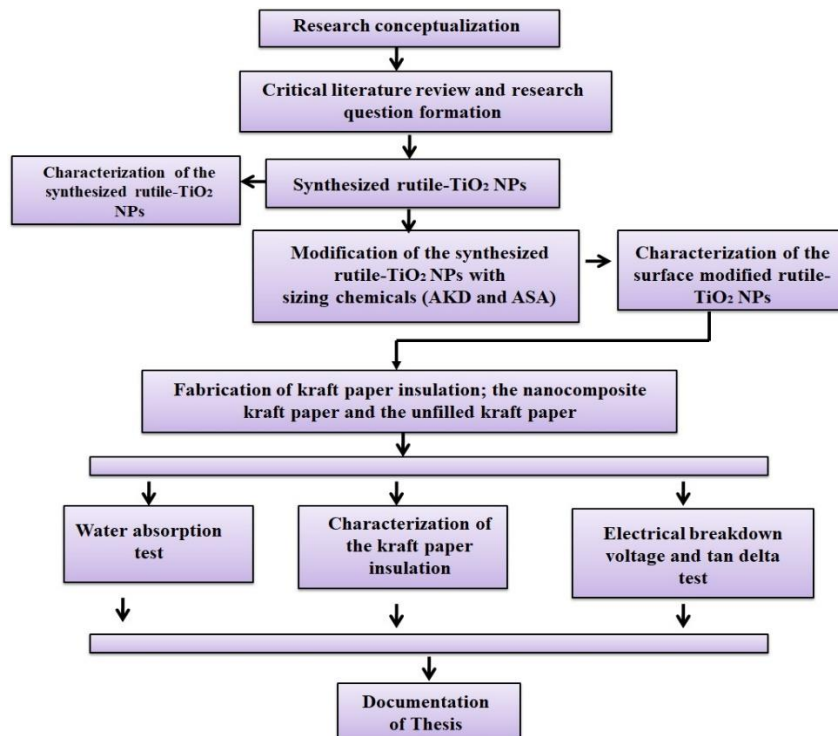
1. Rutile-TiO<sub>2</sub> NPs were synthesized and surface-modified with AKD in one case and ASA in another case. The surface modification was to achieve rutile-TiO<sub>2</sub> NPs with improved resistance to water absorption.
2. The nanoparticle characterization, moisture absorption and thermal examination were conducted to investigate the properties of the synthesized and the modified nanoparticles.
3. Fabricate the nanocomposite kraft paper insulation material. The cellulose pulp was reinforced with the surface-modified and unmodified rutile-TiO<sub>2</sub> NPs. For the control test (reference sample), kraft paper specimen without nanoparticles filler were also prepared.
4. The fabricated kraft paper insulation specimens were characterized. The breakdown strength, thermal stability and mechanical property were investigated. The hydrophilic properties of the fabricated kraft paper were tested and effect of absorbed moisture on the dielectric dissipation factor was studied.

### **1.5 The Research Road Map**

The research work was conducted in collaboration with the following disciplines at the University of the Witwatersrand, Johannesburg: Molecular Science Institute (School of Chemistry), Microscopy and Microanalysis Unit (MMU), School of Chemical and Metallurgical Engineering and School of Electrical and Information Engineering. The

nanocomposite kraft paper and the control specimens were manufactured at the Sappi™ Technology Centre (Innovation Hub, Pretoria). Figure 1.3 depicts the road map of the research methodology. The research work was in three major stages;

- i. First stage was the synthesis and surface modification of the rutile-TiO<sub>2</sub> nanoparticles. This was done in the molecular science institute laboratory at the Wits University School of Chemistry. The samples were then characterized in the Microscopy and Microanalysis Unit (MMU) as well as at the School of Chemical and Metallurgical Engineering.
- ii. The second stage was the fabrication of the unbleached kraft paper with and without the surface-modified rutile-TiO<sub>2</sub> nanoparticles, followed by characterization. These were done at the Sappi™ Technology Centre laboratory (Innovation Hub, Pretoria).
- iii. Then the moisture absorption characteristics, thermal property and electrical breakdown voltage test were investigated. This was done in the School of Chemical and Metallurgical Engineering and Electrical High Voltage laboratory.



**Figure 1.3:** Block illustration of the research road map.

## 1.6 Thesis Structure

Chapter 2 reviews the kraft paper technology and structural characteristics of cellulose fibre used for power transformer insulation. The chapter highlights the hydrophilic nature of cellulose and its effect on the dielectric properties of the kraft paper. It also discussed how moisture is found in power transformers and how it accelerates insulation degradation.

Chapter 3 discusses nanocomposite kraft paper technology. It reviews the application of nanoparticles in kraft paper insulation and the shortfalls associated with the modification. The chapter also presents different nanofillers used for kraft paper insulation and discussed in detail the titanium dioxide nanoparticles as superior nanofiller compared with others.

Chapter 4, discusses various methods of synthesizing rutile-TiO<sub>2</sub> NPs. The synthesis and surface modification of rutile-TiO<sub>2</sub> NPs is then presented. Also, chemicals used to hydrophobize the nanoparticles are highlighted, including the procedure for the surface modification of the rutile-TiO<sub>2</sub> NPs. The chapter also presented the characterization of the nanoparticles and tests the samples against moisture absorption and thermal stability.

Chapter 5 presents the fabrication of the kraft paper insulation and the fibre characterization. The nanofiller retention and dispersion of the fabricated nanocomposite kraft paper are presented. The mechanical and thermal properties of the fabricated kraft paper are measured. Also investigated are the moisture absorption characteristics of the fabricated kraft paper.

Chapter 6 of the report presents the impact of moisture on the dielectric dissipation factor of the kraft paper and also studies the electrical breakdown strength.

Chapter 7 concludes the thesis. The new knowledge contribution and limitation are presented.

# **Chapter 2: Kraft Paper Insulation Technology; a Critical Review**

## **2.1 Introduction**

Paper science and engineering technology provide the fundamental knowledge and understanding to design and fabricate paper for different applications. However, there is still a knowledge deficit in improving the paper's insulation reliability properties for power transformer applications. This chapter presents the kraft paper technology and associated challenges in water absorption.

## **2.2 Kraft Paper Raw Material**

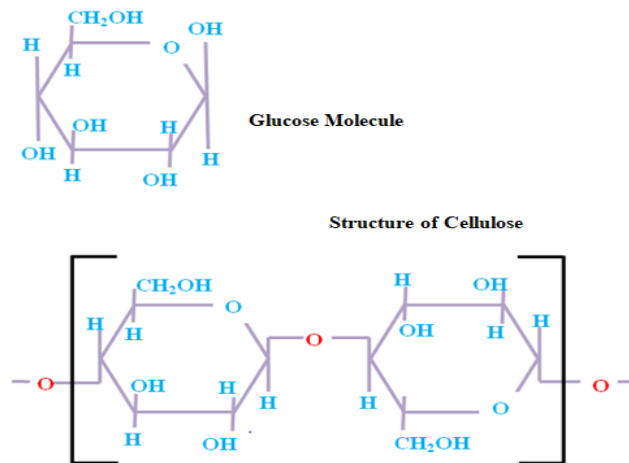
All varieties of vegetable fibres can make different grades of paper [33]. However, the most commonly used cellulose fibres are wood from trees, cotton or grass [34]. Unique purpose papers, kraft paper, tissues, newsprint and corrugated boards are produced using pure, synthetic, or recycled fibres [33]. For power transformer applications, the cellulose wood fibres from trees are commonly used [35], [36]. Wood fibres from trees are the most abundant raw material for cellulose [4]. They are renewable and biodegradable, and this makes wood fibre a sustainable raw material in a society that advocates for environmentally friendly products. Cellulose from wood fibres is a good component for composite materials. The wood fibres are either softwood or hardwood [4], [33]–[35], [37]. Compared to hardwood fibres, softwood has longer and stronger fibres. Hardwood fibres are bleached and used for smooth printing [38]. The softwood unbleached kraft pulp is used for oil-impregnated paper insulation due to its strong fibre-fibre bond [39].

## **2.3 Overview of Kraft Paper Insulation**

Kraft paper is the insulation used for power transformer winding. The winding is wrapped with kraft paper and impregnated in transformer oil, usually mineral or organic oil such as ester [5], [40]. The softwood varieties used for oil-impregnated paper consists of 33-45% cellulose, 22-35% hemicellulose, 27-35 lignin, and 2-3.5% extractives [41], [42]. Through

“sulphate” or “kraft pulping”, the cellulose is refined from the softwood. The process removes the hemicellulose and lignin. After pulping, the unbleached skraft pulp will contain 78-80% cellulose with a small percentage of hemicelluloses and lignin; this improves the mechanical property of the insulation paper [8], [42], [43].

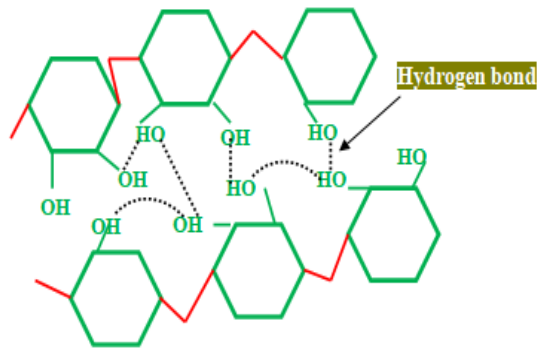
Cellulose molecules contain glucose rings connected in a peculiar format, as in Figure 2.1 [5]. It is represented as  $[C_5H_{10}O_5]_n$  [36], where  $n$  stands for the degree of polymerization (DP). The degree of molecular polymerization is simply the average number of glucose links in the polymer chain. The DP of kraft paper ranges from 1100 to 2000; this implies cellulose fibre comprises 1100 to 2000 glucose molecules [35].



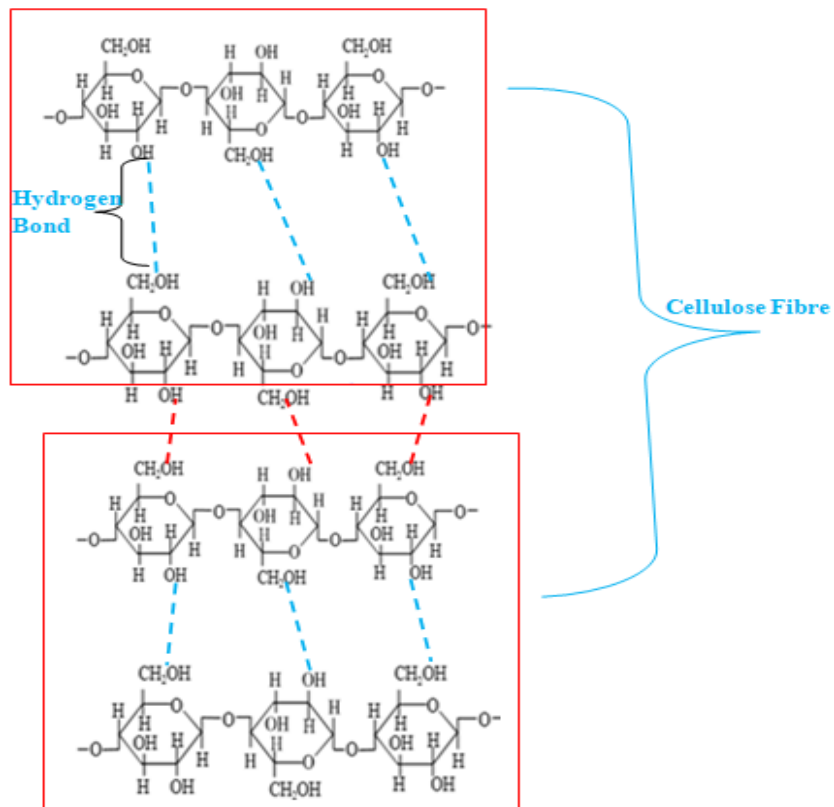
**Figure 2.1:** Glucose molecule and cellulose polymer [36].

In the structure, glucose ( $C_6H_{12}O_6$ ) ring is joined by glycosidic oxygen (O- glycosidic), and linked together via the hydroxyl groups (OH) to form a cellulose [6]. Hydrogen bonds are formed between the OH of the  $C_6H_{12}O_6$  monomers within the cellulose. The hydrogen atoms of the  $C_6H_{12}O_6$  monomer and oxygen atoms of another  $C_6H_{12}O_6$  monomer form the hydrogen bond. Electrons are attracted to oxygen in these groups due to the high electron affinity of oxygen [44], [45]. Since opposite polarities attract,  $O^-$  and  $H^+$  in the groups form a hydrogen bond, as shown in Figures 2.2 and 2.3 of page 10, demonstrating the hydrogen bonding with the fashion of the parallel arrangement of cellulose. The cellulose chains are linked through a hydrogen bond, which contributes to the electrical and mechanical strength of the kraft

paper insulation [35]. The inherent characteristic of cellulosic material to moisture absorption is presented in the following unit.



**Figure 2.2:** Hydrogen bond formation [45].



**Figure 2.3:** Demonstration of the hydrogen bonding that allows the parallel arrangement of the cellulose polymer chains [45].

## 2.4 Moisture Absorption in Paper Insulation

The factors that influence the ageing of kraft paper insulation were studied by Fofana *et al.* [19]. In their experiment, they concluded that the ageing rate of oil-impregnated paper is directly proportional to moisture content. Also, according to the studies done by Arekelian and Fofana on the water in high voltage equipment [46], they realized that cellulose kraft paper is the most water vulnerable insulation. The experiments by Martin *et al.* [39] on moisture absorption of kraft paper insulation revealed that when kraft paper is exposed to atmospheric air, the surrounding moisture is absorbed; this accelerates the deterioration of the kraft paper insulation. Sutan *et al.* [35] studied the effect of moisture on oil-impregnated paper on 43 distribution transformers. Moisture was confirmed as a catalyst for the degradation of kraft paper insulation. From Omicron™ [24], Martin presented a dielectric frequency analysis as a reliable method of assessing water content in an oil-impregnated paper. It is concluded that water is dangerous to the solid insulation of the transformer, and the mechanical properties are compromised when paper absorbs moisture.

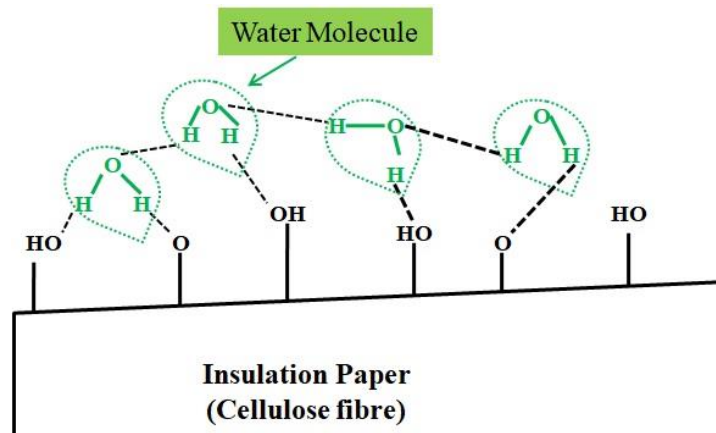
Therefore, the life span of a power transformer is largely dependent on the amount of moisture content in the insulation. The moisture content of solid insulation is between 0.5 and 1% (by dry weight) after factory drying [47]. As the transformer is used, moisture content tends to increase over time and also migrate to the surface of the paper, as vapour, as free water in the capillaries and as bound water to the kraft paper [35], [47], [48]. Several factors facilitate moisture production within the insulation during the transformer's life and these include;

- a) Left over moisture on the oil-impregnated paper after factory drying [47].
- b) Water ingress from the atmosphere [5], [47].
- c) Kraft paper decomposition: small amounts of moisture are produced as a byproduct of the decomposing cellulose. The hydroxide (OH) molecule is released when the solid insulation (cellulose chain) is heat stressed and electrically stressed. During the transformer operation, the liquid insulation becomes a hydrogen source (since most insulating fluids are hydrocarbon-based). And water is formed in chemical reactions involving oxygen and hydrogen [19], [35], [47]–[49].

Therefore, water is usually found in the transformer due to the leftover moisture in the paper (after drying), moisture ingress from the atmosphere and kraft paper decomposition. Water solubility in transformer oil is usually low; therefore, water is more adsorbed by the oil-impregnated paper (>>98% of the water). But as the temperature of the transformer increases, the solubility of water in the liquid insulation is experienced [24], [49]–[52].

## 2.5 The Problem Associated with wet Kraft Paper Insulation

The nano-porous structure with exposed hydroxyl sites (adsorption sites) of cellulose makes it a strong H<sub>2</sub>O-absorbing (hygroscopic) as in Figure 2.4. Water adsorption in cellulose paper causes permanent deformation in its physical and chemical structure, which is identified as hygroscopic growth and failure of mechanical tautness of the kraft paper. The exposed OH site with a large dipole moment attracts water (polar molecules) through Coulomb force [25], [26].



**Figure 2.4:** Attraction of water molecules to hydroxyl groups on the cellulose surface.

There are also several other degradation mechanisms that water cause in wet kraft paper insulation. The dielectric withstand strength [24] is decreased, speeds up cellulose decomposition [35], dielectric loss (loss factor) increased [19], partial discharge initiation level is decreased [46], conductivity is increased and causes the emission of bubbles at high temperatures [47], [49]. The thermal degradation of mechanical properties of the kraft paper is increased with the existence of H<sub>2</sub>O in the kraft paper [46]. In the worst case, transformers can breakdown due to extreme water in the insulation. As the paper's water content increases,

the paper's ageing rate is accelerated [52], [53]. Moisture content diagnosis of power transformer insulation is therefore imperative.

### 2.5.1 Moisture Content Diagnostic Methods in Kraft paper Insulation

Water content in a paper is a relation between the water mass and the insulation mass. The typical range of water content in cellulose insulation is 0.5% under new conditions and 5% under-aged conditions [47]. To determine water content in a power transformer, coulometric Karl Fischer titration has been the popular method. This method now serves as a yardstick (standard scale) for other approaches [47], [54]. Karl Fischer titration in chemistry is used to identify a sample's water trace. It is a chemical method of water analysis using water reaction in a reaction cell. It can measure very precisely how many water molecules react in the cell. However, this method is described to be influenced by moisture interference and temperature variation [47], [54]–[57].

Using temperature ( $T$ ) and vapour pressure ( $P_v$ ), the water content in a paper (WCP) using Fessler equation is calculated thus using the equation 2.1 [58];

$$WCP = 2.173 \times 10^{-7} \times P_v^{0.6685} \times e^{(4725.6)^{-T}} \quad (2.1)$$

Where,

$WCP$  = water content in the paper,

$P_v$  = vapor pressure of water in atmosphere and,

$T$  = temperature in Kelvin.

The capacitive probe is an alternative method of measuring the water saturation in cellulose. It is easy to use both online and on-site [59]. Water molecules cause the change of capacitance measured in this process. The water molecules migrate into the capacitor's dielectric, change the capacitance, and the moisture exchange can be measured [54], [60]. This method only gives moisture saturation but cannot provide moisture content. Using the equilibrium is another method of measuring the water content but has been challenged on the accuracy of measurement and moisture and temperature influence [54], [59], [60].

Dielectric Response Method (DRM) is a method that uses the dielectric properties of the insulation to examine the moisture content in a kraft paper. It is applicable for on-site assessment of moisture content in power transformers. These dielectric properties include recovery voltage, polarization and depolarization current, and Frequency Domain Spectroscopy [47], [54]. Dielectric Response Analyzer (DIRANA) is a new and improved DRM for moisture content study developed by Omicron™. DIRANA determines the water content in kraft paper without the need for oil sampling. To measure water content using the DIRANA, the measurement voltage is applied to the voltage winding. The main insulation of the power transformer is situated between the high voltage (HV) and low voltage (LV) windings and has a cylinder shape. The current flowing from HV to LV winding is measured to measure the dielectric properties. The measurement is influenced by the cellulose and oil conductivity and the interfacial polarization. The DIRANA combines Frequency Domain Spectroscopy (FDS) and Polarization Depolarization Current (PDC) [24], [54], [61]. Since the DIRANA does not requires oil samples, it was used to study the dielectric dissipation factor of the developed nanocomposite kraft paper in this thesis.

## **2.6 Influence of Moisture on the Ageing and Degradation Mechanisms of Kraft Paper Insulation in Power Transformers**

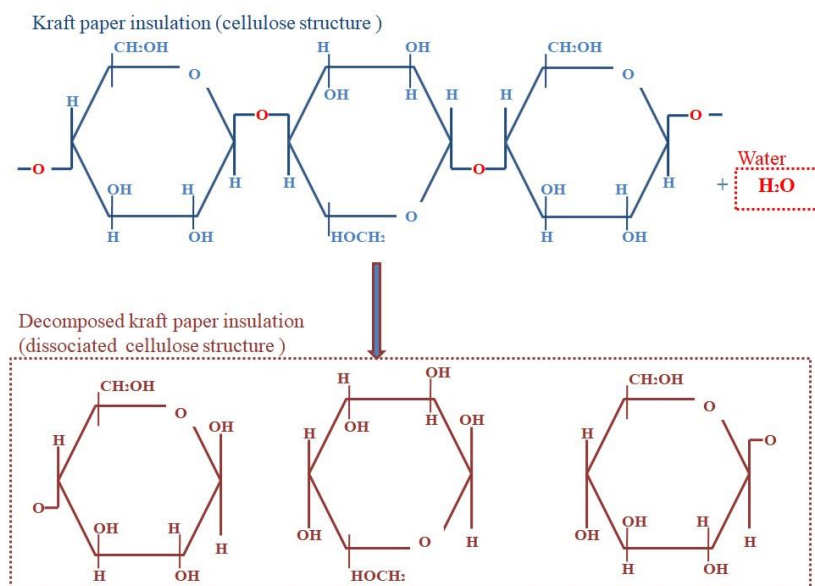
When an insulation paper ages in a transformer, the polymeric chains that makes up the cellulose breaks over time. The ageing mechanism of paper insulation in a power transformer starts when hydrogen peroxide ( $H_2O_2$ ) is produced due to the interaction of metal cation  $Cu^+/Cu^{2+}$  or  $Fe^+/Fe^{2+}$ , water, oxygen, and heat [6]. The  $H_2O_2$  will decompose to create an HO radical and accelerate oil and paper oxidation. The oxidation leads to the generation of water and R-COOH acids. The R-COOH acids are of two types; the Higher Molecular Weight Acid (HMA) and Lower Molecular Weight Acid (LMA). Dissociation of specific acids such as LMA will generate  $H^+$  ions and accelerates the hydrolysis of the paper [6], [62], [63].

The study on the degradation of oil-impregnated paper in power transformers has been on for decades. The factors accelerating the degradation and ageing of paper insulation are temperature, water and oxygen. These three factors are categorized into the following

mechanisms: Hydrolysis, Oxidation and Pyrolysis as reviewed in the following sub-sections [5], [36], [43], [63], [64].

### Hydrolysis:

Hydrolysis is simply the accumulation of water in the transformer insulation. The source of water and carboxylic acids (R-COOH) in a power transformer are traced to originate from the atmosphere, ageing of kraft paper and oil [5], [65]. The presence of water breaks the hydrogen bond and oxygen between the glucose rings, as in Figure 2.5; and this leads to the decomposition of the cellulose, producing free glucose [5], [8], [36]. The insulation paper will eventually depolymerize, weakening its fibre and mechanical properties [63]. The presence of water in the power transformer accelerates the hydrolysis of the kraft paper; this occurs between 60 to 150 °C [8]. It is notable that the process is catalyzed by thermal stress which is a typical operation of power transformers.

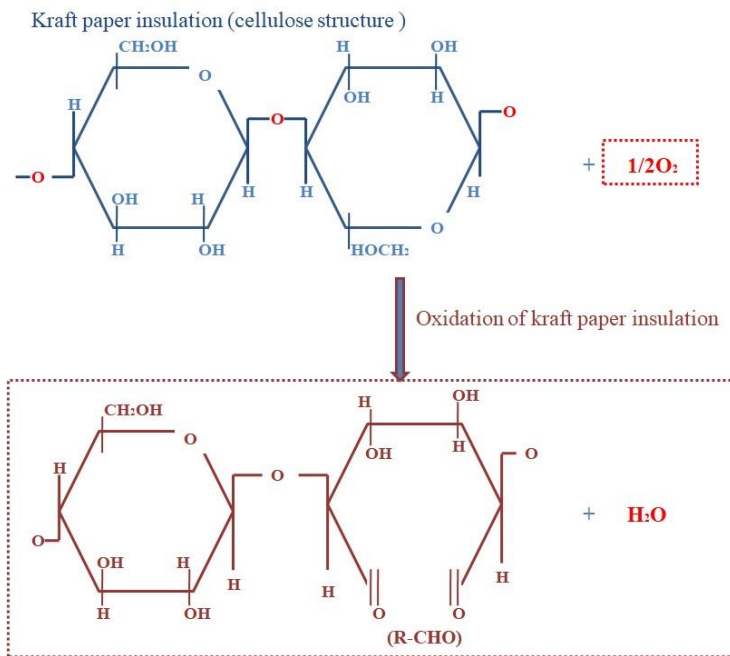


**Figure 2.5:** Hydrolytic degradation reaction of cellulose [61].

### Oxidation:

Thermal degradation and ingress from the atmosphere (small water molecules) cause oxidation of transformer insulation and it is supported by oxygen and copper. When oxidation reactions occur on both primary and secondary alcohol groups (-OH) of the

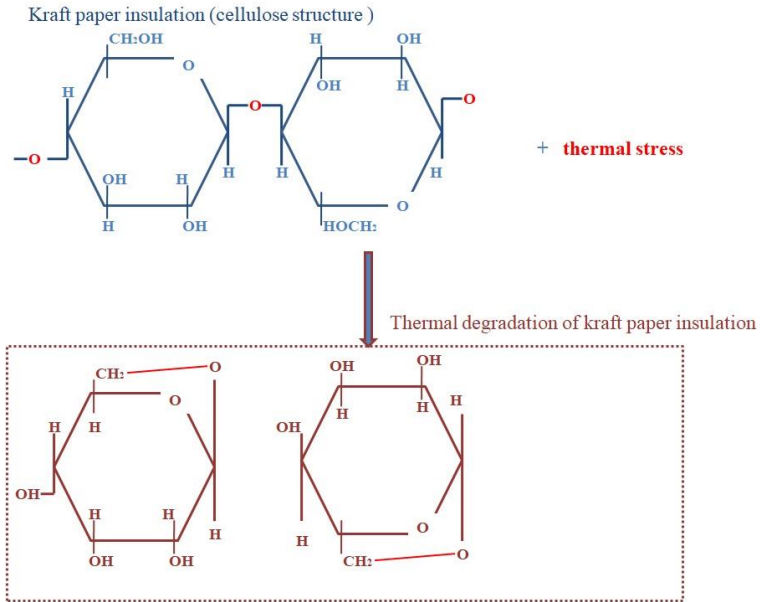
cellulose chain, the oxygen attacks the carbon atoms in the paper molecules. Thus aldehydes (R-CHO), ketones (RC(=O)R), and carboxylic acids (R-COOH) are established [5], [66]. The oxidation of the kraft paper insulation instigates the hydrolysis reaction owing to the production of moisture and acids [8], [66]. The acids produced through the oxidation of the oil insulation also incite the hydrolysis of kraft paper insulation in the presence of water. The moisture molecules produced are easily absorbed by the kraft paper insulation; this opens the glucose ring and disrupts the cellulose chain leading to lower DP [5], [64], as shown in Figure 2.6. A power transformer's oxidation mechanism is experienced at temperatures less than 65 °C [8].



**Figure 2.6:** Oxidation degradation of cellulose [8], [66], [67].

**Pyrolysis:**

When the operating temperature of a transformer is higher than 150 °C, thermal degradation (Figure 2.7 of page 17) on the cellulose called pyrolysis tends to occur. The process often happens without water, oxygen, or both. Pyrolysis occurs at a minimum temperature of 150 °C, at this temperature and above, the glycosidic bonds (oxygen linkage) will be broken at the same time the glucose rings will open. This process creates moisture and gases such as carbon monoxide CO and carbon dioxide CO<sub>2</sub> [5], [60], [63], [67], [70].



**Figure 2.7:** Thermal degradation of cellulose [68].

In summary, paper degradation accelerates due to moisture in the transformer. The presence of water could either be due to leftover moisture on the paper after factory drying, moisture ingress and thermal reaction in the insulation paper. Among the three thermal degradation reactions experienced by the kraft paper insulation, the oxidation and hydrolysis of the kraft paper quickly initiate moisture/water at a lower temperature. This research aims to present the possibilities of modifying the characteristics structure of the cellulose to withstand the experience of moisture created in the transformer due to hydrolysis, oxidation, and pyrolysis.

## 2.7 Chapter Conclusion

From the literature, the application of softwood fibre for fabricating kraft paper insulation is widespread because cellulose softwood fibre has more robust mechanical properties than hardwood. The chemical structure of cellulose wood fibre has been reviewed and discussed with emphasis on its vulnerability to moisture and implication thereof on power transformers. The review elaborated on the impact of moisture on the kraft paper insulation. The degradation of kraft paper insulation is facilitated by the hydrolysis, pyrolysis and oxidation of the kraft paper. However, hydrolysis and oxidation of kraft paper occur at a lower temperature, initiating moisture/water presence which eventually damages the cellulosic structure of the polymer and reduces the degree of polymerization of the kraft

paper insulation. The pyrolysis happens at a much higher temperature. The quest to improve the quality of the insulation paper in terms of thermal stability brought about the application of synthetic fibres; this only address the heat resistance of the kraft paper and produces a toxic byproduct. The compromised dielectric properties of kraft paper insulation due to its moisture absorption becomes a significant concern. The next chapter discusses the application of nanotechnology on kraft paper insulation and the successes achieved in this frontier of technological development.

# **Chapter 3: Nanocomposite Kraft Paper Technology: a critical review**

## **3.1 Introduction**

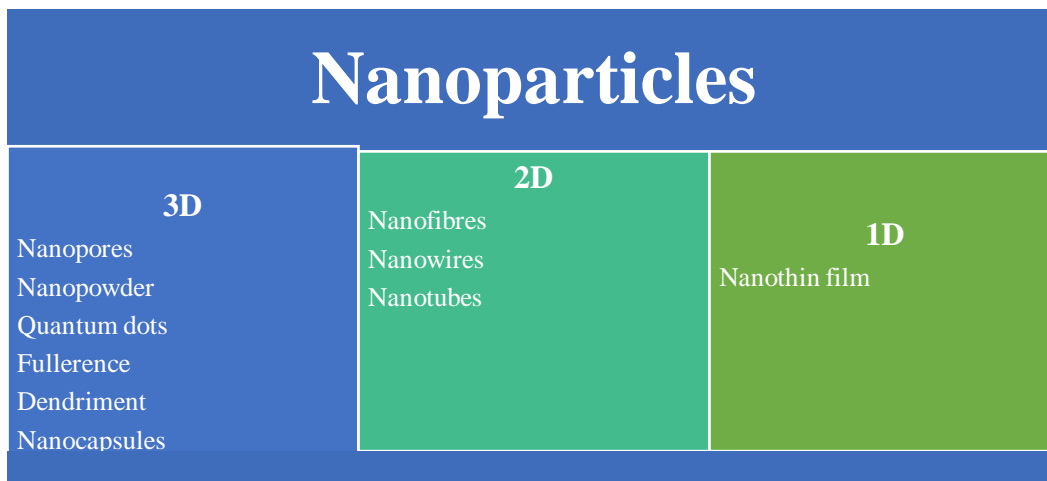
Chapter two presented the raw material and structural characteristics of kraft paper insulation. The chapter also discussed the degradation of the internal mechanism of kraft paper insulation due to absorbed moisture. The shortfall is associated with its strong affinity to polar materials, which poses a severe compromise on the final properties of the kraft paper insulation. The resultant effect could be breakdown of the power transformer. This chapter presents the application of nanotechnology in producing nanocomposite kraft paper that has improved insulation properties. The knowledge that still exists in the technology is highlighted as the rationale of the thesis work.

## **3.2 The Concept of Nanotechnology**

Nanotechnology application has recorded unprecedented recognition and acceptance in several fields of engineering. Due to the limitations of conventional materials to meet modern technology demands, many areas of science and engineering are using nanotechnology to improve their material quality [7], [69], [70]. In transformer winding insulation, nano-cellulose made from cellulose fibres, including nano-fillers (nanoparticles) used to modify kraft paper insulation, attracts attention because of their unique properties. These include excellent flexibility, superior surface smoothness, thermal stability, high optical transmittance and robust tensile strength [68], [69]–[74].

Nobel Prize laureate Richard Feynman introduced nanotechnology in 1959; however, the late Norio Taniguchi in 1974 initially used the expression nanotechnology to describe the skill of engineering a matter precisely at a nanometer scale [78]. Nanotechnology is simply the process of manipulating material properties at its nano-metric level [7]. In the application of nanotechnology, nanoparticles are essential as they connect the tiny materials contained in a matter to the bulk materials. They are defined as objects ranging from 1-100 nm particle size as classified in Figure 3.1 (page 20). Nanoparticles are used for different applications

with distinctive mechanical, photonic, optical, electrical, and catalytic properties. For example, nano-metallic particles produced with zinc, titanium, gold, silver, copper, magnesium and alginate are used in electrical engineering as nano-fillers in insulation. They are also used as insulation barriers in earthing systems. Other areas of application are in medicine, chemical engineering, material science [69], [70], [75], [79]–[81]. Figure 3.2 of page 21 shows the typical dimensional shapes of the nanoparticles. The one-dimensional (1D) nanoparticles are particles with one of their dimension  $<100$  nm. They originate in the form of nanosheets, nanoplates, nanoprism and nanodisk. However, the common 1D nanoparticles are nanographene platelets and Montmorillonite clay. They find application in areas such as sensors, coating, electrical, microelectronics and biomedical [75], [82]–[84].

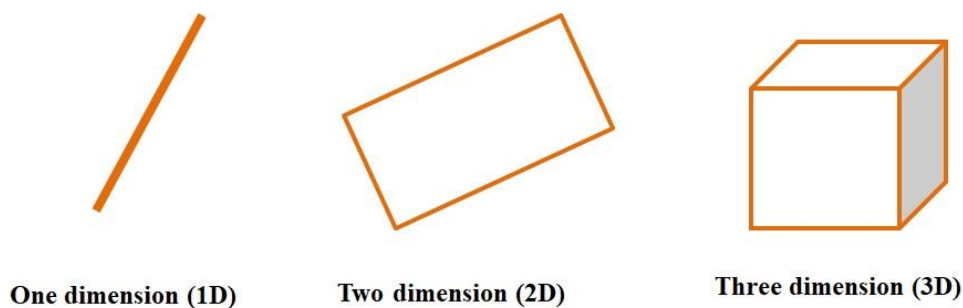


**Figure 3.1:** Nanoparticles Classification.

The whiskers and rod-shaped are two-dimensional (2D) nanoparticles with two dimensions  $<100$  nm. This nanoparticle class applies to electronics, optoelectronics, nanoreactors, and energy sensors. 2D nanoparticles have better flame retardant than 1D and 3D, and higher reinforcement levels than 3D. The most common examples of 2D nanoparticles are; clay nanotubes, cellulose whisker, boron carbon nitride tubes, silver or gold nanotubes, and 2D grapheme [75], [82]–[84].

The three-dimensional (3D) class of nanoparticles is referred to as nanoparticles or isodimensional nanoparticles. The quasispherical particles (3D) have all dimensions in

nanometer. Because of their inbuilt properties, 3D nanoparticles have good advantages in blending of polymer nanocomposites. Some of these nanoparticles have a high refractive index, hydrophilicity, low cost, high photocatalytic activity, and good transparency. 3D nanoparticles are also called nanocrystal, nanoshares and nanogranules. They find application in separation and purification, electrical insulation and biomedicine. Examples of these nanoparticles (3D) are; nano- $\text{Al}_2\text{O}_3$ , nano- $\text{TiO}_2$ , nano- $\text{Fe}_3\text{O}_4$ , nano- $\text{ZnO}$ , Ag, semiconductor nanocluster, carbon black, silica, nanosilica and quantum dots [75], [82]–[84].



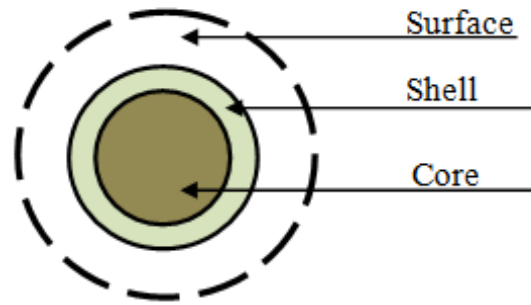
**Figure 3.2:** Typical dimensional shapes of the nanoparticles.

### 3.2.1 Structure of Nanoparticles

In nanoparticles, the core structure of the material is distinctly different from the outer layer. This makes the surface of individual nanoparticles an essential part of the material structure. This unique property of nanoparticles is due to their large surface area-to-volume ratio [83], [85], [86]. The structural layer of nanoparticles is divided into three; the core, the shell and the surface.

As illustrated in Figure 3.3 (page 22), the core is the nanoparticles, which is the material's centre. The composition of the core gives rise to the unique properties of the nano-material. Therefore, the chemistry of the nanoparticles is a product of their core. The shell makes the first layer that surrounds the core. It has surface chemistry that is usually distinct from the core. For example, iron nanoparticles are found to form iron oxide in their shell after preparation. And this does not tend to penetrate the core resulting in different surface chemistry that gives rise to a surface that can be functionalized (producing nanoparticles

with required surface properties). The final layer is the surface which is often functionalized with polymers, surfactants or sizing agents to form a composite [69], [86]. As in the present research, the surface (final layer) of rutile-TiO<sub>2</sub> NPs will be modified with a surfactant to reduce its hydrophilicity. The nanoparticles filled into the host material to produce the resultant material referred to as a nanocomposite.



**Figure 3.3:** Nanoparticles Structure.

### 3.3 Nanocomposite Material

The modification of polymer with nanoparticles (nanofiller) has brought more interest in the area of developing composite material [7], [70]. The use of nanofillers in composite goes way back, but it was first recorded in research carried out by Toyota in 1990 using nylon-6 with clay nanofiller. Ever since, the application of nanofillers in various fields has been studied [69]. In nanocomposites of electrical kraft paper insulation, the reinforcement of nanoparticles to improve the material's properties and performance depends on its interaction and dispersion in the host polymer [87]. Meanwhile, the fabrication of polymer nanocomposites has challenges that might affect the modified material's final properties. These challenges are;

1. Nanoparticles tend to form microscopic clusters (agglomeration of atoms and molecules) with the host polymer; this is due to their higher specific surface area to volume ratio and poor interfacial adhesion. The agglomeration is due to Van der Waals force.

2. Hydrophilic characteristics of nanofiller strongly influence the water absorption rate of the resultant nanocomposite.
3. The fabrication procedure or synthesis of the nanocomposites also influences the final properties of the modified material [75], [88].

### **3.4 Modification of Kraft Paper Insulation with Nanoparticles**

Different nano-metal oxides have been used to modify kraft paper insulation in the technology area of transformer insulation. Kraft papers reinforcement with nanoparticles has shown better and improved dielectric proprieties. Liao *et al.* in [71] and [76] reinforced kraft paper insulation with nano-titanium dioxide (nano-TiO<sub>2</sub>). The breakdown strength of the modified insulation increased by 21%, and the injection of space charge reduced by 50%. In [74], the partial discharge inception voltage (PDIV) of the modified kraft paper insulation was reported to improve by 23%. Also, Liu *et al.* [14] reported that adding TiO<sub>2</sub> NPs suppresses partial discharge (PD) of modified kraft paper insulation and increases the breakdown strength. When Montmorillonite (MMT) was used by Yuan & Liao in 2014 [89] to modify a cellulose wood pulp for transformer winding insulation, the breakdown voltage of the modified insulation paper increased by 13%. In the same experiment, kraft-MMT's resultant properties were influenced by the nanofiller's percentage content and its uniformity of dispersion. When silica nanoparticles (SiO<sub>2</sub> NPs) were used to modify kraft paper insulation in Hollertz *et al.* [90] and Tan *et al.* [91], the mechanical property of the insulation paper increased. Alumina nanoparticles (nano-Al<sub>2</sub>O<sub>3</sub>) in kraft paper speed up the dissipation of space charge under low or high field strength [92] and [93]. The modified kraft paper indicated deformation resistance and improved mechanical properties.

The study of kraft paper reinforced with nanoparticles revealed that the nanofiller's size dramatically influences new material's properties. The interaction, dispersion and adhesion of nanofiller depend on its particle size. Therefore, the nanoparticles' size affects the degree of interaction between the matrixes of the host material [83], [86], [94]. Literature also shows that the method of synthesis, percentage loading, nanofiller retention and rate of dispersion influence the properties of modified kraft paper. Table 3.1 (page 24) summarises improvements recorded on modified kraft papers with different NPs.

**Table 3.1:** Improvements recorded with the application of different nanoparticles on kraft paper insulation.

Nanoparticles	Modified Kraft paper
<p>Nano-TiO<sub>2</sub> [14], [76], [42],[95]</p>	<p>Improvement in breakdown voltage, tensile strength and dielectric constant were recorded.</p> <p>The space charge distribution of modified kraft paper was improved.</p> <p>Reduction in distortion rate of the internal electric field in modified kraft paper was recorded</p> <p>Optimum particle size and mass fraction of TiO<sub>2</sub> nanoparticles were achieved.</p> <p>With TiO<sub>2</sub> NPs, the PDIV and break-down properties of modified insulating paper were greatly improved</p> <p>Homogeneous dispersion within the cellulose pulp was achieved, building a firm internal structure arrangement of the kraft paper.</p> <p>New chemical bonds were formed between the matrix of the kraft pulp and TiO<sub>2</sub> NPs.</p>
<p>Nano-SiO<sub>2</sub> [91],[96], [90]</p>	<p>With SiO<sub>2</sub> NPs, low dielectric losses and improvement in-plane tensile properties were produced.</p> <p>The mechanical, thermal and electrical properties of the Kraft paper modified with SiO<sub>2</sub> NPs were improved</p>
<p>Nano-Al<sub>2</sub>O<sub>3</sub> [92], [93]</p>	<p>Adding Al<sub>2</sub>O<sub>3</sub> NPs to kraft paper; prevents injection, movement and accumulation of space charge in modified insulation, making the space charge distribution more homogeneous in kraft paper.</p> <p>With Al<sub>2</sub>O<sub>3</sub> NPs, the number of hydrogen bonds increased in modified insulation, thereby increasing its thermal stability. A decline in the degree of polymerization was recorded in the modified paper (having Al<sub>2</sub>O<sub>3</sub> NPs) with a record of improvement in breakdown strength.</p>
<p>Nano-ZnO [96]</p>	<p>ZnO NPs can potentially improve kraft paper's surface partial discharge behaviour at AC voltages and under impulse stresses. Other properties like tensile strength and electrical properties were recorded to have improved for insulations have ZnO NPs.</p>
<p>Montmorillonite (MMT) [89]</p>	<p>The breakdown voltage and dielectric constant improve for Kraft paper modified by MMT</p>

### **3.4.1 Selection of most suitable Nanoparticles for Modification of Kraft Paper Insulation in Power Transformer Application**

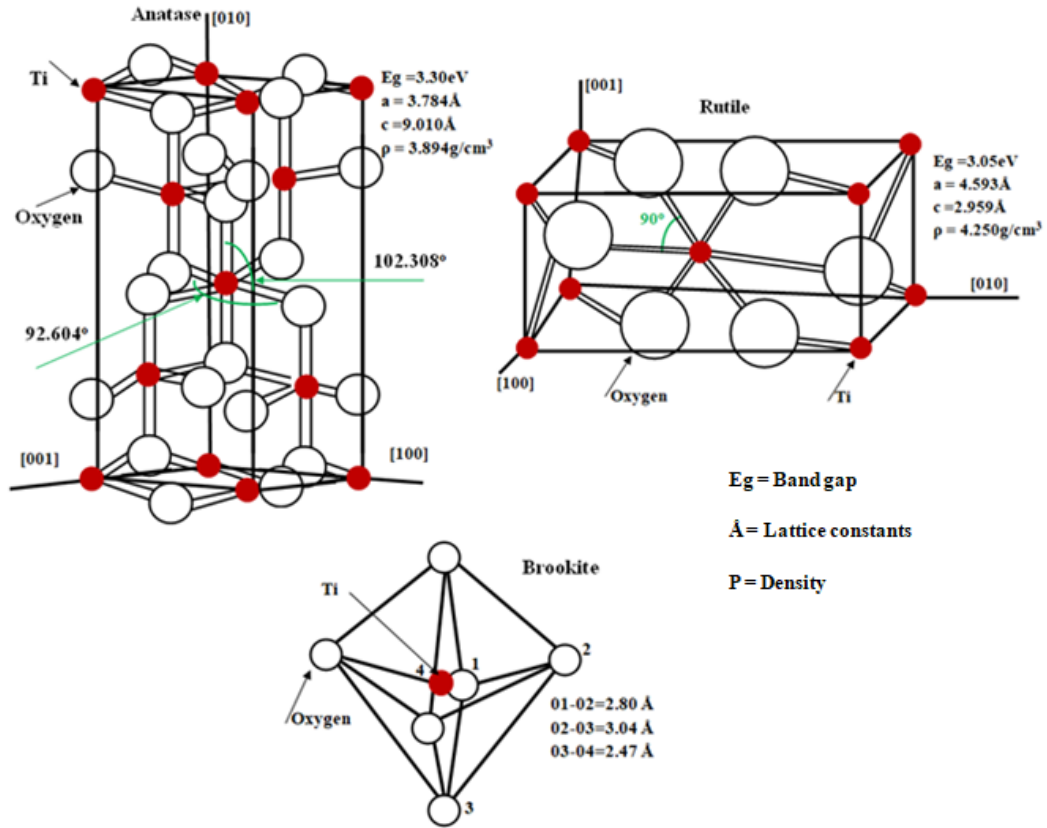
The selection of a particular nanofiller depends on the resulting nanocomposites' desired properties. In insulation for power transformers, the desired electrical, mechanical and thermal properties of the insulation are influenced by its application [7], [69], [70], [75]. Therefore, the required type of nanofiller that enhances a specific insulation performance without significantly affecting the rest of the insulation properties is necessary. Among the nanoparticles used for modification of kraft paper insulation, metal oxides nanoparticles are commonly used and these include  $\text{TiO}_2$ ,  $\text{ZnO}$ ,  $\text{SiO}_2$  and  $\text{Al}_2\text{O}_3$  [14], [74], [92], [96], [97]. Of the options,  $\text{TiO}_2$  NPs are reported to be superior among other possibilities [81]. Its compatibility and ability to improve the performance of kraft paper are notable.  $\text{TiO}_2$  is reported to be more stable in reactions, nontoxic, has a strong polarity, low cost, and can withstand higher temperatures. The rutile phase of nano- $\text{TiO}_2$  has high electrical resistivity, thermal stability and good mechanical strength. In contrast to the other common phases of the  $\text{TiO}_2$  NPs (brookite and anatase), the rutile is chemically stable. It can exist in very high temperatures and pressure without transforming or decomposing. Rutile-  $\text{TiO}_2$  has a relatively high dielectric constant, making it suitable for some dielectric applications [81], [98]–[103]. Although  $\text{TiO}_2$  NPs is an attractive nanofiller for kraft paper insulation, it has a major weakness in being hydrophilic [20], [27], [75], [96], [104], [105]. The hydrophilic properties of  $\text{TiO}_2$  is a major challenge to be mitigated furthermore. It is notable that in the literature, most studies on modifying kraft paper insulation with  $\text{TiO}_2$  have been with the anatase phase and not the rutile, and this is the knowledge gap to be addressed by the present work. Therefore, in this thesis, the nanoparticles investigated are of the rutile- $\text{TiO}_2$ .

### **3.4.2 Titanium Dioxide ( $\text{TiO}_2$ ) NPs fillers in Kraft Paper Insulation**

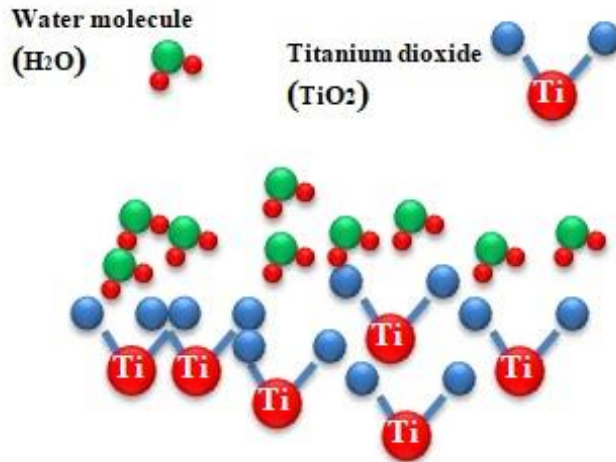
Discovered in 1791,  $\text{TiO}_2$  is a naturally existing mineral referred to as titania. As a well-known metal oxide, titania is mainly used because of its electronic and optical properties, low cost, nontoxic, and chemically stable.  $\text{TiO}_2$  (an inorganic solid) has found application in stabilizers in food, paper, plastic, coating and ceramics, amongst others [81], [102], [106].

Recently many findings revealed encouraging results in applying TiO<sub>2</sub>-nanoparticles as filler in engineering materials. Because of its high electrical resistivity and thermal and mechanical properties, TiO<sub>2</sub> nanoparticles improve the performance and properties of kraft paper insulation in power transformers.

TiO<sub>2</sub> has three intrinsic polymorphs, which are anatase (tetragonal), rutile (tetragonal) and brookite (orthorhombic), as depicted in Figure 3.4 of page 27. Anatase and rutile are more stable than brookite and have more applications. Because of the distinctive nature of anatase and rutile, they have found tremendous application in engineering. Anatase TiO<sub>2</sub> remove organic pollutants in H<sub>2</sub>O. Since it has small band gap energy, anatase absorbs a high percentage of sunlight radiation, making it a better phase for photocatalytic study. The rutile is more stable at high temperatures and pressure than the anatase phase. The rutile TiO<sub>2</sub> has a high dielectric constant ( $\epsilon = 114$  [107]) and electrical resistivity (vary in the range of  $10^{10}$  to  $10^{12}$  m $\Omega$  [81]); this makes it useful in the field of electrical and electronic engineering. It is also used in the power circuit, filter, temperature compensating condensers and capacitor. Rutile TiO<sub>2</sub> is chemically stable compared to other phases of TiO<sub>2</sub> NPs [103], [106], [108]. However, rutile-TiO<sub>2</sub> NPs, like other metal oxides, have surface oxygen vacancies that act as active sites in the dissociative absorption of water. The process of water absorption to the rutile-TiO<sub>2</sub> surface could be molecularly or dissociative. It is an interaction between the surficial Ti and hydroxyl group of the water molecule while the bridging oxygen forms a bond with the H atom as depicted in Figure 3.5 of page 27 [20], [27], [104]. How to mitigate the hydrophilic properties of TiO<sub>2</sub> for use as a nanofiller to improve hydrophilic properties of the nanocomposite kraft paper becomes a major research question in the present work.



**Figure 3.4:** Structures of  $\text{TiO}_2$  phases [100], [109].



**Figure 3.5:** Surficial Ti interaction with water molecules.

### **3.5 Chapter Conclusion**

This chapter has reviewed and discussed the application of nanotechnology on kraft paper insulation for transformer application. Nanoparticles are classified into one-dimensional (1D), two-dimensional (2D) and three-dimensional (3D) particles. Among these classes, the 3D blends better in composites; therefore, kraft paper insulation is modified with the 3D particles. Nanocomposites of kraft paper insulation are affected by particle size, method of synthesis, nanoparticle dispersion and retention within the host polymer. Nano-metal oxides made from Ti, Mg, Zn, Cu, Al, and Si are commonly used to modify the cellulose pulp for the application of kraft paper insulation. However, TiO<sub>2</sub> NPs have shown superior improvement when used in modification. The major setback associated with metal oxides, including the TiO<sub>2</sub> NPs, is their being hygroscopic. In the present research work, the rutile phase of TiO<sub>2</sub> NPs was chosen due to its good thermal endurance and stability in a chemical reaction. The next chapter presents the synthesis of rutile-TiO<sub>2</sub> NPs and a possible technique to mitigate the hydrophilic characteristic of the rutile-TiO<sub>2</sub> nanoparticles.

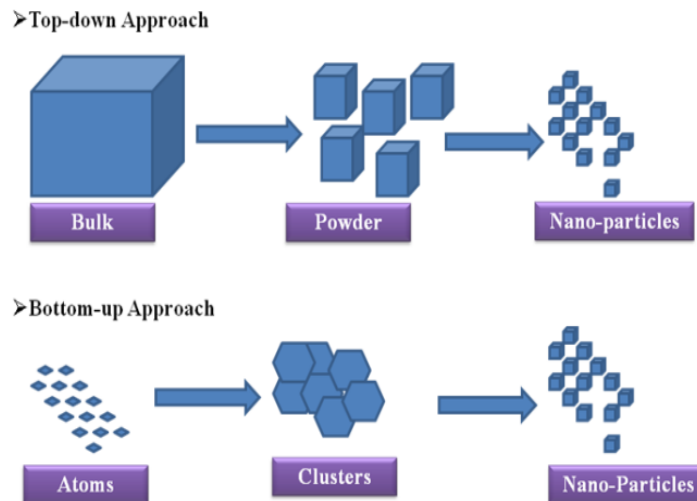
# **Chapter 4: Synthesis, Surface Modification and Characterization of Rutile-TiO<sub>2</sub> Nanoparticles for use in Power Transformer Kraft Paper**

## **4.1 Introduction**

As discussed in the previous chapter, polymer nanocomposites are organic polymers with reinforced inorganic nanofiller particles. Nanofillers tend to form clusters in the nanocomposite of kraft paper insulation, affecting a uniform dispersion of the particles within the host polymer. This is often influenced by the method of synthesis and nanoparticle size. Therefore, producing a kraft paper insulation modified with nanoparticles demands on a very reliable method of synthesizing the filler nanoparticles. This chapter presents the synthesis, surface modification (to reduce vulnerability to surrounding moisture) and characterization of rutile-TiO<sub>2</sub> NPs to fabricate nanocomposite kraft paper insulation. The findings in this chapter have been published in the scholarly knowledge domain titled; *“Improving thermal stability and hydrophobicity of rutile-TiO<sub>2</sub> nanoparticles for oil-impregnated paper application”*.

## **4.2 Synthesis of TiO<sub>2</sub> Nanoparticles**

The synthesis of TiO<sub>2</sub> nanoparticles involves two approaches. The first is bottom-up technique, which consists of assembling atoms onto one another to synthesise nanostructures. The second approach is top-down and it involves the breaking of atoms from the substrate. The building blocks are removed from the substrate to produce the nanostructure, as illustrated in Figure 4.1 (page 30) [7], [110]. Fabrication of proper particle size and shape of nanoparticles is difficult with methods under the top-down approach [111]. However, the most frequent methods of synthesizing TiO<sub>2</sub> nanoparticles are the categories of the bottom-up approach such as: Sol-gel, hydrothermal, Solvothermal, Direct Oxidation, Sonochemical synthesis, Microwave synthesis, Chemical Vapor Deposition (CVD)/ Physical Vapor Deposition (PVD) methods; all these methods have been used in different experiments to synthesize nano-TiO<sub>2</sub> [102].



**Figure 4.1:** Bottom-up and Top-down approaches to synthesizing TiO<sub>2</sub> nanoparticles [110].

The merits and the demerits of the commonly used methods of synthesizing TiO<sub>2</sub> NPs are presented in Table 4.1, including the sol-gel process.

**Table 4.1:** Merit and demerits of different methods of synthesizing TiO<sub>2</sub> NPs.

Methods of Synthesis	Merit	Demerit
Hydrothermal and Solvothermal [80], [100], [109], [112].	It provides a simple mode of operation; it can grow sizeable high-quality crystals	Impossibility of observing the reaction process and the need for expensive autoclaves and Teflon
Sonochemical [100], [102], [109], [113].	The method is faster and consumes far less energy compared to other conventional methods of synthesis	This method is still limited in application because of its uncontrollable rapid reaction, and most precursors are not suitable for this kind of synthesis
Microwave [102], [109], [113].	It has uniform heat on the solution, and it saves energy due to the short thermal induction period, selective heating, manageable control and low cost	Unfeasible for reaction monitoring, limited applicability to materials that absorb microwave and lack of scalability

**Table 4.1 cont.’**

Methods of Synthesis	Merit	Demerit
Sol gel method [114], [115], [116, p. 4], [117]	Easy to perform in the laboratory, able to get uniform and small particles, uniform distribution of components and porosity, control of reaction path way and feasible for reaction monitoring	Moisture sensitive, hard to fabricate in large scale, high temperature required to form, anatase and rutile, expensive.
CVD/PVD [102], [113].	Lower power input  Lower temperature rage, PVD doesn't require a special precursor  Produce a relatively pure product  PVD is environmental friendly	CVD precursors are often hazardous and toxic, producing a by-product that is harmful to health and is a slow process  CVD precursors are expensive  Not all precursors can be used with CVD  PVD is a costly method  and requires a skilled operator

Compared to other methods, sol-gel is easy to perform, and the process involved can be monitored and controlled; as such, the sol-gel method was chosen for the synthesis. In the present work therefore the sol gel method was chosen for the of the rutile-TiO<sub>2</sub> NPs.

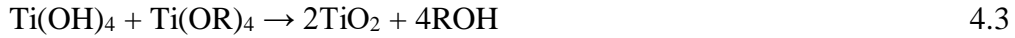
**Sol-gel method:**

Sol-gel is a wet chemical method of synthesis. It involves two steps: hydrolysis and condensation, then obtaining the TiO<sub>2</sub> nano-crystalline particles through annealing. The precursor (Ti(OBu)<sub>4</sub>, TiCl<sub>4</sub>, TiCl<sub>3</sub> or TiBr<sub>4</sub>) are dissolved in some suitable solvent (example, distilled water, de-ionized water or ethanol) to form a solution called sol; the sol is then converted to gel. The gel is then dried to get the required nanoparticles. This method has been used in much literature to synthesise TiO<sub>2</sub> NPs [105], [106], [107]–[109]. The process is shown in the following equations:

Hydrolysis



Condensation



In the equation, R can either represent n-butyl, ethyl, i-propyl and so on [123].

Sol-gel approach is a well-developed fabricating method to synthesise inorganic (metal oxide) NPs and also for the preparation of organic and inorganic nanocomposites [75], [100]. The rest of the section presents the procedures for synthesizing and characterising the nanoparticles.

### 4.3 The Overview Process of Synthesizing Rutile-TiO<sub>2</sub> Nanoparticles using the Sol-gel Method

The steps followed in the present work in synthesizing rutile-TiO<sub>2</sub> NPs via the sol-gel method are shown in Figure 4.2. The water in the sol-gel creates a reaction between the Ti(OBu)<sub>4</sub> (precursor). The process decomposes the solvent and the solute (precursor) and the reaction is referred to as hydrolysis. This later condenses the precursor into Ti-O-Ti; which will then be suppressed due to Ti-OH formation. Annealing is necessary in a furnace to remove the organic molecules from the process to complete the crystallization [102].



**Figure 4.2:** Steps involved in synthesizing TiO<sub>2</sub> NPs via the sol gel.

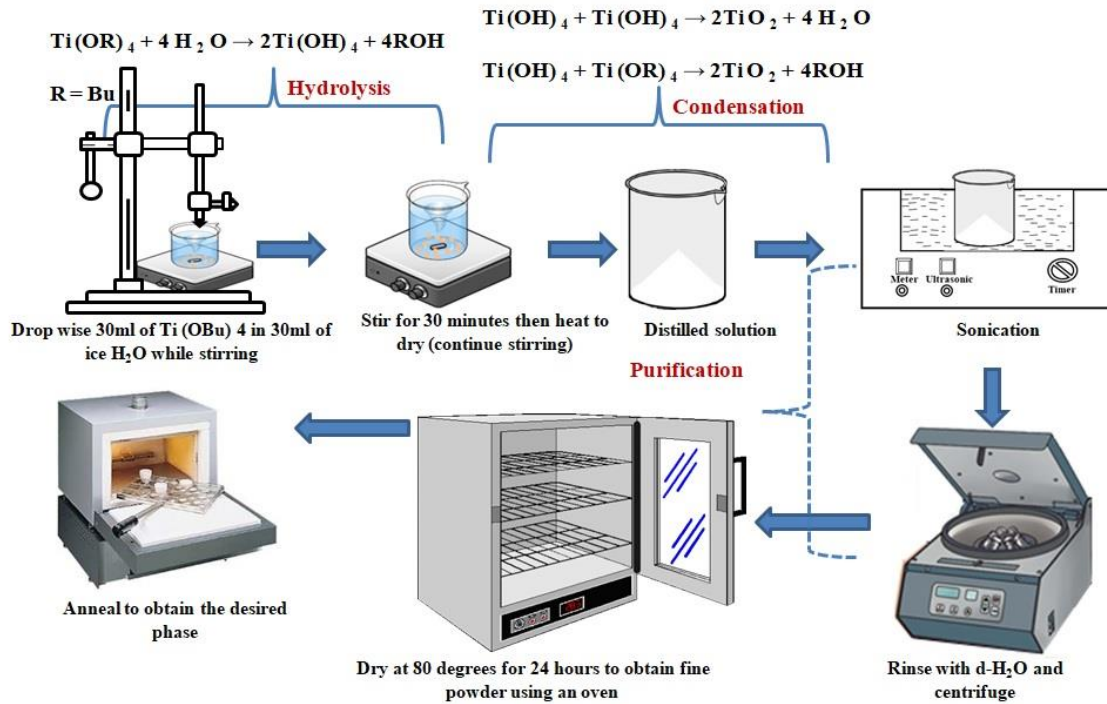
#### **4.3.1 The Designed and Implemented Process of Fabricating TiO<sub>2</sub> Nanoparticles of Specific Size (19.72nm)**

To optimally synthesize the rutile phase of TiO<sub>2</sub> nanoparticles size, 10 ml, 20 ml and 30 ml of Ti(OBu)<sub>4</sub> were drop-wise in a beaker containing distilled water (ice water). As shown in Figure 4.3 of page 34, the synthesis sequence involves continuous stirring of the mixture after dropping the precursor. After 30 minutes of stirring, the samples were heated and sonicated to reduce agglomeration. The samples were then rinsed, centrifuged and dried in an oven at 80°C for 24 hours.

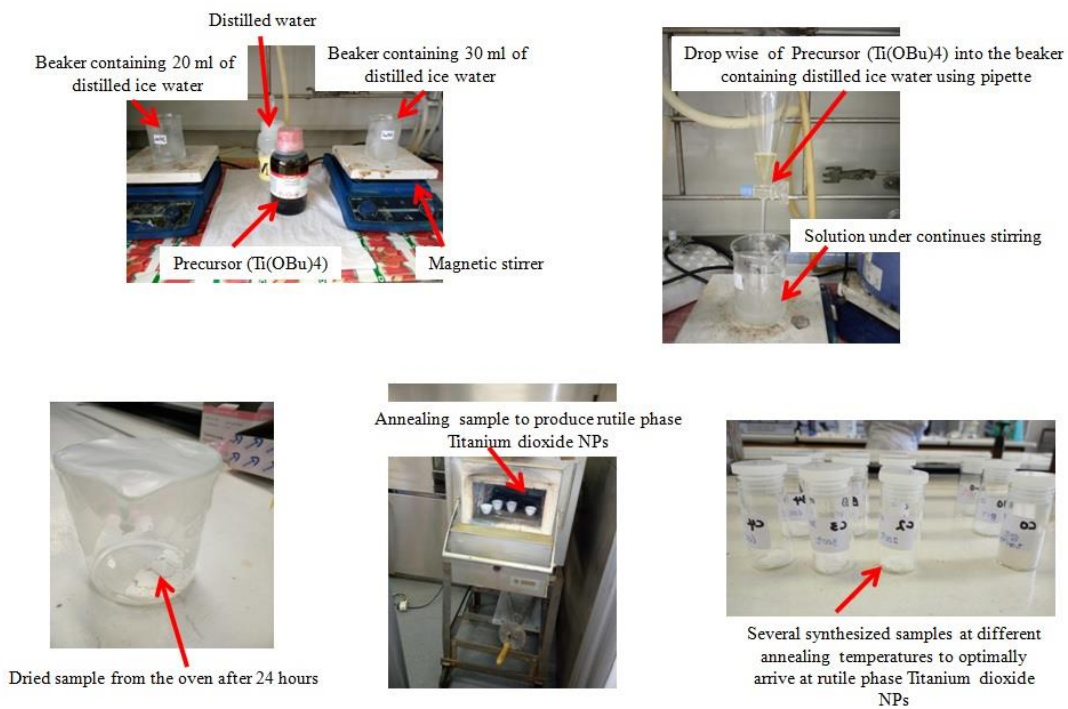
To obtain the rutile phase, 500 mg of each dried sample was weighed and annealed in a muffle furnace. Different temperatures, ranging from 300°C to 900°C were selected to produce the rutile phase. For each temperature chosen, the ramping and holding period were varied several times. This process was repeated until an optimal mixing ratio, temperature, ramping and holding period were identified. The following ratio of precursor to the solvent, annealing temperature, ramping and holding period was finally optimal to produce the rutile-TiO<sub>2</sub> NPs with a resultant NPs size of 19.7 nm on average;

- a. 30 ml of Ti(OBu)<sub>4</sub> dropped wise in 30 ml of distilled water
- b. The mixture was continuously stirred for 30 minutes
- c. Then was heated to remove impurities
- d. The obtained solid sample was sonicated, washed and centrifuged
- e. The sample was dried at 80°C for 24 hours in an oven

500 mg of the dried powder was annealed in a muffle furnace at 700°C, ramped for 2 hours and held for 2 hours resulting in the formation of the rutile phase of TiO<sub>2</sub> NPs. Figure 4.4 (page 34) shows the practical images of the experiment.



**Figure 4.3:** Sequence of synthesizing rutile- $TiO_2$  NPs.



**Figure 4.4:** Images of various stages of the synthesis.

### 4.3.2 Characterization of the obtained Rutile-TiO<sub>2</sub> Nanoparticles

The obtained nanoparticles were taken through various characterization techniques to review important parameters as summarized in Table 4.2. The detail procedure for each characteristic technique are explained in subsequent sub-sections.

**Table 4.2:** Summary of characteristic techniques.

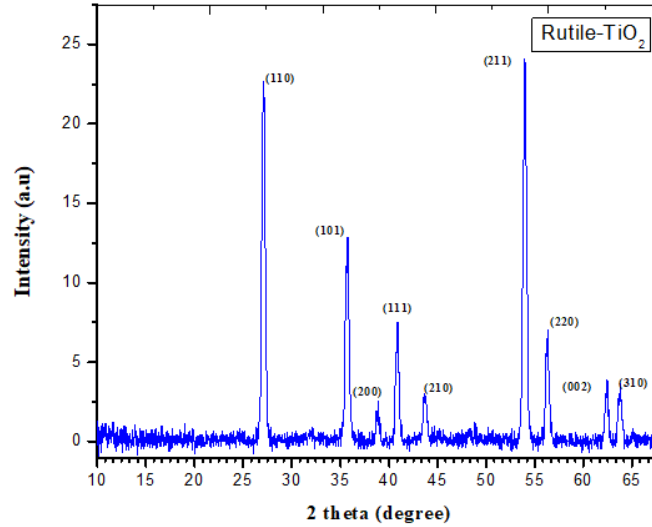
Characterization	Examination
X-ray Diffraction (XRD)	Phase identification, particle size and phase composition
Raman Spectroscopy	Phase identification
Fourier Transform Infrared (FT-IR)	Identification of unknown sample through its fingerprints or new functional group.
Transmission Electron Microscopy (TEM)	Morphology on particle shape and dispersion

#### 4.3.2.1 Phase Identification of the obtained Nanoparticles using X-ray Diffraction Spectrometry

X-ray powder diffraction (XRD) of the synthesized nanoparticles was done on the Bruker MeasSrv (D2-205530)/D2205530 diffractometer using CuK $\alpha$  radiation ( $\lambda = 1.5406 \text{ \AA}$ ) at 30 kV/10 mA. The synthesized nanoparticle crystallinities were studied using the X-ray diffraction technique with a computerized data acquisition facility and analytical tools. 30 kV operating voltage and 10 mA of filament current was used for the X-ray source. All samples were scanned at a speed of 5°/min in the 2 $\theta$  range between 10° and 90° for diffraction pattern

From the results, the XRD pattern exhibited distinct diffraction peaks at 2 $\theta$  of 27.18°, 35.96°, 38.92°, 40.96°, 43.68°, 53.98°, 56.34°, 62.87°, and 63.91° correspond to (110), (101), (200), (111), (210), (211), (220), (002) and (310) planes. This matches the standard rutile-TiO<sub>2</sub> reference peaks; all peaks are in good agreement with the standard spectrum (JCPDS no.:

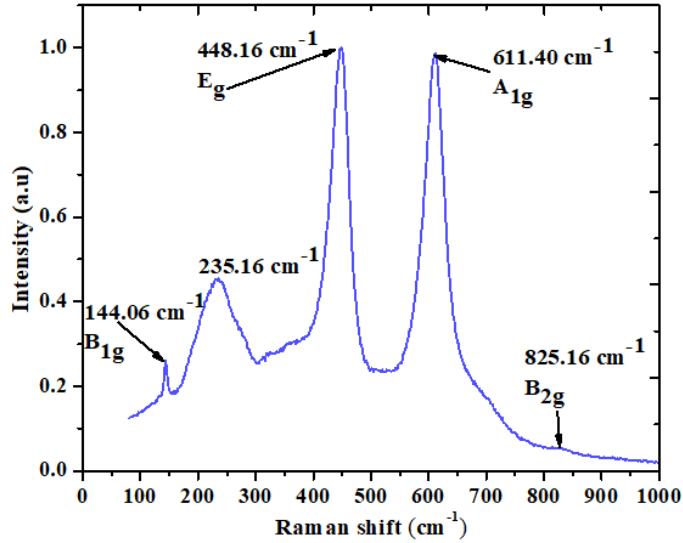
88-1175). As shown in Figure 4.5, the diffraction depicted sharpness of the peaks indicates highly crystalline nanoparticles [108], [124], [125]



**Figure 4.5:** XRD pattern (signature) of the obtained rutile-TiO<sub>2</sub> nanoparticles.

#### 4.3.2.2 Raman Spectrometry of the obtained Nanoparticles

Raman spectroscopy was done on the Bruker Infinity 1 spectrometer fitted with a 50x objective lens for imaging. Four random spots were scanned on each sample. Raman spectroscopy was used to check the quality and phase of the synthesized rutile-TiO<sub>2</sub> NPs. From the results obtained, the spectrum in Figure 4.6 (page 37) shows the Raman peak shifts for the rutile-TiO<sub>2</sub> NPs. The rutile-TiO<sub>2</sub> has four characteristic phonon modes at  $143 \pm 2 \text{ cm}^{-1}$  ( $B_{1g}$ ),  $445 \pm 5 \text{ cm}^{-1}$  ( $E_g$ ),  $610 \pm 1 \text{ cm}^{-1}$  ( $A_{1g}$ ), and  $235 \pm 5 \text{ cm}^{-1}$ . From Figure 4.6 (page 37), rutile exhibits dominated peaks at  $448.16 \text{ cm}^{-1}$  and  $611.04 \text{ cm}^{-1}$ . These peaks are attributed to  $E_g$  and  $A_{1g}$  active modes of rutile-TiO<sub>2</sub> correspondently. The graph's third most active optical phonon mode of rutile is the  $144.06 \text{ cm}^{-1}$  which is attributed to  $B_{1g}$ . The peak at  $825.16 \text{ cm}^{-1}$  is the weakest and poorly observed. This peak is assigned  $B_{2g}$ . A visible broad band at  $235.76 \text{ cm}^{-1}$  as observed on the graph does not correspond with any fundamental rutile phase modes. This may be assigned to the disorder-induced scattering or second-order effect (SOE) as a consequence of multi-phonon processes [126]–[130].



**Figure 4.6:** Raman peak shifts of the obtained rutile-TiO<sub>2</sub> NPs.

#### 4.3.2.3 Average Crystallite Size and Phase Composition of the obtained Rutile-TiO<sub>2</sub> Nanoparticles

##### Crystallite Size:

The crystallites and average size were calculated from the XRD data using the Scherrer equation [20] as given in equation 4.4.

$$S = \frac{k\lambda}{L\cos\theta} \quad (4.4)$$

where,  $S$  = crystallites size (nm),

$K = 0.9$  (Scherrer constant),

$\lambda = 0.15406$  (wavelength of the X-ray source),

$L$  = Full Width – Half Maximum – radians (FWMH) and,

$\theta$  = peak position

The XRD data determined the peak position and FWHM using the OriginLab. OriginLab is a program that runs on Microsoft Windows and is produced by OriginLab Corporation. It is used for graphing and data analysis [131]. The values were then substituted in the equation in excel to calculate the crystallites and average crystallite size of the obtained rutile-TiO<sub>2</sub> NPs. Table 4.3 (page 38) shows the particle size from the Scherrer equation.

**Table 4.3:** Particle size of the synthesized rutile-TiO<sub>2</sub> NPs.

Peak Position (2 θ)	FWMH	Crystallite Size (nm)
27.17508	0.57616	14.19
35.95979	0.4924	16.96
38.91545	0.52005	16.20
40.96045	0.45061	18.82
43.67634	0.41322	20.71
53.97556	0.43772	20.37
56.340028	0.35633	25.29
62.32229	0.42764	21.71
63.90541	0.41364	22.64
68.62027	0.47475	20.26
Average crystallites size: 19.72		

**Phase Composition:**

Also, the amount of phase composition was calculated using the Spurr formula [125].

$$X = (1 + 0.8 I_A/I_R)^{-1} \quad (4.5)$$

Where  $I_A$  and  $I_R$  are the peak intensities of Anatase (101) and Rutile (110)

(110) rutile intensity at 27.18 is 16.7

(101) Anatase intensity at 25.29 is 0.185

Substituting the values into equation 4.5

$$X = (1 + 0.8 I_A/I_R)^{-1} = 99.13\%$$

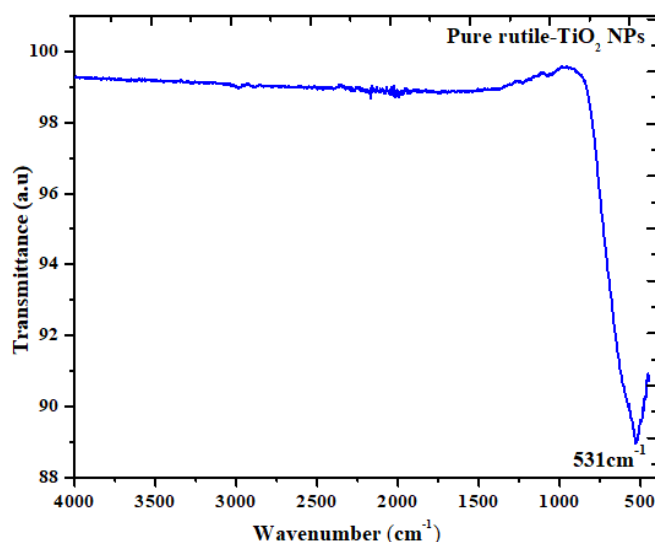
$$A (\%) = 100 / \{1 + 1.265(I_A/I_R)\} = 0.87$$

$$R (\%) = 99.13 - 0.87 = 98.26\%$$

This indicates that only small traces of anatase (0.87%) are in bulk. The percentage could be due to factors affecting the kinetics of phase transformation between the two main polymorphisms of TiO<sub>2</sub> (anatase to rutile). This includes heating rate, sample volume, impurities, measurement technique, atmosphere and particle size [126].

#### 4.3.2.4 Fourier Transform Infrared (FT-IR) Spectroscopy of the obtained Rutile-TiO<sub>2</sub> Nanoparticles

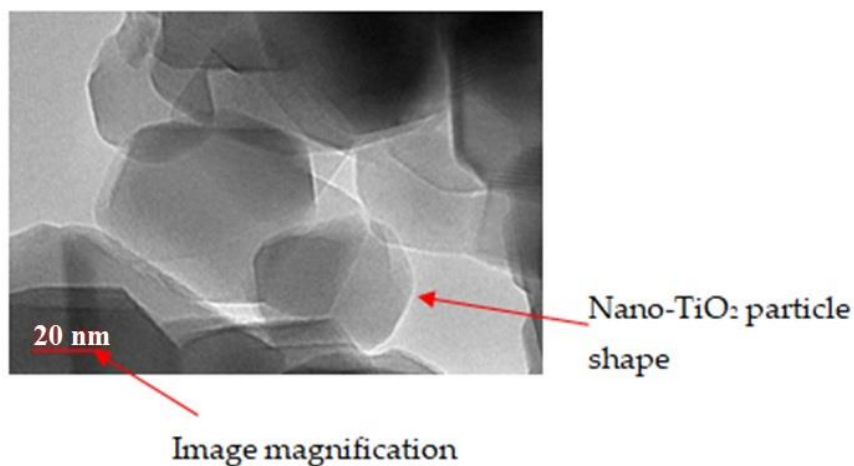
The FT-IR spectroscopy was performed using a Perkin Elmer Fourier transform-attenuated total reflectance – infrared spectrometer (FT-UATR-IR-2). The instrument was used to identify the synthesized nanoparticles and new functional groups after surface modification. The FT-IR spectra of the samples were obtained in the wavelength range of 4500–420 cm<sup>-1</sup> and was recorded at room temperature. As shown in Figure 4.7, the spectrum of the obtained sample (rutile-TiO<sub>2</sub>) was examined and compared with the rutile-TiO<sub>2</sub> FT-IR spectrum in the literature. The appearance of a band in the region 531 cm<sup>-1</sup> of the TiO<sub>2</sub> NPs spectrum indicates the presence of metal to oxygen bonding which corresponds to O-Ti-O bonding. Compared with what is available in the literature, the characteristic of the -OH group (3650-3200 cm<sup>-1</sup>) is not evident in the TiO<sub>2</sub> spectrum. This could be due to the annealing temperature and time; leading to the removal of the hydrolysable surface group, thereby fabricating ligand-free TiO<sub>2</sub> NPs [20]. The FT-IR results confirm the the fabricated nanoparticle is a rutile-TiO<sub>2</sub>.



**Figure 4.7:** FT-IR spectrum of the obtained rutile-TiO<sub>2</sub> NPs.

#### 4.3.2.5 Transmission Electron Microscopy (TEM) of the obtained Rutile-TiO<sub>2</sub> Nanoparticles Morphology

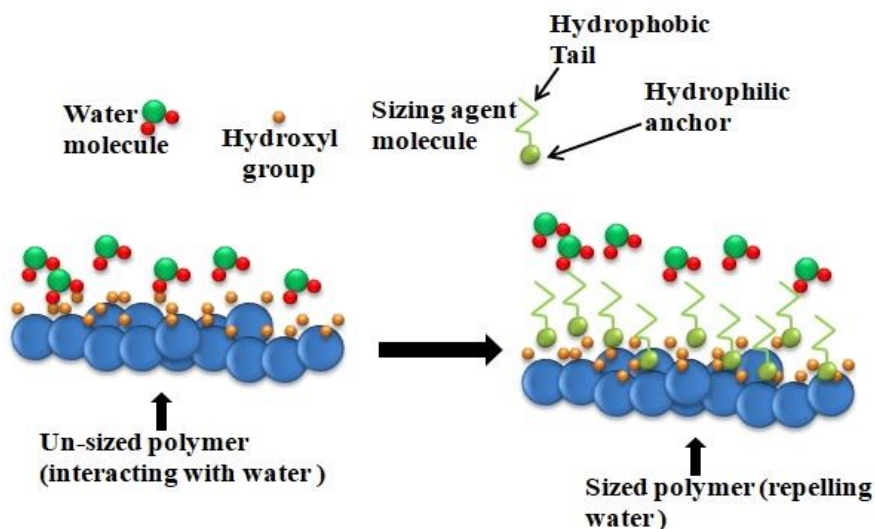
Transmission electron microscopy (TEM) was done on the FEI Technai T12 microscope. At an accelerating voltage of 120 kV, the TEM was used to examine the morphological features of particles. The TEM specimens were prepared by sonicating in ethanol to disperse the samples. A drop of the solution was then added to an SPI-carbon coated copper grid and dried in the air before inserting into the microscope. After insertion into the microscope, the beam was aligned, and sample images were taken. As shown in Figure 4.8, the particles are agglomerated; therefore, particle size distribution cannot be ascertained from the images obtained. However, as earlier reported in the XRD analysis using the Scherrer equation, the average nanoparticle size of 19.7 nm was calculated. The agglomeration obtained in the particles could be due to the high temperature used during calcination (that exists between the transitions of the two polymorphous of TiO<sub>2</sub>). Also, for small particles, Van der Waals attraction force between the NPs leads to agglomeration [20]. From the TEM images, a hexagonal like shape is evident. For effective uniform dispersion in the host kraft pulp and to reduce its affinity to water/moisture, the particles had to be surface conditioned as presented in the next section.



**Figure 4.8:** TEM images of the obtained rutile-TiO<sub>2</sub> NPs.

#### 4.4 Surface Modification of the obtained Rutile-TiO<sub>2</sub> Nanoparticles

In the paper manufacturing technology such as the ones used in printing, writing and packaging, Alkyl ketene dimer (AKD), alkenyl succinic anhydride (ASA), rosin products and copolymer are used to make the paper to be hydrophobic for different applications [132]. AKD and ASA are water resistive agents (sizing) most commonly used. The sizing agent reduces the surface-free energy of the material. The mechanism involves anchoring the hydrophilic head of the agents (AKD and ASA) with the host material while the hydrophobic tail extends out to repel water, as illustrated in Figure 4.9. As far back as the 1960s, AKD and ASA have been used to control the wettability of a paper. The hydrophobicity of modified kraft paper depends on the interaction of sizing chemicals [132]–[134]. Paper sizing provides resistance or limits the water absorption rate by adding chemicals to a slurry of cellulosic fibres to produce a kraft paper that resists water penetration. Sizing agents are the chemicals used in sizing a kraft paper [132], [135].



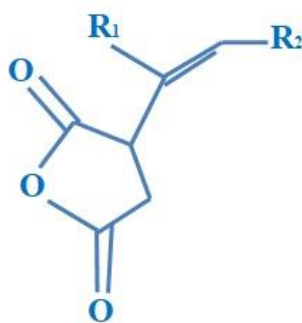
**Figure 4.9:** Sizing agent and mechanism of sizing orientation [20].

The rosin products, usually called “acidic sizes”, have been used for many years for sizing. However, papermaking condition has changed from an acidic approach to neutral and alkaline. This has displaced the applicability of rosin-type sizing agents in most paper manufacturing. Meanwhile, copolymer products are applicable where a tough sizing degree

is needed. They are used as surface sizing and require the combination of conventional sizing agents (AKD and ASA) [132], [133], [135]. The next section review ASA and AKD, respectively.

#### **Alkenyl Succinic Anhydride (ASA):**

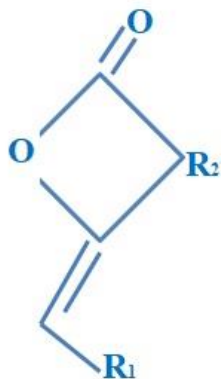
First mentioned in 1959 and patented in 1964 as a sizing agent [134], ASA structured as shown in Figure 4.10, is an oily and hydrophobic liquid. As a neutral/alkaline agent, it applies over a wide pH-range (5-9) and has a high degree of ageing resistance. The structure of ASA comprises two parts; the reactive succinic anhydride (the hydrophilic anchoring part with cellulosic material) and the alkenyl rest (the tail), which provides the needed hydrophobicity to the composite material. The tail (alkenyl rest) consists of iso-olefin having a chain length from C16 to 22 [132]–[134].



**Figure 4.10:** ASA Structure.

#### **Alkyl Ketene Dimer (AKD):**

Alkyl ketene dimer (AKD) was developed before ASA [132]. Like ASA, AKD components are a hydrophilic anchor ( $\beta$ -keto lactone ring) and a hydrophobic tail (consisting of two hydrogen chains with chains of C7 to C22). The structure of AKD is shown in Figure 4.11 of page 43. When AKD is used as a sizing agent, the hydrophilic anchor component forms  $\beta$  keto ester bonds with polymer, and the surface free energy is reduced as the hydrophobic groups align. They are use in pH range of 7-10 with melting point of about 50 °C [136], [137]. In the present research, AKD and ASA were chosen to be used to limit the surface free energy of the kraft paper insulation through surface modification of the nanoparticles.

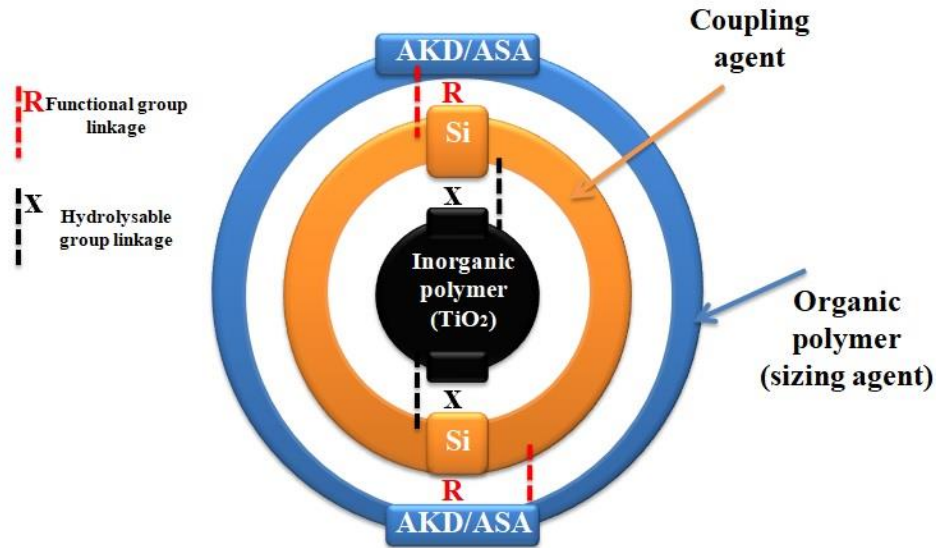


**Figure 4.11:** AKD Structure.

The presence of moisture in transformer insulation forms hydrogen bonds with the cellulose exposed OH group, thereby decomposing the glucose chain. However, by reinforcing the kraft paper insulation with surface-modified nanoparticles, the surface properties could be transformed from a high energy state to a reduced free energy surface, thereby increasing its contact angle. In this form, the ease of penetration of H<sub>2</sub>O and formation of hydrogen bonds becomes difficult [132]. The following section presents the process involved in surface modification of the rutile-TiO<sub>2</sub> nanoparticles.

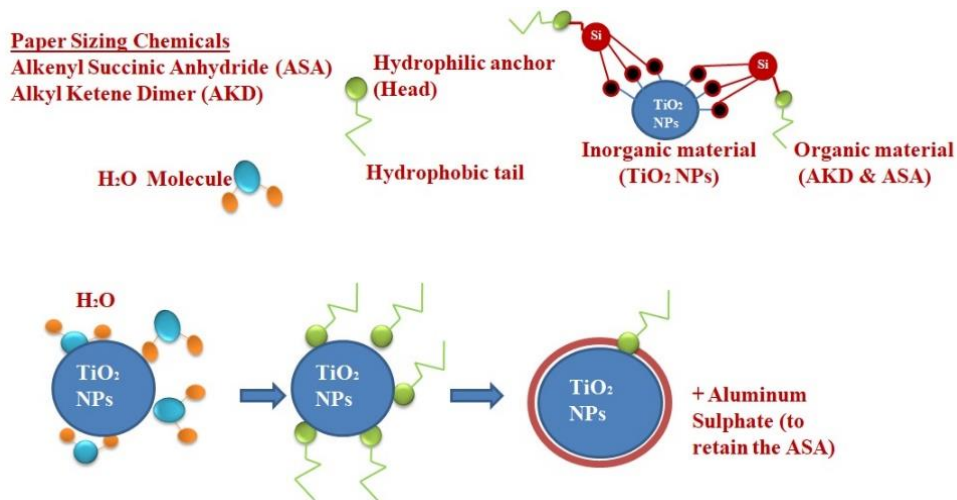
#### **4.5 The Theoretical Concept of Surface Modification of the Rutile-TiO<sub>2</sub> Nanoparticles**

Bonding of inorganic nano-fillers such as rutile-TiO<sub>2</sub> NPs with an organic sizing agent can be difficult. A coupling agent is often used to bond the two [138]. The coupling agent can be represented by the formula R (CH<sub>2</sub>)<sub>n</sub> SiX<sub>3</sub> [75]. The “X” is the hydrolysable group forming bonds with TiO<sub>2</sub> NPs. “R” is the functional group; it bonds with the polymer (cellulose) or organic material, which is the sizing agent in this case. Figure 4.12 (page 44) illustrates the interface bonding of organic (sizing agents) and inorganic (TiO<sub>2</sub> NPs) material with silane. The nanofiller reacts with “X” to produce silanol (forming metal hydroxide) while “R” produce a covalent bond with organic material [20], [75], [138]–[140].



**Figure 4.12:** Silane interface bond between organic and inorganic material [20].

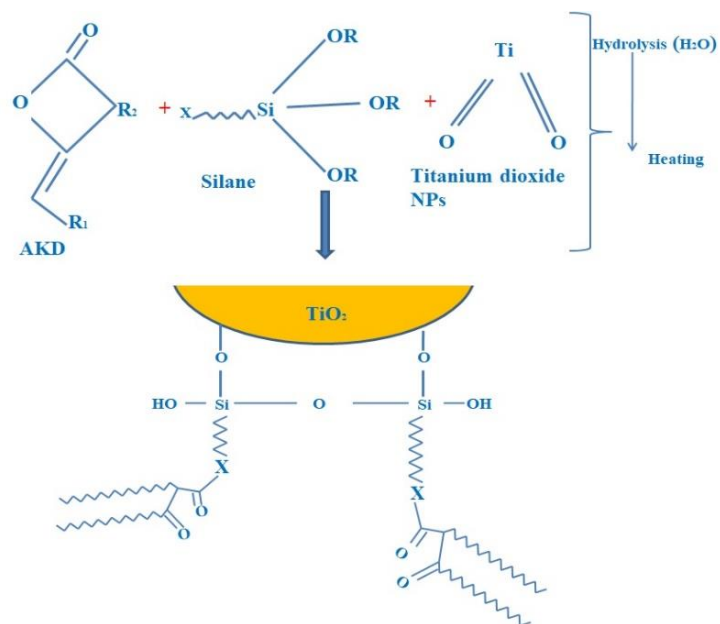
The block diagram of Figure 4.13 illustrates the modification stages of  $\text{TiO}_2$  NPs with the water-resistive agents (AKD and ASA). The silane coupling agent is employed to connect the dissimilar material, while due to the oily nature of ASA, alum is used to fuse the components further together.



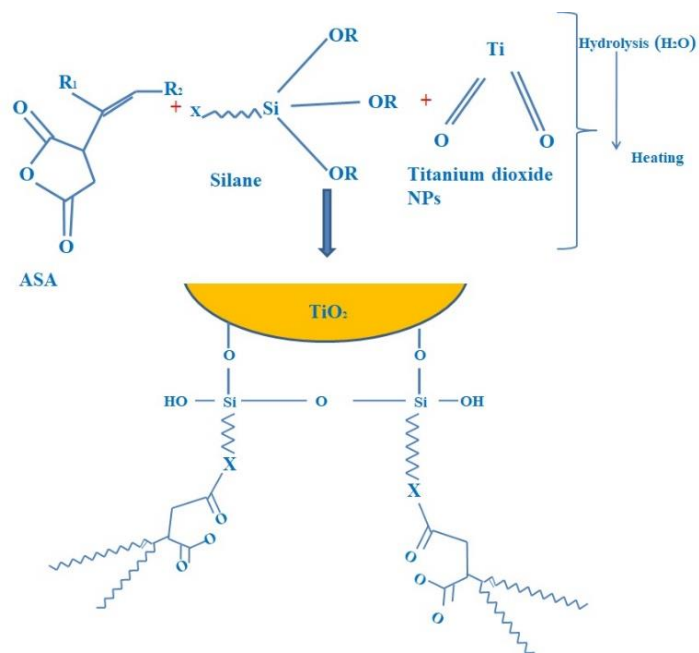
**Figure 4.13:** Illustration of surface modification mechanism of rutile- $\text{TiO}_2$  NPs [20].

The reaction model of surface-modified  $\text{TiO}_2$  NPs is shown in Figure 4.14 a & b (page 45); for AKD modified and ASA modified, respectively. During the hydrolysis of silane ( $\text{Si-OH}$ ),

the hydrolysable group ( $(\text{OH})_3\text{Si}$ ) reacts with rutile- $\text{TiO}_2$  NPs, and the organofunctional group reacts with sizing agents (AKD and ASA) [20], [138].



**Figure 4.14a:** Reaction model of surface-modified rutile- $\text{TiO}_2$  NPs/AKD.

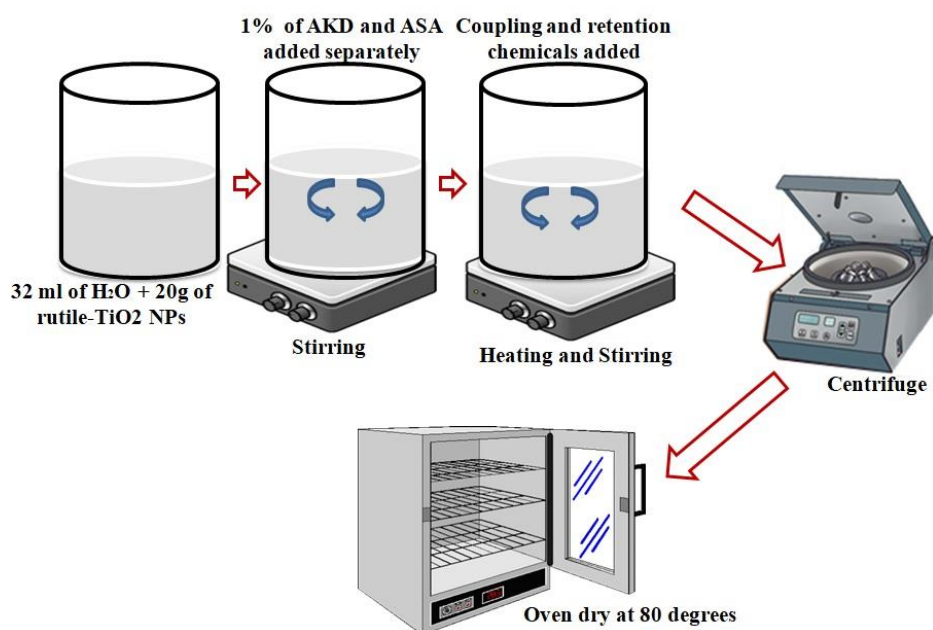


**Figure 4.14b:** Reaction model of surface-modified rutile- $\text{TiO}_2$  NPs/ASA.

#### 4.5.1 The Practical Procedure Implemented in Surface Modification of Rutile-TiO<sub>2</sub> Nanoparticles

Three portions of 10g of TiO<sub>2</sub> nanoparticles were dispersed in 32 ml of distilled water and sonicated for 30 minutes. Three portions were made comprising of 5 vol/vol%, 3 vol/vol% and 1 vol/vol% of AKD, making X, Y and Z. The same procedure was repeated for ASA, making samples A, B, and C. After 35 minutes of stirring, 1.5 vol/vol% silane was added to each mixture to connect the dissimilar compounds and was stirred for 1 hour. For ASA, alum was added to the solution to further fuse and retain the ASA with the TiO<sub>2</sub>. Both mixtures were heated for 20 minutes at 60°C with continued stirring. The samples were centrifuged, rinsed with distilled water to remove the impurities, and dried at 80°C. Figure 4.15 shows the block illustration of the modification model.

The obtained surface modified nanoparticles were then characterized for (a) constituent composite using FT-IR, (b) thermal stability using thermogravimetric analysis (TGA), and (c) water absorption using an experimental procedure as presented in the next section.



**Figure 4.15:** Schematic illustration of surface modification of rutile-TiO<sub>2</sub> NPs.

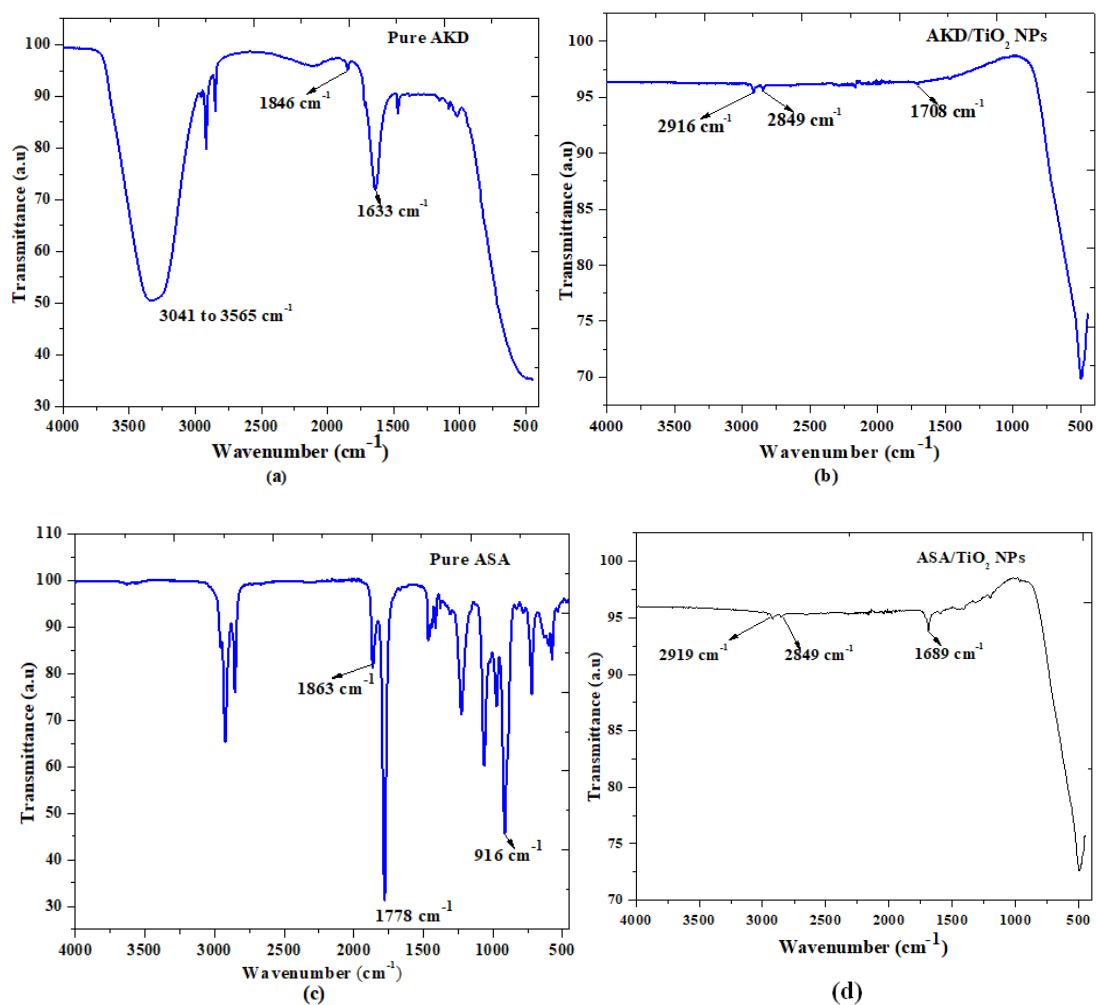
#### 4.5.1.1 Fourier Transform Infrared Spectroscopy (FT-IR) of the Surface Modified Rutile-TiO<sub>2</sub> Nanoparticles

The FT-IR was recorded at room temperature using a Perkin Elmer Fourier transform-attenuated total reflectance – infrared spectrometer (FT-UATR-IR-2) ranging from 4000-420 cm<sup>-1</sup>. The FT-IR of the modified TiO<sub>2</sub> NPs was conducted to examine the spectra of each sample. Figure 4.16a (page 48) shows the FT-IR spectra of pure AKD. From the plot, a weak and broad peak is evident between 3041 and 3565 cm<sup>-1</sup>, which is characteristic of (OH) vibrations in the AKD spectrum [20], [141]. Comparing Figures 4.16a and 4.16b of the modified TiO<sub>2</sub> NPs, the modified TiO<sub>2</sub> NPs show the presence of AKD features in their structure. The double bond carbon-carbon stretching vibration absorption peak at 1708 cm<sup>-1</sup> relates to the absorption band characteristic peak 1846 and 1633 cm<sup>-1</sup> in the spectrum of AKD, which usually correspond to C=O and C=C [20]. However, the OH frequency absorption band was absent in the modified TiO<sub>2</sub> NPs, suggesting the dehydration of water molecules in the complexes. The appearance of double bond carbon stretching at 1708 cm<sup>-1</sup> is very weak (almost not existing). This indicates that the functional group is very symmetrical but does not imply that the functional group is absent [20].

The adsorption bands at 2849 and 2916 cm<sup>-1</sup> of the modified TiO<sub>2</sub> NPs are from –CH<sub>2</sub>– symmetric and asymmetric stretching vibration [20], [142]. Therefore, the spectra of the modified TiO<sub>2</sub> NPs with AKD show that new absorption bands are present, evidence of new chemical bonds formed through modification. There is a reaction and connection between the TiO<sub>2</sub> NPs and AKD.

The FT-IR spectrum of ASA is shown in Figure 4.16c. The spectrum peaks for ASA arising from anhydride carbonyl stretching were identified at 1778 cm<sup>-1</sup> and 1863 cm<sup>-1</sup>, which correspond with the literature. The 1778 cm<sup>-1</sup> represents the stretching vibration of (C=O), which conforms with 1785 ± 5 cm<sup>-1</sup>. At 916 cm<sup>-1</sup>, the stretching vibration band of five-membered cyclic anhydrides (succinic anhydride) is identified. In Figure 4.16d, which characterizes the modified TiO<sub>2</sub> NPs with ASA, there is an absence of succinic anhydride grouping (1778 cm<sup>-1</sup> and 1863 cm<sup>-1</sup>). This is due to the hydrolysis of the anhydride, which results in the appearance of a band at 1689 cm<sup>-1</sup>. The band corresponds to the stretching vibration of the C=O bond [20], [143]–[145]. The absence of the bands at 1863 to 1778 cm<sup>-1</sup>

<sup>1</sup>indicates that the composite is free of an un-reacted modifier (ASA). The adsorption bands at 2849 and 2919  $\text{cm}^{-1}$  of the modified  $\text{TiO}_2$  NPs are also from  $-\text{CH}_2-$  symmetric and asymmetric stretching vibration [142]. Figure 4.16d demonstrates that new adsorption bands and chemical bonds are formed after modification. The signatures shows the presence of both ASA and rutile- $\text{TiO}_2$ , confirming the success of the modification process.



**Figure 4.16:** FT- IR Spectra; (a) pure AKD (b) AKD surface-modified rutile- $\text{TiO}_2$  NPs (c) pure ASA (d) ASA surface-modified rutile- $\text{TiO}_2$  NPs.

#### 4.5.1.2 Moisture Absorption Characteristics of the Surface Modified Rutile-TiO<sub>2</sub> Nanoparticles

Each sample of the surface-modified TiO<sub>2</sub> NPs, including the unmodified, was weighed using an analytical weigh balance. 10 ml of distilled water was dropped in each piece and left exposed to air for three (3) days. The experiment was triplicated, and the average values and the error deviations are summarized with initial sample mass of 500 mg as in Table 4.4.

**Table 4.4:** Change in mass due to absorbed moisture.

Sample	Average triplicated sample mass after 3 days exposure to moisture	Mass change (%)
T(unmodified)	519.40 ± 0.46	3.88 ± 0.09
A (5%ASA)	494.40 ± 0.62	-1.12± 0.12
B(3%ASA)	497.00 ± 0.36	-0.60± 0.07
C(1%ASA)	497.70 ± 0.70	-0.46± 0.14
X(5%AKD)	486.70 ± 0.20	-2.66± 0.04
Y(3%AKD)	492.30 ± 0.44	-1.54± 0.09
Z(1%AKD)	494.00 ± 0.30	-1.20± 0.06

After being exposed to air, the unmodified rutile-TiO<sub>2</sub> NPs (sample “T”) absorbed moisture and had a weight increase of 3.88%. In contrast, the modified samples generally lost weight by releasing water into the atmosphere. These results demonstrate the hydrophilic nature of TiO<sub>2</sub> and the effect of sizing agents on reducing the hydrophilicity behaviour of TiO<sub>2</sub>. The hydrophilic rutile-TiO<sub>2</sub> nanoparticles were therefore successfully converted into being hydrophobic by surface modification. Another method of water affinity characterization of the nanoparticles is presented in the next section.

#### 4.5.1.3 Thermal Stress Induced Weight Loss of Surface Modified rutile-TiO<sub>2</sub> Nanoparticles

To determine thermal stress induced weight loss characteristics, 300 mg portion of each sample were measured separately and placed in a furnace. The furnace temperature was set to ramp up to 400°C in 20 minutes and then stayed constant for 40 minutes. The samples

were then placed in a desiccator with silica gel to avoid moisture absorption as the samples cooled off. Analytical weight balance was used to measure each sample mass change. This experiment was triplicated, and Table 4.5 shows the average value of each case's weight loss and error deviation. Note, the initial sample mass was 300 mg.

**Table 4.5:** Weight loss analysis of surface-modified rutile-TiO<sub>2</sub> NPs under thermal stress.

Sample	Average triplicated sample mass after 3 days	Weight loss (%)
T(unmodified)	298.80 ± 0.78	0.40 ± 0.26
A (5% ASA)	293.00 ± 0.50	2.33 ± 0.17
B(3% ASA)	292.30 ± 0.61	2.57 ± 0.21
C(1% ASA)	291.50 ± 0.50	2.83 ± 0.17
X(5% AKD)	295.60 ± 0.53	1.47 ± 0.18
Y(3% AKD)	296.70 ± 0.20	1.10 ± 0.07
Z(1% AKD)	297.20 ± 0.36	0.93 ± 0.12

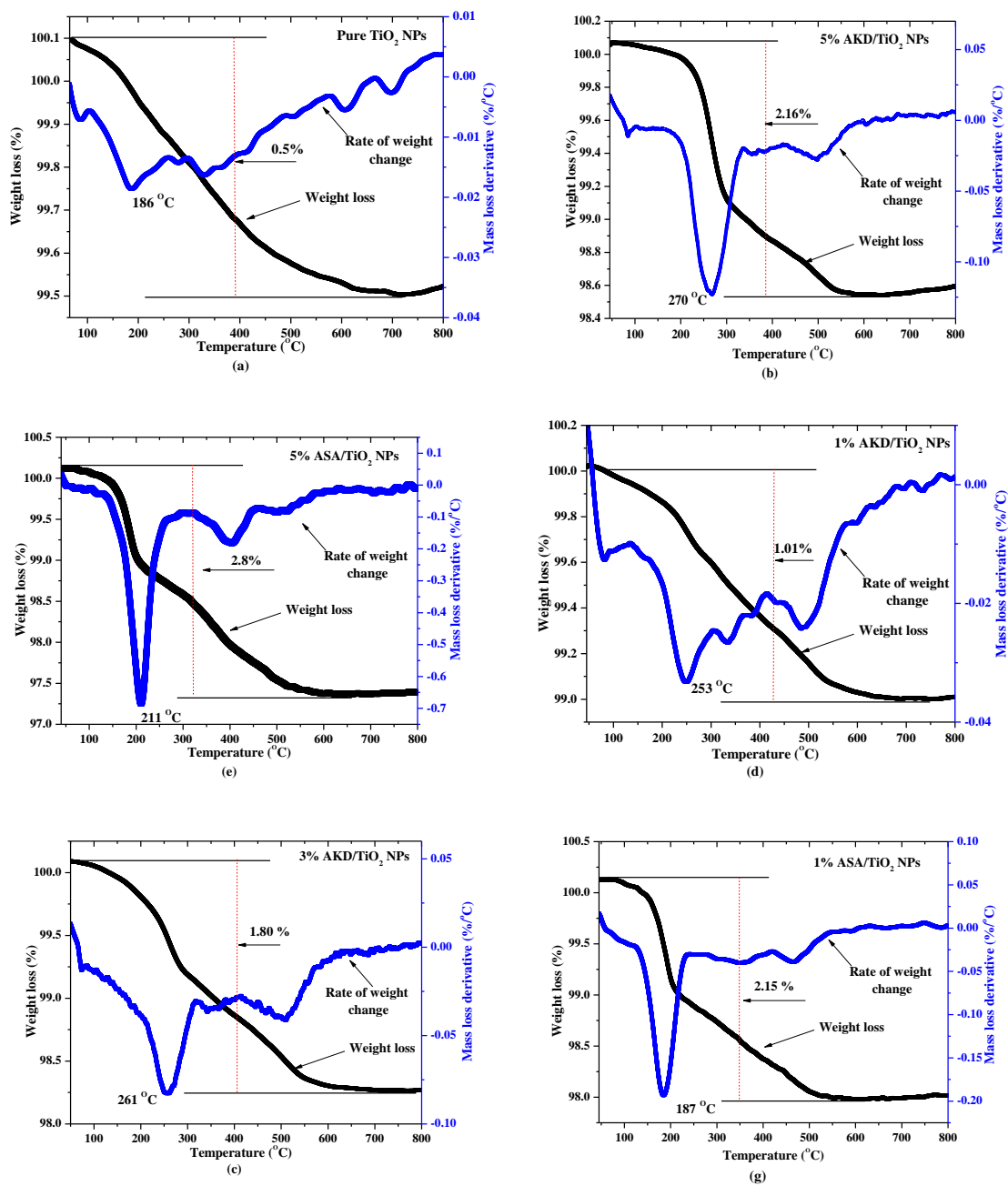
From the table, the surface-modified samples lost more weight than the unmodified samples, and the amount lost is directly proportional to the percentage content of the sizing agent applied to each sample. The weight loss of the composites can be attributed to the breakage or disintegration of the bond between organic and inorganic compounds [146]. This indicates that the modified samples contain more than one compound. In essence, the weight loss under heating is predominated by the decomposition of the surfactants. This phenomenon is further confirmed in the thermogravimetric analysis presented in the next section.

#### 4.5.1.4 Thermogravimetric Analysis (TGA) of the Surface-Modified Rutile-TiO<sub>2</sub> Nanoparticles

Perkin Elmer STA 4000 analyzer was used to study thermal stability of the nanoparticles. A constant flow rate of 10 mL/min and sample mass (10 mg) were maintained in all investigations to reduce the error. The instrument temperature was set at 900°C at a rate of 10 °C/min in a controlled environment. The TGA data profile was come with the derivative curve (DTG) to determine the oxidation and decomposition temperature.

The thermogravimetric analysis (TGA) of the samples was conducted under nitrogen gas. From the graph of pure TiO<sub>2</sub> NPs (Figure 4.17a page 52), a rapid loss of moisture occurred

between 75-90°C, followed by a significant degradation at about 186°C, which is attributed to the decomposition of the TiO<sub>2</sub> [20], [147], [148]. The initial steep gradient (representing a rapid loss of moisture) and the subsequent steep depression on the graph further confirm the results obtained in Table 4.3 about moisture absorption of the unmodified sample. As for the 5% AKD modified rutile-TiO<sub>2</sub> NPs, there is drastic thermal decomposition at 270°C, which is about 45% higher than that of pure rutile-TiO<sub>2</sub> NPs. For the reduced AKD content of 3%, the decomposition of modified rutile-TiO<sub>2</sub> NPs occurs at a lower temperature of 261°C, which is about 40% higher than that of the pure rutile-TiO<sub>2</sub> NPs. A further reduction of the AKD to 1% resulted in the modified rutile-TiO<sub>2</sub> NPs decomposing drastically at 253°C, which is about 36% higher than that of pure rutile-TiO<sub>2</sub> NPs. For AKD, in all cases of surface medication of rutile-TiO<sub>2</sub> NPs, there is increased thermal stability of at least 36%. In the case of ASA-modified NPs, the temperature at which the modified NPs drastically decomposed were 211°C, 194°C, and 187°C for 5%, 3% and 1% ASA content, respectively. Notably, for all cases of ASA modification, the temperature at which drastic decomposition occurred was lower than the least % AKD content modified sample. This shows that AKD-modified samples are more thermally stable than the ASA. However, the ASA-modified samples show improvement in thermal stability except for 1% content, whose thermal stability is the same as that of the pure rutile-TiO<sub>2</sub> NPs. Table 4.6 (page 53) summarizes the effects of surfactant content and type on the thermal stability of the resultant modified samples.



**Figure 4.17:** Thermogravimetric Analysis of the nanoparticles (TGA) graph; (a) pure TiO<sub>2</sub> NPs (b) 5% AKD/TiO<sub>2</sub> NPs (c) 3% AKD/TiO<sub>2</sub> NPs (d) 1% AKD/TiO<sub>2</sub> NPs (e) 5% ASA/TiO<sub>2</sub> NPs (f) 3% ASA/TiO<sub>2</sub> NPs (g) 1% ASA/TiO<sub>2</sub> NPs.

**Table 4.6:** Effects of surfactant content and type on thermal stability.

Sample	The temperature at which drastic decomposition occurred (°C)	The difference in temperature to the pure rutile-TiO <sub>2</sub> NPs (%)
T(unmodified)	186	0
A (5%AKD)	270	45.2
B(3%AKD)	261	40.3
C(1%AKD)	253	36.0
X(5%ASA)	211	13.4
Y(3%ASA)	194	4.3
Z(1%ASA)	187	0.5

The decomposition of the modified rutile-TiO<sub>2</sub> NPs samples at higher temperatures is attributable to improved heat resistance associated with the long-chain organic compounds from surfactants [117], [145], [149], [150]. Both cases of the modified TiO<sub>2</sub> NPs show that the modified samples have better thermal stability than pure rutile-TiO<sub>2</sub> NPs. The thermal resistance of the surface modified rutile-TiO<sub>2</sub> nanoparticles is major improvement recorded in the present research.

#### 4.6 Chapter Conclusion

This chapter has presented the successful synthesis, surface modification and characterization of rutile-TiO<sub>2</sub> nanoparticles. The sol-gel method of nanoparticles synthesis was used. Rutile-TiO<sub>2</sub> NPs of 19.72 nm in size were successfully fabricated and then surface-modified using sizing chemicals. The surface-modified rutile-TiO<sub>2</sub> NPs are less vulnerable to surrounding moisture/water and have higher thermal stability. The surface modification of rutile-TiO<sub>2</sub> NPs using the sizing chemicals is a novel approach to mitigate the hydrophilic characteristic associated with nanoparticles used for kraft paper insulation, and this is a major new knowledge contribution of this thesis. The next chapter presents the development of the nanocomposite kraft paper insulation.

# **Chapter 5: Fabrication and Characterization of Rutile-TiO<sub>2</sub> Nanocomposite Kraft Paper for Power Transformer Application**

## **5.1 Introduction**

The previous chapter discussed the synthesis and surface-modification of rutile-TiO<sub>2</sub> NPs. The surface-modified rutile-TiO<sub>2</sub> NPs exhibited better thermal and hydrophobic properties than the unmodified surface of TiO<sub>2</sub> NPs. The inherent hydrophilic characteristics of cellulose fibre and that of metal oxide NPs are regarded as a threat to the viability of nanocomposite kraft paper technology. This chapter presents the possibility of reducing the hydrophilicity associated with kraft paper insulation. The synthesized and surface-modified rutile-TiO<sub>2</sub> NPs are filled into unbleached kraft pulp to fabricate a nanocomposite kraft paper insulation. The findings in this chapter have been presented at a conference and also published in the scholarly knowledge domain.

## **5.2 Papermaking**

In papermaking, cotton, wood, and grass are the typical raw material used, and for special purposes, synthetic fibres are commonly used [33], [34], [151]. The process of making a paper involves the production of kraft pulp, refining and treatment of the pulp. Where necessary modification with chemicals is done, the pulp could be reinforced with filler or coated and finally cast using a handsheet former machine [151]–[153].

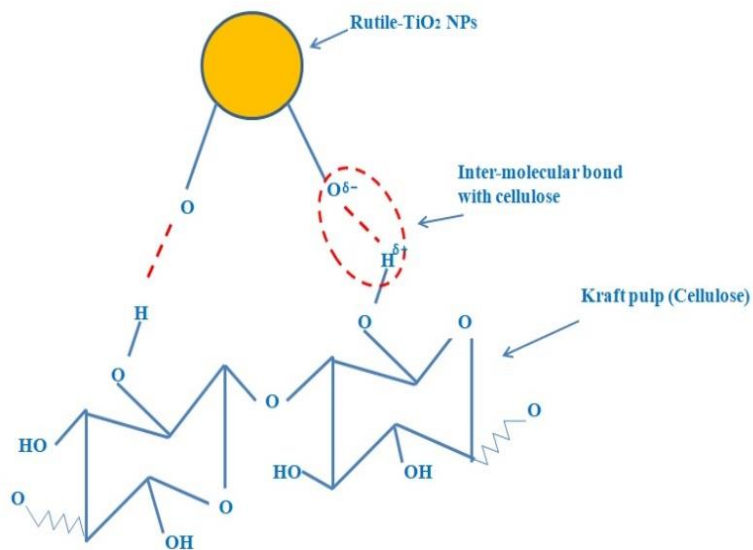
The characteristics of a kraft paper are better described as a ‘reconstituted wood’ [154]. Before 1719, kraft paper was made from disintegrated cotton rags. However, after observing the creative skill of an insect, using maceration of trees to build their nests, Antoine de Reamur suggested the same technique for papermaking [154], [155]. Kraft paper consists of cellulose, hemicellulose and lignin; all these fibre constituents are a buildup of a living plant. Cellulose is the major constituent of the wood fibre used in forming paper; the cellulose fibre is detached from the wood by chemical or mechanical means. The fibre is then dissolved in

water and sprained. The water absorption characteristics of the cellulose wood fibre lead to fibre contraction, forming hydrogen bonds between the separate fibres. This mechanism forms a matrix referred to as paper. The final properties and the nature of the fabricated kraft paper depend on the species of the plant used, and the chemical and mechanical treatment of the pulp [154]–[156]. The following section presents the bonding of the nanocomposites kraft paper insulation.

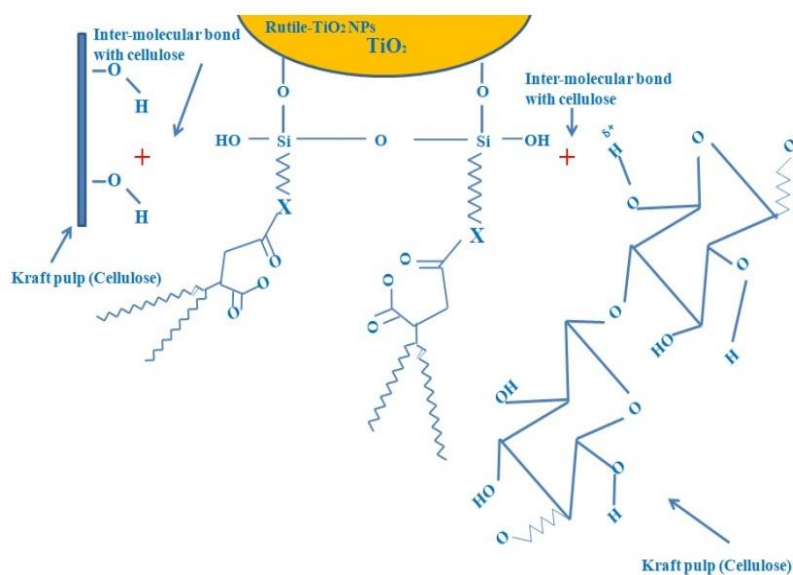
### **5.3 Bonding and Structural Mechanism of the Fabricated Nanocomposites Kraft Paper Insulation**

This section describes the bonding and structural mechanism between the cellulose, rutile-TiO<sub>2</sub> NPs and the surface modifying rutile-TiO<sub>2</sub> NPs.

Cellulose has an intrinsic affinity for self-adhesion, with a material containing hydroxyl groups (-OH). It forms inter-molecular and intra-molecular hydrogen bonds. For inter-molecular and intra-molecular bonding of cellulose, a hydrogen bond is formed between O<sup>-</sup> and H<sup>+</sup> [44], [157]–[160]. The interaction and bonding between the cellulose and the surface-modified rutile-TiO<sub>2</sub> NPs can be established because cellulose wood fibre is hydrophilic and can contain or attract water from surrounding moisture even under room temperature. These attracted molecules of water can react to hydrolyze the silane (the coupling chemical). According to Zhang *et al.* [142], the dioxygen complex nature of TiO<sub>2</sub> NP attracts H<sub>2</sub>O to complete its number of the crystal lattice. The rutile-TiO<sub>2</sub> NPs have surface oxygen vacancies which act as an active site in water absorption. During this process, the silane coupling agent's hydrolysable group (alkoxy) is activated, forming a reactive surfactant and setting free the alcohols. The hydrolyzed silane group (organic functional group) has a high affinity with one another and the organic functional group on the cellulose wood fibre, forming a fibre-filler-fibre bond. The amount of hydrolysable groups influences the bond between the silane, rutile-TiO<sub>2</sub> NPs and the cellulose fibre (kraft paper) [138], [142], [161], [162]. However, For the unmodified TiO<sub>2</sub> NPs, hydrogen bonds are formed between the oxygen atom and the hydrogen atom of the TiO<sub>2</sub> NPs and the cellulose [71]. The interactions between TiO<sub>2</sub> NPs with cellulose and surface-modified TiO<sub>2</sub> NPs with cellulose are shown in Figure 5.1a-c (page 56 and 57).



**Figure 5.1a:** Interaction mechanism of cellulose kraft paper with unmodified rutile-TiO<sub>2</sub> NPs.



**Figure 5.1b:** Interaction mechanism of cellulose kraft paper with surface modified rutile-TiO<sub>2</sub> NPs having ASA.



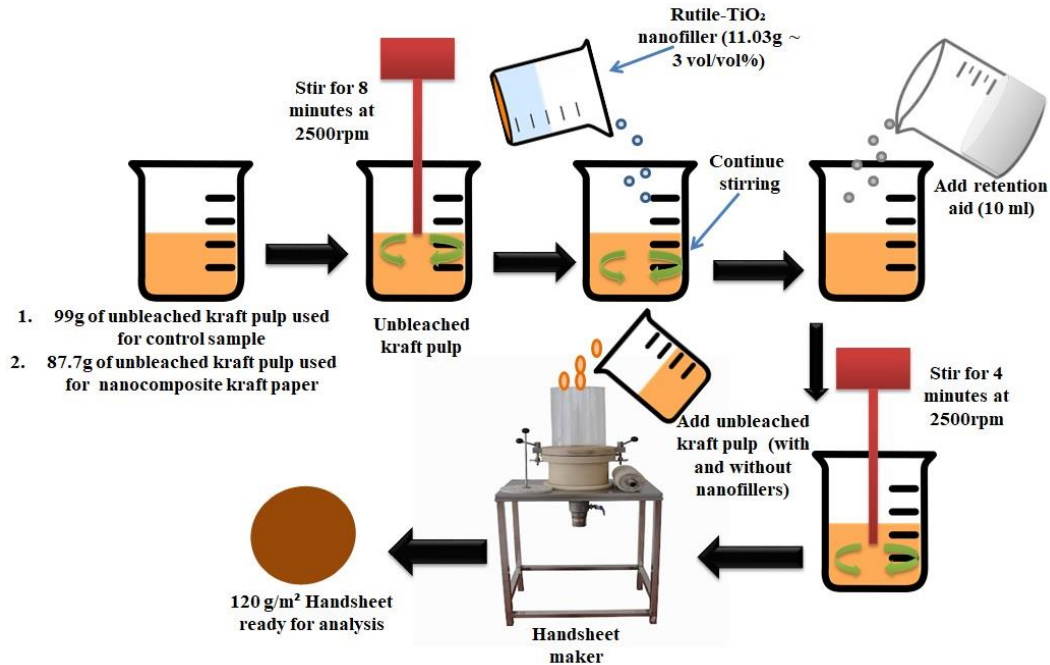
Electrical grade unbleached kraft pulp (wood pulp) is commonly used for power transformer insulation. It is produced in a controlled condition and environment (laboratory) using handsheet former machine for research and experimental purposes [72, ], [86], [92], [157]. Different paper insulation specimens are fabricated, including the reference (unfilled kraft paper) sample, nanocomposite kraft paper with unmodified rutile-TiO<sub>2</sub> NPs and surface-modified rutile-TiO<sub>2</sub> NP samples.

#### **5.4.1 Materials and Chemicals used to Fabricate the Kraft Paper Insulation**

The raw materials for the kraft paper fabrication process were electrical grade unbleached kraft pulp (unbleached sulphur) as supplied by Sappi™ Technology Centre (Pretoria, South Africa), distilled water, surface-modified rutile-TiO<sub>2</sub> nanoparticles (the nanoparticles were surface modified with AKD and ASA to condition the surface against water; refer to section 4.4. and 4.5 of chapter 4), and the filler retention aid; the retention aid was used to retain the nanofiller due to the particle size.

#### **5.4.2 Experimental Procedure for Fabricating the Kraft Paper Insulation**

The procedure involved two experiments: the fabrication of the control (reference/unfilled kraft paper) sample and the fabrication of samples filled with nanoparticles (with rutile-TiO<sub>2</sub> NPs). The procedure of the handsheet making complied with procedures in TAPPI T 205 [153]. The rutile-TiO<sub>2</sub> nanocomposite kraft paper was fabricated following the process illustrated in Figure 1. The same procedure was followed for the control (reference) sample but without adding the nanofillers and retention aid. Detailed experimental calculations and steps are presented in Appendix A of this thesis. Figure 5.2 of page 59 shows the process of the paper fabrication, while Figure A (Appendix A) presents some images taken at some stages of the process. The following section presents the characterization and results obtained from the kraft paper specimens.



**Figure 5.2:** Steps involved in fabricating the kraft paper insulation.

## 5.5 Fibre Characterization and Scanning Electron Microscope (SEM) Analysis of the Fabricated Kraft Paper Insulation

Characterization of the fibre in kraft paper reveals in detail the internal features of the fibres that make up the paper. The features such as fibre length, fines, coarseness and fibre wall thickness are best seen and analyzed by special machines having a microscopic lens. The fibres' characteristics of kraft paper insulation significantly influence the modified and unmodified kraft paper insulation performance.

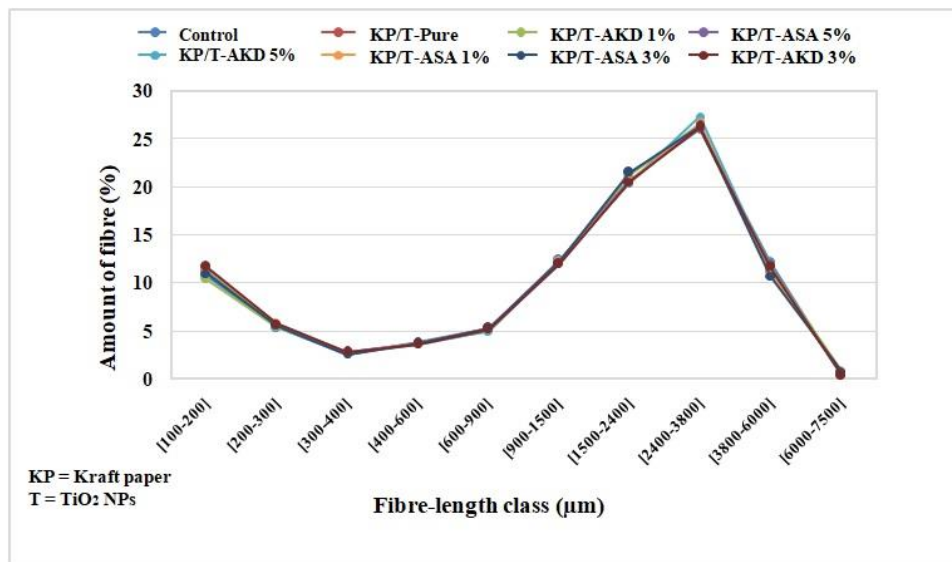
### 5.5.1 Fibre Analysis of the Fabricated Kraft Paper Insulation

The L&W FT+ tester was used to determine morphological characteristics of cellulose fibres and fine elements through size criteria. L&W FT+ (Code 912+) has different optics and uses a camera with higher resolution; these features allow for better measurement of small particles in the pulp, fines or macro fibrils. Up to six beakers containing disintegrated pulp samples can be placed on the sample-changer carousel. After a test is started with the software, the sample is drawn into the tester and diluted to the proper concentration for testing. The fibre suspension is pumped through a measuring cell, where it is photographed. The photographs are then

processed in an image-analysis program for further analysis [165]. The procedures involved in sample preparation and analysis using the L&W FT (Code 912+) are presented in Appendix B. The characteristics results of fibre length, fines, coarseness and fibre wall thickness of the kraft paper specimens are presented in the next subsections.

**Fibre Length:**

The results on the fibre length are plotted as shown in Figure 5.3. From the graph of the fibre length distribution, the fibre length of all the sampled specimens falls within the fibre length class of softwood. The fibre length analysis also shows that the nanofiller does not influence the fibre length. Unbleached softwood cellulose fibres have a length measured between 1.8 to 4 millimetres. These woods are more robust and have a longer length compared to hardwood. This makes it a preferred raw material for fabricating kraft paper insulation for power transformers [34], [37]–[39], [166]–[168].

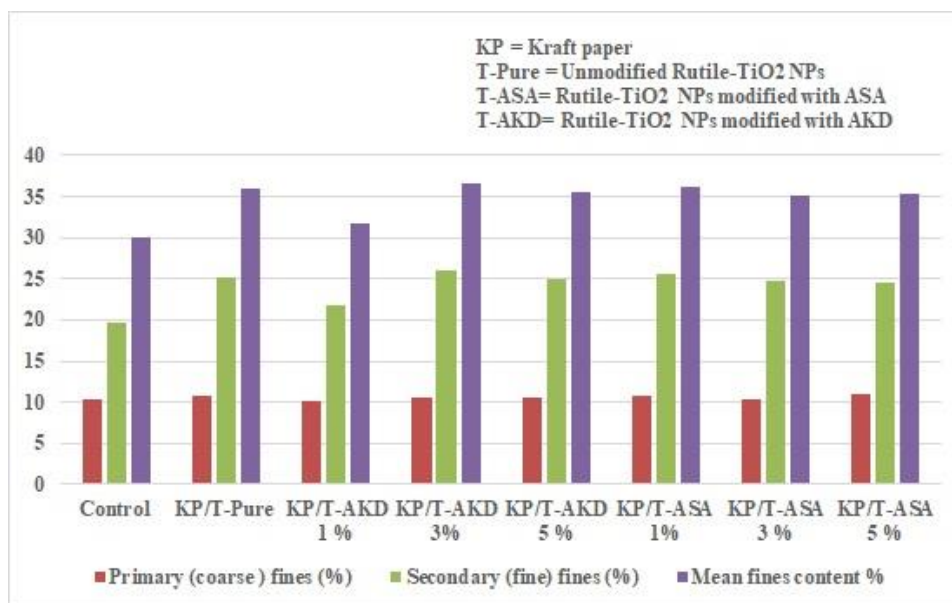


**Figure 5.3:** Graphical representation of the fibre length constituents in the various specimens.

**Fines:**

Fines are detached fibrils from the fibre [38], [169]. They are the smallest component of the fibre and are defined as particles that can pass through a 200 mesh screen with a hole diameter of 76 µm [170], [171]. Fines are of two types; the primary fines which are produced

during pulping and bleaching, and the secondary fines are generated during refining of pulp which is a mechanical process. Primary fines comprise less than 2% of the entire fines content, the rest secondary fines [38]. Concerning Figure 5.4, the percentages of secondary fines content are approximately twice that of the primary, which conforms with the literature [38]. Compared to other samples, the control (unfilled) sample has less fines content. This could be due to the filler retention aid added to the other samples containing nanofillers. Fines increase the bond between fibre by filling the voids during the dewatering. The fibre-fibre interaction increases the sheet density, resulting in an increase in tensile strength. [34], [38], [172]–[175].

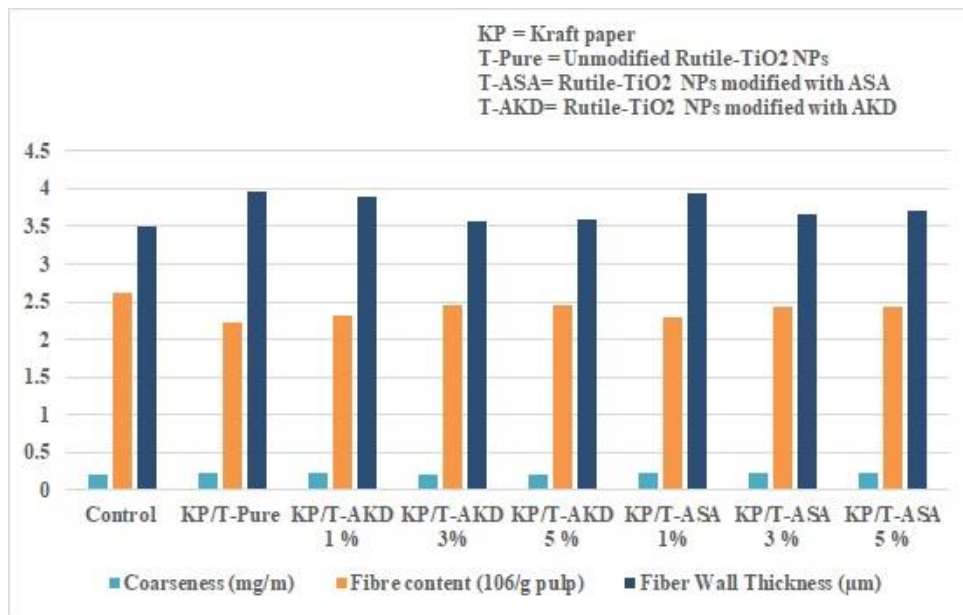


**Figure 5.4:** A graph representing fines in different test specimens of the kraft paper.

### Coarseness and Wall thickness

The coarseness of a fibre is the measure of its mass per unit length. A handsheet with a high coarseness value affects its ability to form strong fibre bonds [176]. Such fibre forms weaker fibre links that can easily be broken under stress [34], [176]. Concerning Figure 5.5, the coarseness is directly proportional to the fibre wall thickness and inversely proportional to fibre content (refer to table B1 of Appendix B). Although there is not much difference in coarseness because the same pulp was used throughout, the reinforced handsheets were slightly coarser than the pure sample sheet. Since coarser fibre has thicker walls, they are

bulkier with a more open fibre network resulting in more porous sheets [174]. The wall thickness of a fibre influences the paper's strength. The fibre wall thickness controls the bonding potential of the kraft paper [34]. Thick walls are known to contain fewer fibre per volume, as depicted in Figure 5.5 (refer to table B 1 of Appendix B) [38]. The tensile strength of a paper is affected by its wall thickness. From the specimen analysis, the wall thickness of all the samples falls within the same range; however, the control sample has a smaller thickness [174], [176]–[179].



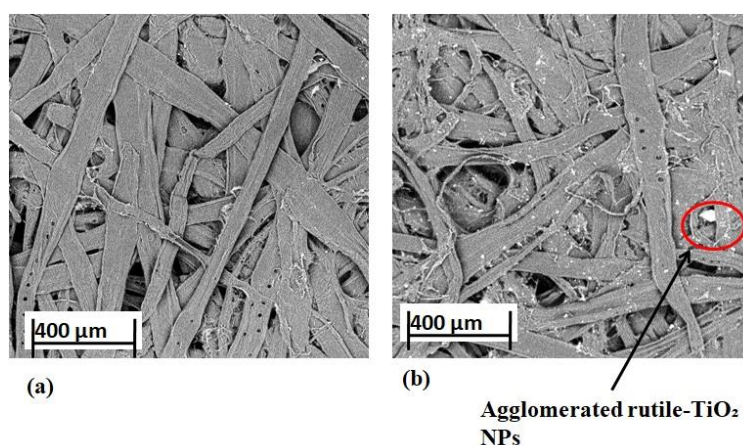
**Figure 5.5:** A graph representing coarseness, fibre content and the wall thickness of the kraft paper developed in this thesis work.

### 5.5.2 Scanning Electron Microscope (SEM) Analysis of the Fabricated Kraft Paper Insulation

The Phenom ProX SEM is a high-resolution desktop imaging tool that combines an optical camera and a scanning electron microscope for detailed imaging of various samples. Custom software allows analysis of fibres and particles, as well as elemental analysis and particle size distribution analysis. The equipment consists of the Phenom microscope ProX with rotary knob; flat panel monitor and mouse; Pre-vacuum pump; Power supply; ProX hard drive with application system software, flat panel monitor and mouse. The steps involved in sample preparation and visualization with an optical/electron microscope of the kraft paper specimen

are detailed in Appendix C. The images obtained from the fibre examination of the samples are presented.

The images of Figure 5.6 are for the paper sheet with and without nanoparticles. The handsheet without nanoparticles is represented in Figure 5.6a; no trace of nanoparticles within the fibre web. Figure 5.6b shows a more even distribution of the nanoparticles within the fibre matrix with small trace of agglomeration. The images of the selected handsheets depict the general footprint of the rest sheets. The distribution of the nanoparticles influences the final properties of the kraft paper.

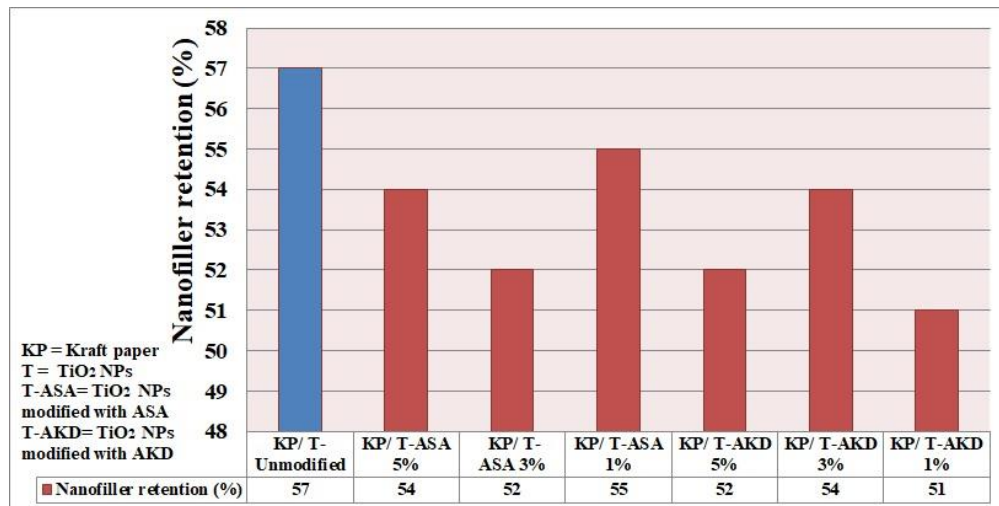


**Figure 5.6:** Surface morphology of the handsheets (a) without nanofiller (b) with nanofiller uniformly distributed with trace of agglomerated nanoparticles.

### 5.5.3 Percentage of Filler Retention (Rutile-TiO<sub>2</sub> NPs) in the Nanocomposite Kraft Paper

Nanofiller retention is the amount of filler content in the composite kraft paper retained in the manufacturing process [180]. The nano-filler retained in the sheets was determined using the ash content method, in compliance with the procedures in International Standard ISO 2144:1997(E) [181]. A muffle furnace set at 900 °C was used to determine the ash content. The samples were weighed before and after heating using the analytical weigh balance. Figure 5.7 depicts the quantity of nanofillers that were retained. At least half of the nanofillers are retained in all the samples within the kraft paper reinforced with surface-modified TiO<sub>2</sub> NPs and the unmodified rutile-TiO<sub>2</sub> NPs. The kraft paper reinforced with unmodified nanoparticles has the highest retention of 57%.

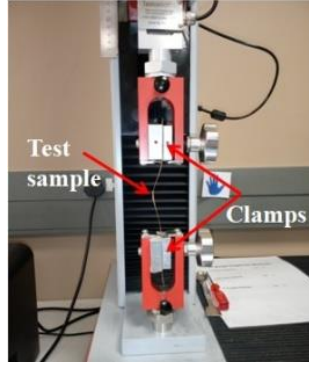
The retention of the nanofillers is an indication of fibre-filler-fibre bond being formed between the cellulose fibre and the nanofillers; the bonding is enhanced by the retention aid. The significance of the modification and the resultant performance of the nanocomposite kraft paper depends on the amount of the nanofiller retained within the fibre web. Since on average 50% of the initial nanofiller loading was retained, this translates to percentage loading of about 1.5wt%. This optimal nanoloading is consistent with the literature.



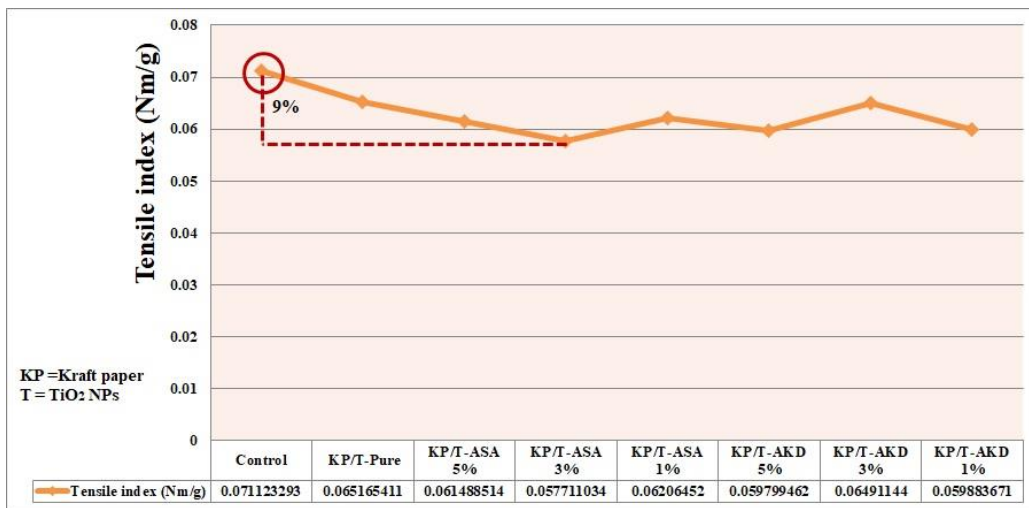
**Figure 5.7:** Percentage of nanofiller particles retained in the rutile-TiO<sub>2</sub> nanocomposite kraft paper.

#### 5.5.4 Tensile Strength of the Fabricated Kraft Paper Insulation

The tensile strength is an indicator of the mechanical property of the kraft paper insulation. It reveals the extent of the structural bonding. The tensile strength test is done by stretching out the paper specimen. A steady pulling force at 10 mm/min speed was applied until the kraft paper insulation mechanically broke. All tests were done using Testometric (TC.PT.003) tensile machine. Tensile strength of the paper sheets were measured in according with the ISO 1924-2 standards [182]. Figure 5.8 shows the image of a failed clamped strip of one sample kraft paper, while the results on the tensile index are plotted in Figure 5.9.



**Figure 5.8:** Image of mechanically failed sample strip.



**Figure 5.9:** Tensile strength of the fabricated kraft paper samples.

From Figure 5.9, it is evident that the control sample has highest tensile strength compared to all versions of the nanocomposite kraft paper specimens. The difference in tensile strength of the modified and unmodified kraft paper is about 9%. In the work of Liao *et al.* [71], the tensile strength of oil-impregnated paper reinforced with TiO<sub>2</sub> NPs decreased by 3%. Yuan and Liao [89], also recorded a decrease of about 12% in tensile strength when montmorillontine was used to modify transformer insulation paper. However, Tang *et al.* [91] reported that the tensile strength of aramid insulation paper reinforced with SiO<sub>2</sub> NPs increased by 8% at 1 wt% of nanofiller loading and declined as the percentage content increases. The variation in the tensile strengths could possibly be due to the influence of nanofiller and agglomeration. According to El Omari et al [183], nanoparticle dispersion and

agglomeration affects fibre sheet interaction resulting to decrease in mechanical property of the composite kraft paper. Tensile strength in kraft paper insulation is related to its degree of polymerization (DP of a kraft paper is defined on page 9 of this thesis).

The need to measure the tensile strength of oil-impregnated might be perceived as less significant in the design of the electrical winding of the power transformer. However, The hydrogen bond of cellulose fibres are form between the hydroxyl (OH) of glucose links, which contributes to the tensile strength of the kraft paper. To this regard, the DP of a kraft paper which is the number of glucose chain that forms cellulose can be measured by its tensile strength [184]. It is important to note that the measure of DP is difficult and costly therefore, tensile strength is often used to measure the remaining life of oil-impregnated paper [185]. If the tensile strength drops to 20% of the initial value, DP is reduced to approximately 200; this defines the end of life of the oil-impregnated paper [184]–[186].

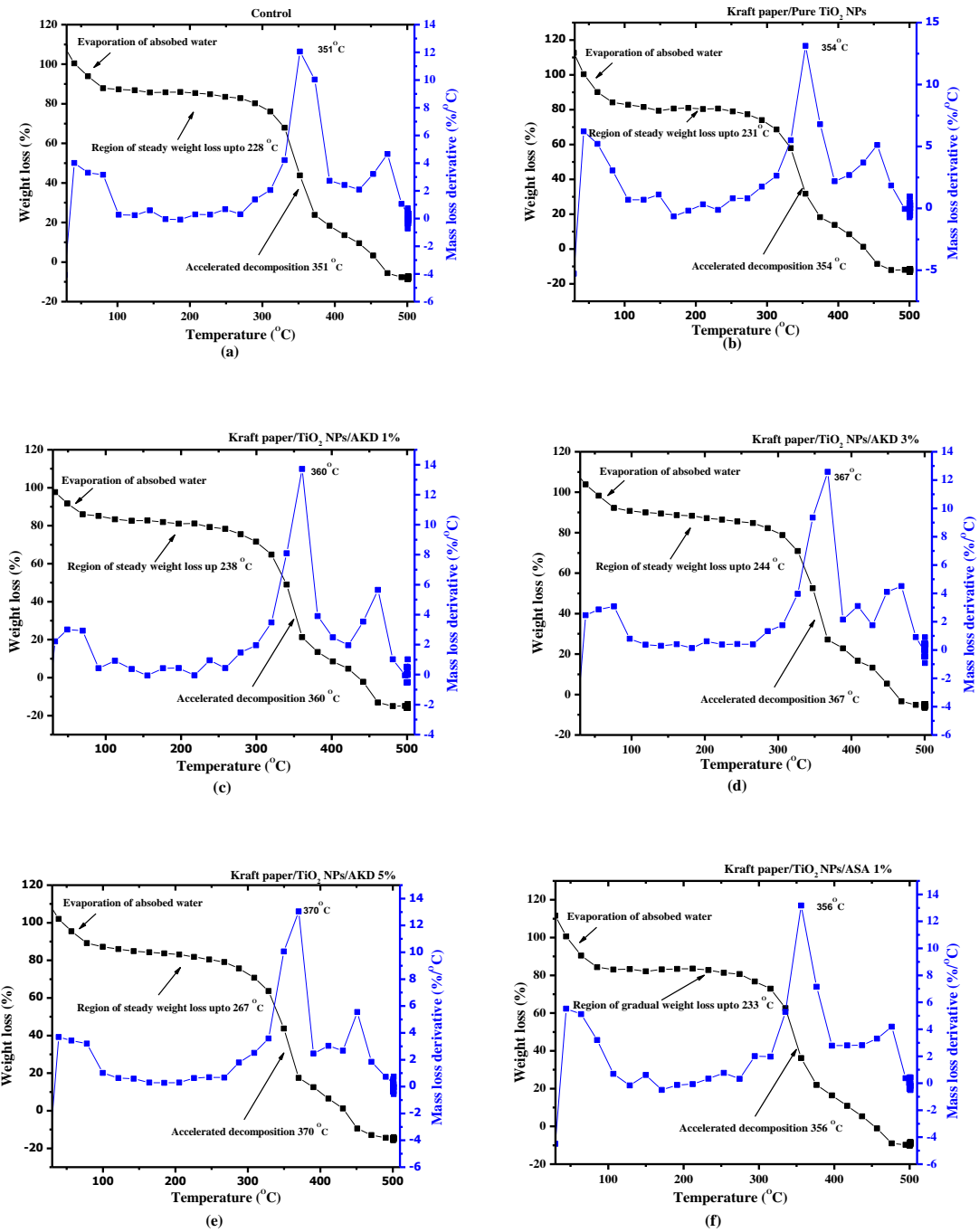
*Tensile strength mainly decreases with ageing which in turn is mostly influenced by moisture content in the kraft paper. Although the designed nanocomposite kraft paper showed 9% less tensile strength as depicted in Figure 5.9, this initial value however is not expected to deteriorate the kraft paper significantly due to ageing because it has better performance in moisture. Meanwhile, the longtime ageing effect of the nanocomposite kraft paper need to be pursued as future research work.*

### **5.5.5 Thermal Stability of the Fabricated Kraft Paper Insulation**

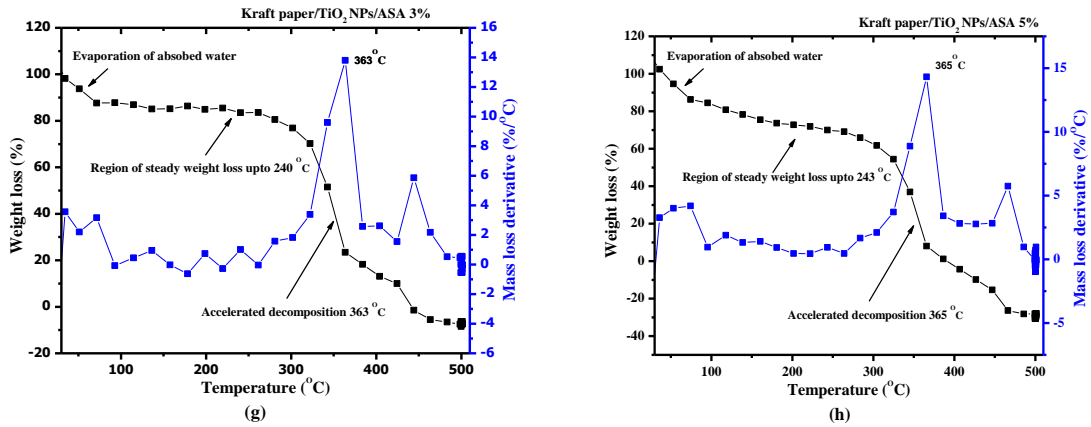
A thermogravimetric analyser (TGA701, LECO Corp. USA) was used to study the thermal stability of the samples. Temperature rise in power transformer is a threat to its insulation therefore, the measure of TGA will reveal the thermal withstand of the fabricated kraft papers. 10 mg of each sample of the kraft paper insulation were weighed and placed in ceramic crucibles. The temperature was set to ramp from 20 °C to 900 °C. The thermogravimetric graph of the control sample (unfilled), kraft paper filled with unmodified rutile-TiO<sub>2</sub> NPs and kraft paper having surfaced modified rutile-TiO<sub>2</sub> NPs are presented in Figure 5.10.

With reference to the TGA graphs (in Figure 5.10), the first sharp slope on each curve indicates the release (removal) of absorbed water. Then the region of steady weight loss; at this stage, a gradual thermal depolarization is seen. The kraft paper filled with modified rutile-TiO<sub>2</sub> NPs/5% AKD takes about 267 °C to give up its thermal strength, and at 370 °C maximum thermal decompositions was obvious. Compared with the control sample (unfilled), the kraft paper filled with rutile-TiO<sub>2</sub> NPs/5% AKD is 5.4% more thermally stable.

The sizing chemicals used in this thesis to surface modify the rutile- TiO<sub>2</sub> NPs are described in literatures to have high thermal resistance. This attribute is due to their characteristic long organic chain length, resulting to a stronger van-der-waals interactions among the bonds. Moreso, TiO<sub>2</sub> NPs especially the rutile phase are known to have higer thermal resistance compare to other nano-metalic fillers [20], [149], [187]–[190]. As such, the fabricated nanocompiste kraft paper exhibits higher thermal resistance than the unmodified kraft paper insulation Table 5.1 of page 69 presents the thermal stability of the fabricated kraft paper samples from the TGA results.



**Figure 5.10:** TGA of the sample papers (a) control sample, (b) kraft paper with unmodified NPs, (c) kraft paper filled with rutile-TiO<sub>2</sub>/AKD1%, (d) kraft paper filled with rutile-TiO<sub>2</sub>/AKD3%, (e) kraft paper filled with rutile-TiO<sub>2</sub>/AKD5%, (f) kraft paper filled with rutile-TiO<sub>2</sub>/ASA1%.



**Figure 5.10:** cont.’ (g) kraft paper filled with rutile-TiO<sub>2</sub>/ASA3% and (h) kraft paper filled with rutile-TiO<sub>2</sub>/ASA5% .

**Table 5.1:** Thermal stability of the fabricated kraft paper samples.

Sample	The temperature at which drastic decomposition occurred (°C)	The difference in temperature to the control (unfilled) kraft paper specimen (in %)
Samaple A (Control)	351	0
Sample B (Rutile) Kraft paper	354	0.9
Sample C (Rutile/1% AKD) Kraft paper	360	2.6
Sample D (Rutile/3% AKD) Kraft paper	367	4.6
Sample D (Rutile/5% AKD) Kraft paper	370	5.4
Sample E (Rutile/1% ASA) Kraft paper	356	1.4
Sample F (Rutile/3% ASA) Kraft paper	363	3.4
Sample G (Rutile/5% ASA) Kraft paper	365	3.9

Oxidation, hydrolysis and pyrolysis mechanisms in power transformer all depend on temperature rise and affects the insulation as shown in Figure 1.2 of chapter 1. The 5.4% increase in thermal resistance entails that the fabricated nanocomposite kraft will withstand more stress induced by thermal reaction than the unfilled kraft paper before degrading.

*It can be argued that with the 5.4% increase in thermal resilience, the loading of power transformers can be increased in order of 5%. This translates into significant savings in power transformer assets investment. In this regard, this present reseach work has successfully upgraded the thermal withstand capabilities of kraft paper using nanofiller and surfactants for power transformer application. This work has also presented an alternative*

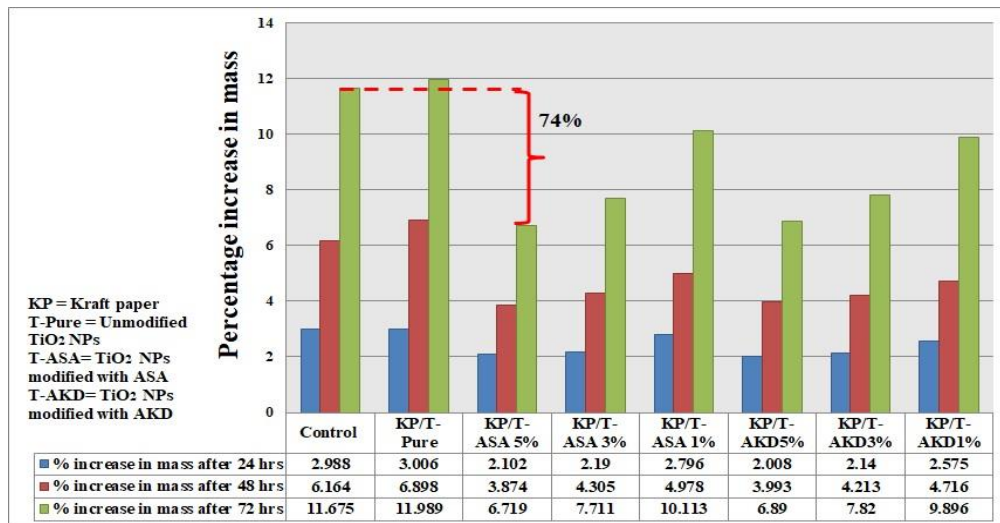
technique of producing thermally upgraded insulation materials. The following section presents the tests on moisture and water absorption characteristics of the fabricated kraft paper.

### 5.5.6 Hydrophilicity Test on the Fabricated Kraft Paper Specimens

The vulnerability of the fabricated kraft paper specimens to surrounding moisture and the rate of water absorption is tested. The next subsections presents the experimental test procedure and the results.

#### Moisture Absorption Test:

The fabricated kraft paper specimens were exposed to humid atmospheric air for 72 hours. The atmospheric conditions were temperature and relative humidity were respectively  $23 \pm 3^\circ\text{C}$  and  $53 \pm 5\%$ . At least three specimens of each specimen type were tested. The samples were cured (dried) in a laboratory oven at  $105^\circ\text{C}$  for 20 minutes and weighed. They were then exposed to the atmospheric air for 72 hours after which they were weighed again. This approach to measuring moisture absorption characteristics of kraft paper has also been used by other researchers such as; Gasser *et al.* [191], Cigre Working Group A2.30 [47] and Koch [192]. Figure 5.11 represents the percentage increase in mass due to moisture absorption.



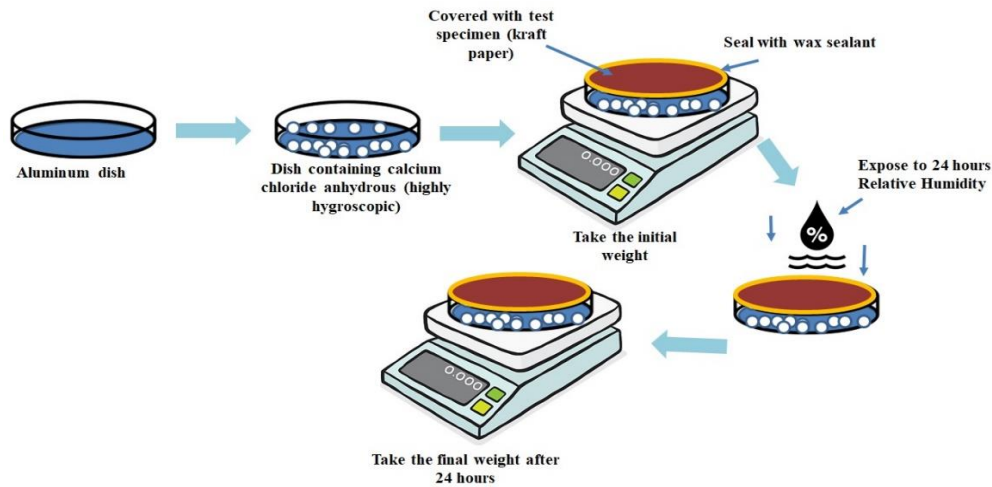
**Figure 5.11:** Percentage increase in mass due to absorbed moisture of the fabricated kraft paper samples.

The results show significant increase in mass in all samples due to the absorbed moisture. However, the reference (unfilled) and the nanocomposite kraft paper filled with unmodified rutile-TiO<sub>2</sub> NPs specimens show a significantly higher percentage increase in mass than the rest of the samples. Specimens filled with AKD surface-modified nanofiller show more hydrophilic properties than those with nanoparticles modified with ASA. After 72 hours, the kraft paper specimens filled with surface-modified rutile-TiO<sub>2</sub> NPs (KP/T-ASA5%) absorbed the least moisture; about 74% less than the unfilled paper.

*The vulnerability of cellulose insulation to surrounding moisture has been reduced by distributing the surface modified hydrophobic nanofillers within the fibre of kraft paper. This outcome infers that if the nanocomposite kraft paper is used for transformer insulation winding, the moisture absorption and moisture ingress on the kraft paper will significantly be reduced. This research work has therefore successfully fabricated a nanocomposite kraft paper with hydrophobic characteristic for improved power transformer insulation design possibilities.*

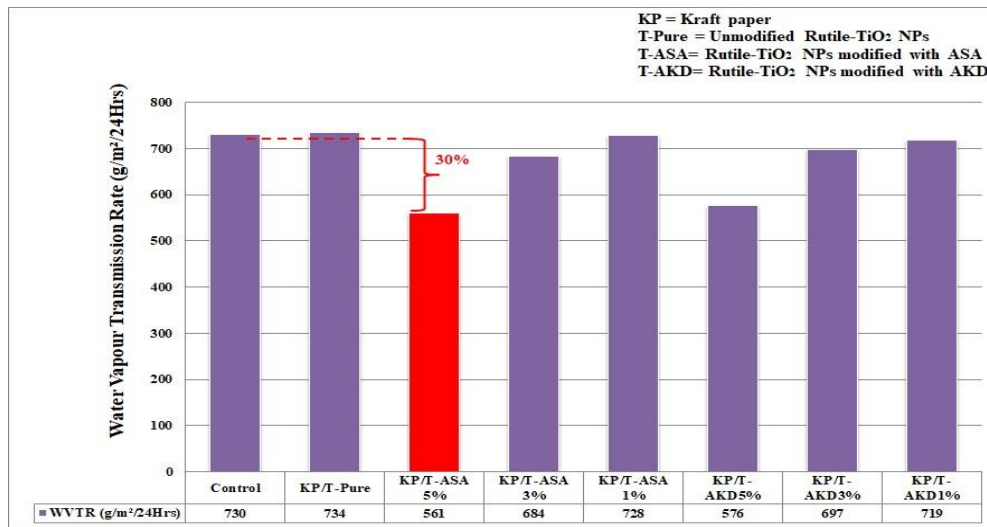
### Water Vapour Transmission Rate (MVTR):

The water vapour transmission rate (WVTR) of the kraft paper specimens were measured following the ISO 2528 standard procedure [193], and the conditions were as specified in ISO 187 [194]. The experimental process is illustrated in Figure 5.12 and Figure 5.13 presents the results. The practical detail of the test is explained in Appendix D.



**Figure 5.12:** Experimental setup and process of water vapor transmission rate test.

Figure 5.13 presents the results of the WVTR of the samples, and each bar is an average of three measurements on each specimen. The nanocomposite kraft paper filled with unmodified rutile-TiO<sub>2</sub> has the highest transmission rate. Nanocomposite kraft paper filled with modified rutile-TiO<sub>2</sub> with ASA has about 30% less transmission rate than the unfilled kraft paper specimen. The kraft paper filled with 5 vol/vol% ASA surface-modified TiO<sub>2</sub> nanoparticles proves to scale down moisture absorption tendencies of kraft paper. The long-term sustainability of the effects, however need to be further investigated. There is a possibility that the characteristics of the surfactant chemicals could change over time [137], [195]–[197].



**Figure 5.13:** Water Vapour Transmission Rate (WVTR) of the kraft paper specimens.

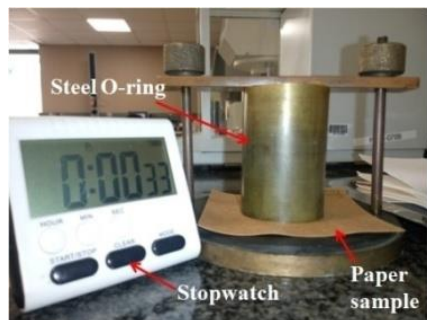
In addition to moisture absorption and transmission characteristics, the rate at which water droplets (deposited onto the kraft paper surface) are absorbed into the kraft paper is an important characteristic.

*The WVTR further confirmed that the fabricated nanocomposite kraft paper filled with surface modified nanofiller are less hygroscopic to the surrounding moisture. The next subsection presents the water cobb test and contact angle.*

### Water Cobb Test:

The Cobb test measures the quantity of water absorbed by a paper specimen. For the experiment, three test determinations were carried out. The experimental procedures were in

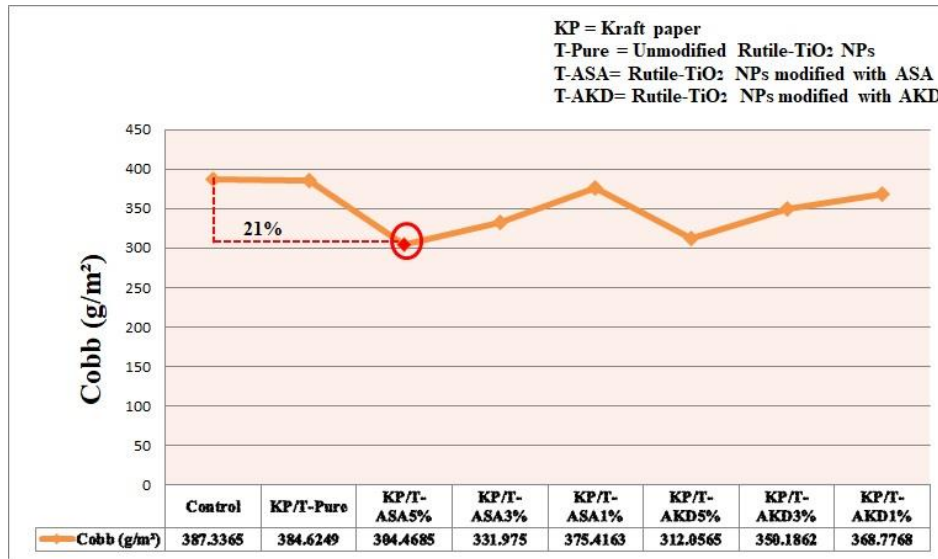
accordance with ISO 535 [25], and all samples were preconditioned and conditioned in accordance with ISO 187. Figure 5.14 shows the image of the test setup. A detailed explanation of the test setup is presented in appendix D.



**Figure 5.14:** Image of the water Cobb test setup.

The results from the water Cobb test are represented in Figure 5.15. The control sample has the highest Cobb value indicating vulnerability to water. The value obtained from the kraft paper reinforced with surface-modified rutile-TiO<sub>2</sub> NPs shows an indication of sizing with KP/T-ASA5% recording the least Cobb value; decreased by 21% as compared with the control sample.

A Cobb value usually varies according to dosage and method of sizing. According to Seppanen [195], about a 60% decrease in Cobb was recorded when the kraft pulp was internally sized with AKD and ASA. Also Varshoei *et al.* [199] reported a 92% decrease in Cobb value as they added 1% AKD internally to kraft pulp. In this present research, the kraft pulp was not internally sized; instead, the rutile-TiO<sub>2</sub> NPs were surface conditions. Internal sizing implies that the sizing chemical is added to the pulp stock before fabricating the sheet. In another development by Zhang *et al.* [142], TiO<sub>2</sub> NPs were surface condition with AKD and reinforced in a bleach kraft pulp. From the report, an 84% decrease in Cobb values was recorded. In the experiment, kaolin a titanium oxide extender was added to the experiment. When Al<sub>2</sub>SiO<sub>5</sub> (kaolin) is added to paper, it increases the covering power (coating), barrier resistance, nanofiller quantity and resists the undesirable effect of liquids [200].



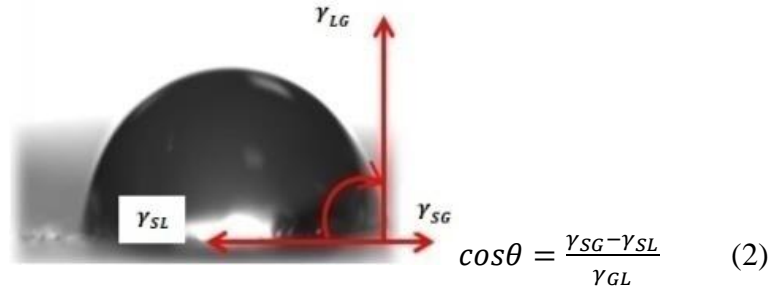
**Figure 5.15:** Graphical representation of Cobb test of the fabricated kraft paper samples.

There are no universal Cobb values for papers; however, cardboard, packaging and printing paper are expected to have Cobb values ranging from 20-35g/m<sup>2</sup>. According to their application, some kraft papers are moderately sized, and the Cobb value goes beyond 140 g/m<sup>2</sup> [201], [202]. In power transformer application, the required Cobb value can only be identified when the paper undergoes accelerated laboratory ageing, which subjects the kraft paper to a typical power transformer condition. With this, the response of the modified kraft paper to ageing will be examined. The same verification is done on thermally upgraded kraft papers (defined in IEEE C57.100) [203].

The Cobb test basically studies the wetting characteristics of the kraft paper. In power transformer, accumulation of water is usually due to moisture ingress (small water molecules) and thermal degradation which results to oxidation as well as hydrolysis mechanism. The water molecules produced in these processes are absorbed by the kraft paper. The wet kraft paper will eventually disrupt the glucose rings thereby breaking the hydrogen bond of the cellulose and compromising the mechanical property of the insulation. The Cobb test and the results indicate the resistance of the fabricated kraft papers to water; however, this experiment is conducted on papers that are exposed to higher volume of water and stress. The contact angle test which involves a droplet of water is presented in the subsection.

### Contact Angle of the Nanocomposites Kraft Paper Insulation:

The Young's model by Thomas Young described the interaction between the surface of a dry fibre sheet and a wet droplet in 1805. His model under an ideal fibre sheet defines the wetting characteristic as related to the contact angle of surface energy at three interphases. The equation provided an interphase relation between contact angle  $\theta$ , solid, liquid and gas as in equation 2 and illustrated in Figure 5.16 [136], [204].



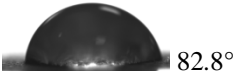
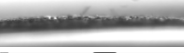


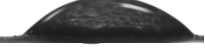


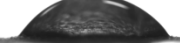


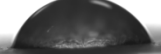
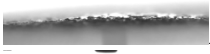

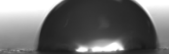


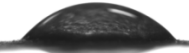



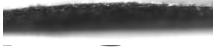



**Figure 5.16:** Contact angle illustration of a water droplet.

Where  $\gamma_{SG}$ ,  $\gamma_{SL}$  and  $\gamma_{GL}$  are the surface energy at the interphase of solid and gas, solid and liquid and gas and liquid, respectively.

The experimental test examined the contact angle and rate at which the contact angle changes with time as the water is absorbed into the kraft paper surface. The measurements were carried out using a Kruss EasyDrop (Model FM40Mk2). A droplet of distilled water was placed on the sample and captured by a high-resolution camera. Five spots were tested on each three replicated samples. The angle and the rate the contact angle changes were recorded. The test was done in accordance with TAPPI T 558 standards [205].

As per the contact angle measurement (Table 5.2), the nanocomposite kraft paper specimens filled with surface-modified rutile-TiO<sub>2</sub> NPs (KP/T-ASA5%) have the biggest contact angle manifesting the highest hydrophobicity. Compared with the control paper, the contact angle improved by 12%. The results also show that the water absorption rate is 4 times slower in the KP/T-ASA5% specimen than in the unfilled kraft paper specimen.

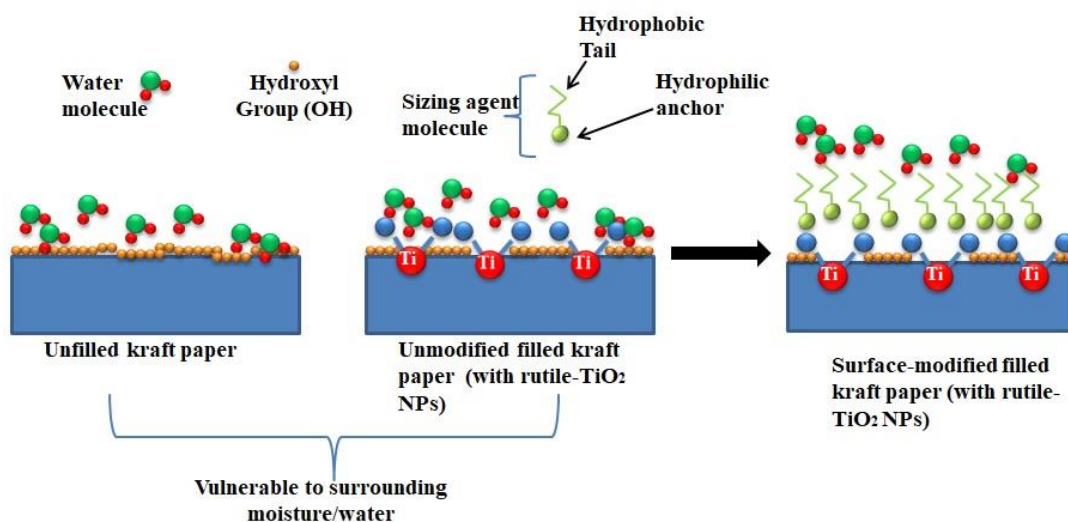
**Table 5.2:** Contact angle and time taken to absorb water.

Sample	Contact with sheet	After 5 seconds	Water absorbed by the sheet
Control	 82.8°		 After 5s
KP/T-Pure	 83.7°		 After 7s
KP/T-AKD 1%	 85.4°		 After 8s
KP/T-AKD 3%	 89.6°		 After 11s
KP/T-AKD 5%	 91.8°		 After 17s
KP/T-ASA 1%	 85.6°		 After 8s
KP/T-ASA 3%	 90.1°		 After 14s
KP/T-ASA 5%	 92.5°		 After 19s

In summary, the examinations of the fabricated kraft paper insulation's moisture and water absorption characteristics using various tests shows that the unfilled kraft paper and kraft paper filled with unmodified nanofillers are more hydrophilic. The hydrophilicity is attributable to the hygroscopic nature of kraft paper (cellulose) insulation due to its exposed hydroxyl site [20] and the reinforced rutile-TiO<sub>2</sub> NPs. The rutile-TiO<sub>2</sub> NPs have surface

oxygen vacancies which act as an active site for water absorption. The process of absorption of water to the rutile-TiO<sub>2</sub> surface could be molecularly or dissociative. This causes an interaction between the surficial Titanium and the hydroxyl group of the water molecule while the bridging oxygen forms a bond with the H atom [27]–[29], [104]. The characteristic of cellulose and rutile-TiO<sub>2</sub> NPs being hydrophilic, in effect, made the control kraft paper and the nanocomposite kraft paper filled with unmodified rutile-TiO<sub>2</sub> NPs hygroscopically to the surrounding moisture and water.

The hydrophobicity of the nanocomposite kraft paper filled with surface-modified rutile-TiO<sub>2</sub> NPs is attributed to the role of AKD and ASA sizing agents. How the sizing agents interact with the surrounding moisture is illustrated in Figure 5.17. Consequently, the kraft paper reinforced with the modified rutile-TiO<sub>2</sub> NPs reacts more hydrophobically with the surrounding moisture.



**Figure 5.17:** Interaction of sized nanocomposite kraft paper with surrounding moisture.

It is essential to note that hydrolysis of the ester bond (of AKD and ASA) between the sized molecules and polymer can result in sizing reversion over time. In the literature, it is explained as a loss of size response [137], [195], [196], [201].

*This thesis has produced a novel nanocomposite kraft paper with 74% less moisture absorption properties and 12% less water absorption rate capability compared to the unfilled kraft paper. Moisture/water are the main agents of kraft paper degradation. With*

*reference to Figure 1.2 in chapter 1, on average, moisture contributes 6% to power transformer failure and also the deterioration of the insulation (insulation failure) are most affected by the moisture which contributes 26% of the transformer failure. Therefore, hypothetically if all the power transformers were to be installed using nanocomposite kraft paper, the percentage of moisture induced faults will reduce to about 1.5% compared to 6% with current kraft paper technology. Therefore, the improved moisture performance of the fabricated nanocomposite kraft paper translates into improved power transformer reliability.*

*In summary, the achieved hydrophobicity of the nanocomposited kraft paper samples filled with surface modified rutile-TiO<sub>2</sub> NPs produced in this present research work is an unprecedented contribution to the kraft paper technology used for power transformer winding insulation. The inherent hydrophilic nature of cellulosic kraft paper material has been a significant setback in its applications.*

## **5.6 Chapter Conclusion**

This chapter has presented the fabrication and evaluation of nanocomposite kraft paper insulation. The application of surface-modified rutile phase of TiO<sub>2</sub> NPs as filler in fabricating composite kraft paper is a novel approach to reduce the hydrophilic characteristic associated with cellulose kraft paper insulation. The fabricated kraft paper insulation were tested for moisture absorption. The results show that kraft papers filled with surface-modified nanoparticles has significantly improved hydrophobic properties. The thermal stability of the kraft paper insulation filled with nanoparticles was also improved. However, the tradeoff in the design of the nanocomposite kraft paper in the 9% decrease in its tensile strength as compared with the unfilled kraft paper. The next chapter looks into the dielectric properties of the fabricated kraft paper insulation.

# Chapter 6: Dielectric Characteristics of the Fabricated Kraft Paper Insulation

## 6.1 Introduction

The previous chapter presented the fabrication of kraft paper insulation; three different specimens were fabricated and characterized. The moisture absorption and rate of water absorption of unfilled and filled kraft paper insulation were studied and analyzed. It was shown that the kraft paper filled with surface-modified rutile-TiO<sub>2</sub> NPs (KP/T-ASA5%) had significantly improved in its hydrophobicity properties, and compared with the unfilled: (a) moisture absorption rate dropped by 74%, (b) WVTR decreased by 30% and (c) the water droplet contact angle increased by 12%. While moisture and water absorption properties are important, the electrical properties of the resultant nanocomposite kraft paper are equally important and are therefore evaluated in this chapter. The findings in this chapter also form part of the published scholarly article.

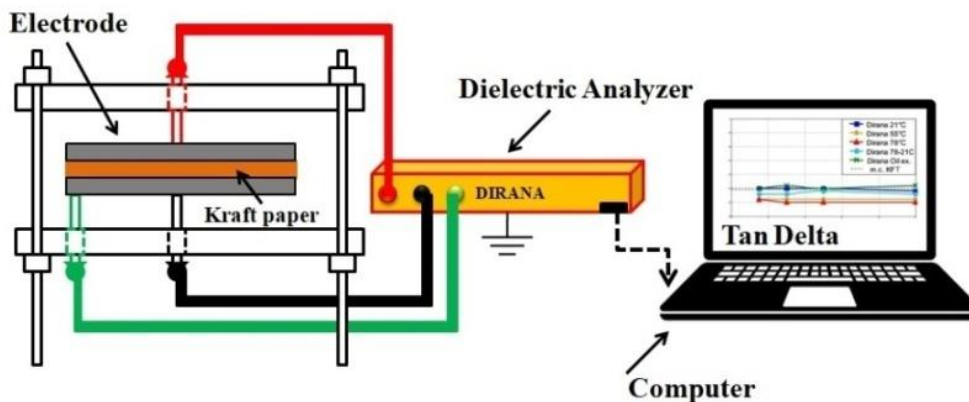
## 6.2 Dielectric Dissipation Factor (Tan Delta) of the Fabricated Kraft Paper Insulation

Since moisture and water are detrimental to the insulation integrity of kraft paper, the presence of moisture in kraft paper insulated equipment needs to be diagnosed. In that regard, a dielectric loss measurement is a common tool for moisture condition diagnosis of kraft paper-based insulation.

Dielectric dissipation factor (tan delta) or dielectric loss is a diagnostic tool used to indicate the presence of moisture and contaminations in insulation. The measured value of tan delta indicates the moisture effect in the kraft paper [32], [206]. For sound insulation, the tan delta is very low (less than 0.5%), and high values imply the existence of moisture. Tan delta is a non-dimensional value as in equation 6.1 [207].

$$Dissipation\ factor\ (tan\delta) = \frac{current\ loss}{charge\ current} = \frac{I_{loss}}{I_{charge}} \quad (6.1)$$

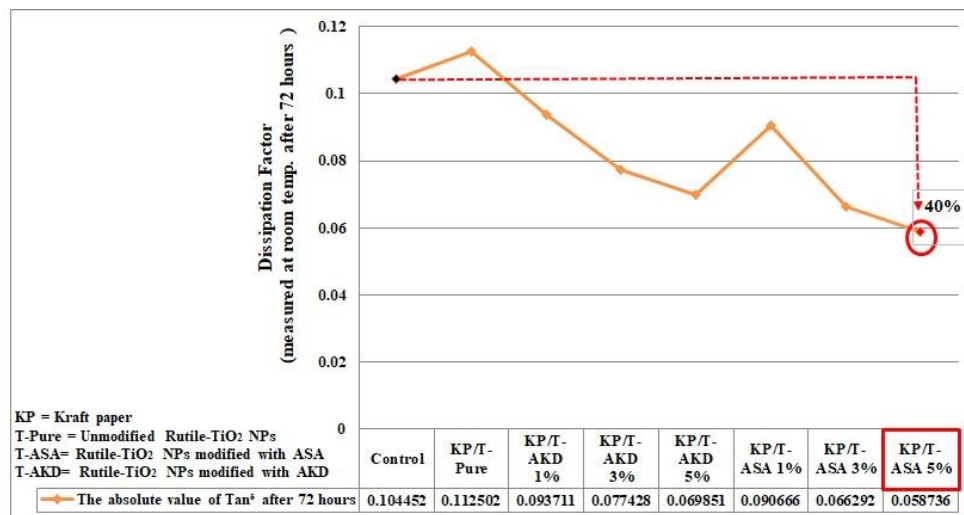
To study the effect of moisture absorption on the paper samples, Omicron™ Dielectric Response Analyzer (DIRANA) was used in this work. DIRANA combine the time domain measurement (polarization and depolarization current) and frequency domain measurement (dielectric dissipation factor) [61], [208]. The test specimens were dried in an oven at 105 °C for 20 minutes, and DIRANA was used to measure the value of the tan delta on the dry specimens at about the same high temperature. The samples were then exposed to moisture at a relative humidity of  $53 \pm 4\%$  and at a temperature of  $23 \pm 2$  °C for 72 hours. Figure 6.1 shows a schematic of the experimental setup and the data values from DIRANA are presented in the table and Appendix E.



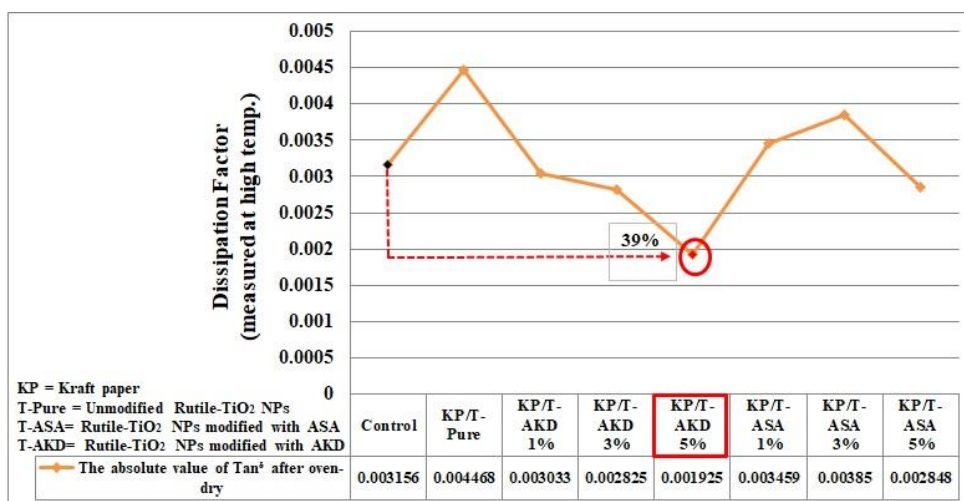
**Figure 6.1:** Experimental setup of measuring dissipation factor using DIRANA.

Figure 6.2 presents the tan delta measurement set up at room temperature 72 hours after the specimens were taken out of the drying oven. The results show that the kraft paper specimens reinforced with surface-modified rutile-TiO<sub>2</sub> NPs (KP/T-ASA5%) has the lowest tan delta values. Notably, the difference with that of the unfilled is 40% which is quite significant. Figure 6.3 presents the tan delta measurement results of the specimens at high temperature immediately after oven curing. The tests were done at high temperature. As expected, the test specimens' tan delta values were lower than the corresponding values after 72 hours of exposure to the atmospheric air at room temperature. It is notable that instead of the KP/T-ASA5% that of KP/T-AKD5% has the lowest tan delta value which manifests the temperature dependence of ASA and AKD surfactants.

AKD efficiency depends on temperature and takes a longer time to cure. At a higher temperature, AKD is expected to perform better [137], [195], [196], [201]. The efficiency of ASA-sized handsheets could also be retarded by its speedy hydrolysis [197], [201].



**Figure 6.2:** Absolute values of tan delta measured after 72 hours at 50 Hertz.

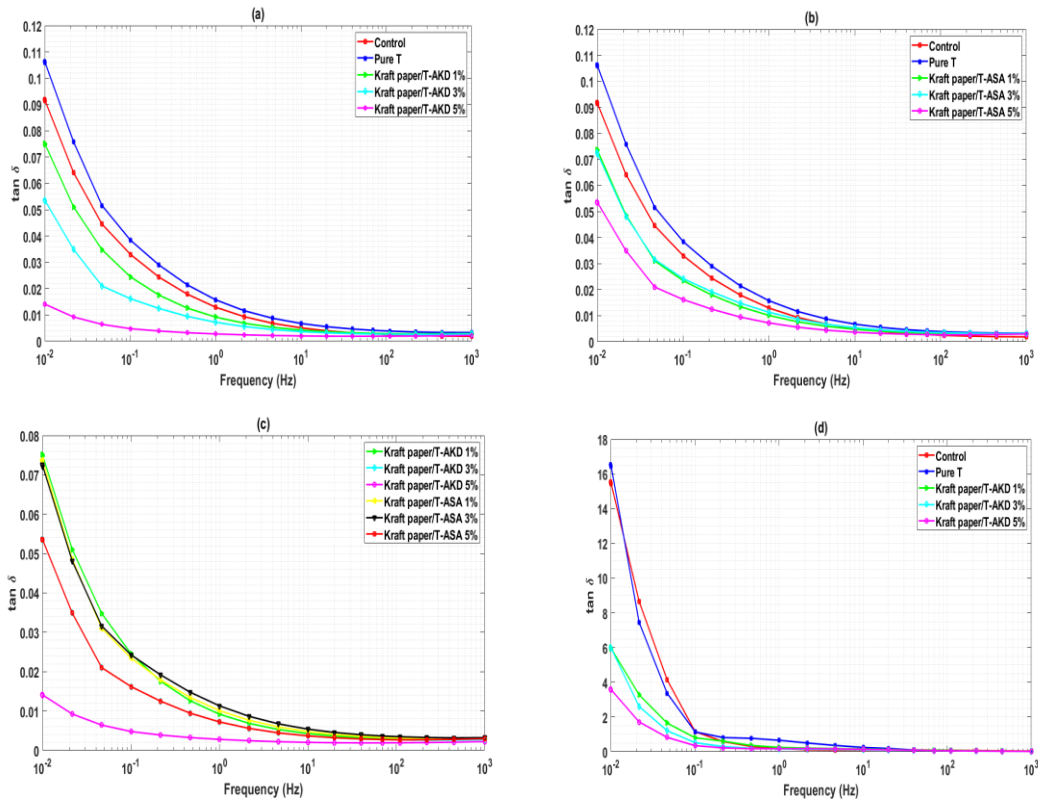


**Figure 6.3:** Absolute values of tan delta measured after curing at 50 Hertz.

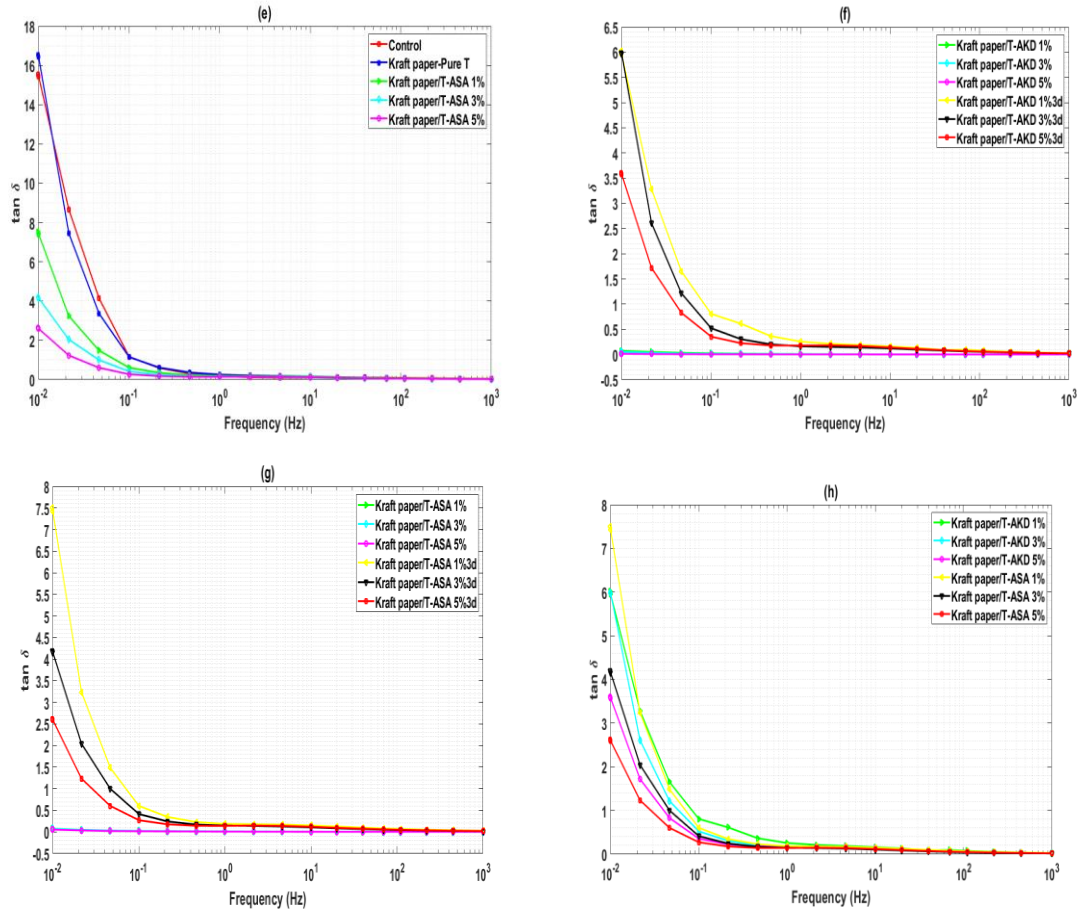
Figure 6.4. (page 82) shows the graphs of tan delta against the frequency. The kraft paper insulation reinforced with surface-modified rutile-TiO<sub>2</sub> NPs has lower tan delta values for both graphs plotted for high temperature and after 72 hours of direct exposure to humid atmospheric air. However, the control (unfilled) sample and the sample containing

unmodified rutile-TiO<sub>2</sub> NPs increased more in tan delta towards the low frequency. In general, moisture has a higher effect at lower frequency, and kraft paper with absorbed moisture has an increase in conductivity [32], [192], [207]. It is worth noting that a dielectric loss increase, especially in kraft paper, is largely attributed moisture presence.

It is evident from the graphs that all the curves appeared sloppy, while a typical tan delta curve of oil-impregnated paper is usually in an S-shape (showing the moisture absorption, oil-conductivity and geometry). This is because the experiment was done on a single insulation material (kraft paper), and the dissipation factor curves of the kraft papers were only displayed, excluding the steep slope of the oil. The graphs also show that the samples that absorbed more moisture tend to move right (outward), This effect is assigned to moisture presence, especially in the kraft paper [19], [47], [54].



**Figure 6.4:** (a)  $\tan \delta$  graph of kraft paper/T-AKD after curing, (b)  $\tan \delta$  graph of kraft paper/T-ASA after curing, (c) combined  $\tan \delta$  graph of kraft paper/T-AKD and ASA after curing, (d)  $\tan \delta$  graph of kraft paper/T-AKD after 72 hours.



**Figure 6.4:** cont' (e)  $\tan\delta$  graph of kraft paper/T-ASA after 72 hours, (f) combined  $\tan\delta$  graph of kraft paper/T-AKD after curing and 72 hours later, (g) combined  $\tan\delta$  graph of kraft paper/T-ASA after curing and 72 hours later, (h) combined  $\tan\delta$  graph of kraft paper/T-AKD and ASA after 72 hours.

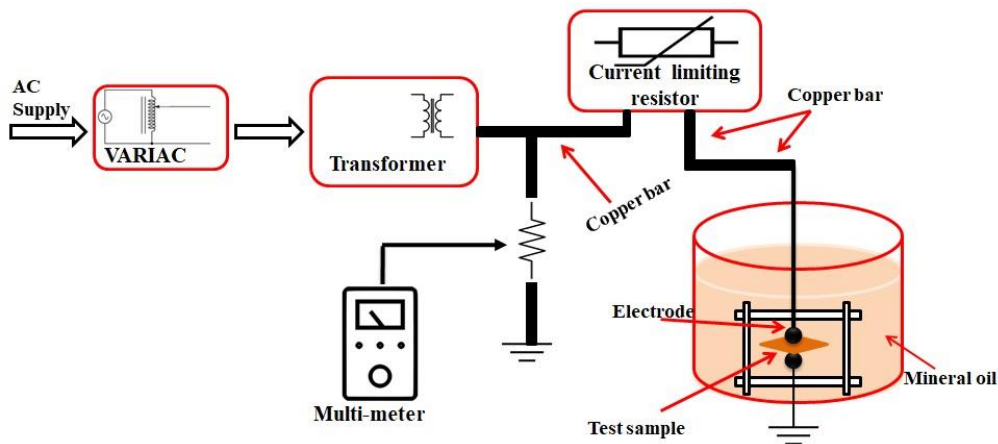
### 6.3 Electrical Breakdown Strength of the Fabricated Kraft Paper Insulation

One of the essential characteristics of kraft paper insulating material used in a power transformer is its ability to withstand electric field stress without breaking down easily. Kraft paper modified with nanoparticles has shown significant improvement in its breakdown strength. Liao *et al.* [71] reinforced kraft paper insulation with  $\text{TiO}_2$  NPs, and the breakdown voltage of the modified kraft increased by 21%. Yuan and Ruijin [89] modified kraft paper insulation with montmorillonite (MMT), and the breakdown voltage of the oil-impregnated paper increased by 13%. Tang *et al.* [93] used  $\text{Al}_2\text{O}_3$  NPs to modify kraft paper insulation;

it was reported that adding  $\text{Al}_2\text{O}_3$  NPs greatly improved the AC breakdown strength of the kraft paper insulation. In a similar effort, Tang *et al.* [91] used  $\text{SiO}_2$  NPs to modify kraft paper insulation, and from the experimental results, the breakdown voltage of the modified insulation increased by 14%. The breakdown voltage of modified kraft paper insulation was reported to have improved when  $\text{TiO}_2$ -NPs were optimized for power transformer application [14]. The breakdown test of kraft paper specimens is presented in the next subsection.

### Experimental procedure for the Breakdown Strength of the Fabricated Kraft Paper Specimens:

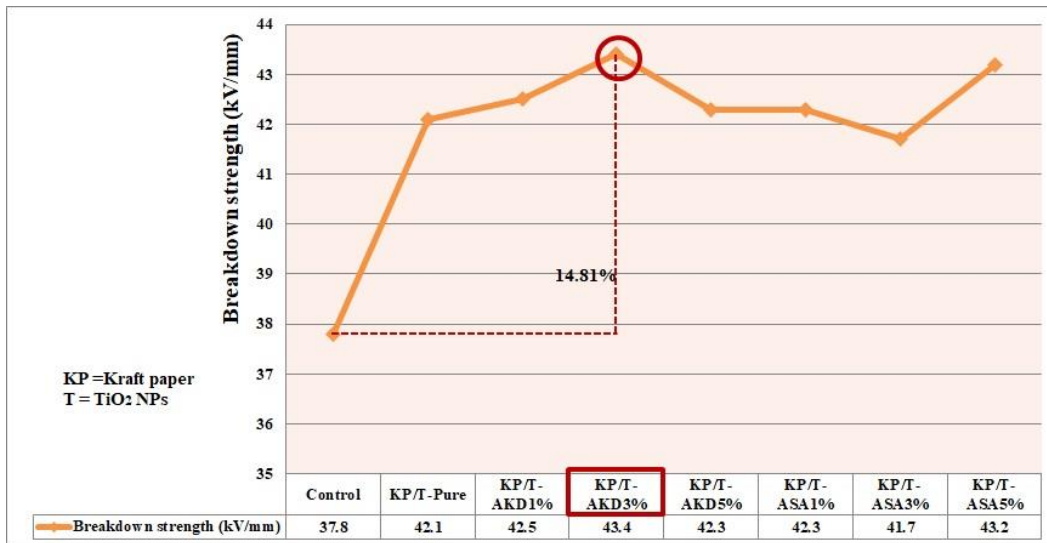
To determine the effect of modification on the new material, the dielectric breakdown strength of each sample paper was studied. Before the breakdown tests were carried out, the samples were oil-impregnated. This was done by drying the kraft paper at  $90\text{ }^\circ\text{C}$  for 48 hours. Transformer oil (mineral) was added, and the oven temperature was controlled at  $40\text{ }^\circ\text{C}$  for another 24 hours. The breakdown test was set up with homemade equipment as in Figure 6.5 and was done accordance with IEC 60243 standard [209]. Three replicates of each sample were tested on seven different spots.



**Figure 6.5:** Breakdown test setup.

From Figure 6.6, the breakdown strength of all the fibres containing either modified or unmodified rutile- $\text{TiO}_2$  NPs increased while the control sample had a lower value. The highest breakdown strength was  $43.4\text{ kV/mm}$ . A 14.81% increase in breakdown strength

was recorded as compared to the reference sample. It was however notable that the specimen that gave the best result was kraft paper filled with surface-modified rutile-TiO<sub>2</sub> NPs (KP/T-AKD3%) and not the surface-modified rutile-TiO<sub>2</sub> NPs (KP/T-ASA5%) which gave best performance in other characteristics such as hydrophobicity. The result of having another specimen performing better in other properties of the fabricated nanocomposite kraft paper could be attributed to either loss of sizing chemical or rate of nanofiller dispersion within the fibre web. It also worth noting that, the rate of nanofiller dispersion and particles size has influence on the percentage increase of the breakdown strength.



**Figure 6.6:** Breakdown voltage of the fabricated kraft paper.

### Impact of the nanoparticles on the resultant breakdown strength of the fabricated nanocomposite kraft paper

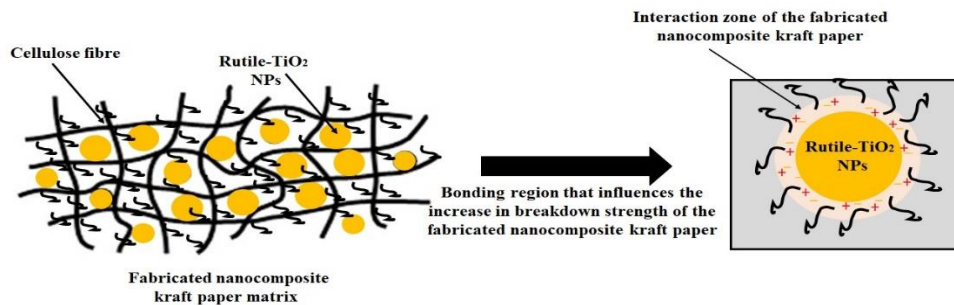
To understand the interaction between the nanofiller (rutile-TiO<sub>2</sub> NPs) and cellulose fibre which results in the suppression of the electric field stress and increases the breakdown strength of the nanocomposite kraft paper, the proposed model by Tanaka *et al.* and Li *et al.* are employed.

Tanaka [210], [211] 2005 proposed a model to explain the interaction around the polymer and nanoparticles. In his work, a multi-layered core model for polymer nanocomposites interface was presented for electrical insulation. His model including the New Potential

Barrier model of Li *et al.* [212] could be used to explain the interaction that results in improved electrical field withstand of the fabricated nanocomposite kraft paper.

The interface in the nanocomposite kraft paper is the channel that bonds the rutile-TiO<sub>2</sub> NPs with the cellulose fibre, from Tanaka model, the interface of the fabricated nanocomposite kraft paper is made of three layers with the first corresponding to the layer that is bonded to both rutile-TiO<sub>2</sub> NPs and cellulose fibre (kraft pulp). This connection is facilitated by the unsaturated bond and organic groups (surfactants) on the surface of the rutile-TiO<sub>2</sub> NPs. The rutile-TiO<sub>2</sub> NPs then connect with the cellulose fibre by hydrogen, ionic and covalent bonds. The second layer (transitional region) is a region within the model that consists of the cellulose chain which bound with the surface of the rutile-TiO<sub>2</sub> NPs and the first layer. The third layer (loose layer) interacts with the second layer. This layer comprises of various chain structure/shape, chain mobility and free crystallinity from cellulose chain (polymer matrix). The bonded and transition region (interaction zone) together define the electrical field strength of the fabricate nanocomposite kraft paper as illustrated in Figure 6.7.

Based on the interaction zone, Li *et al.* proposed a new potential barrier model in 2011. The proposed model considered the interaction zone (with in the nanocomposite kraft paper) as an independent region and the thickness of the transition region to be smaller than the mean free path of the carriers. According to the model, charge carriers are trapped in the interaction zone when the rutile-TiO<sub>2</sub> nanoparticle is in scattered dispersion of the fabricated nanocomposite kraft paper. This result to a decrease in mobility and density of carriers which cause an increase in breakdown strength of the fabricated nanocomposite kraft paper by 15%.



**Figure 6.7:** Interaction zone in nanocomposite kraft paper.

*The approximately 15% increase in breakdown strength of the nanocomposite kraft paper can be translated into decrease in winding insulation failure due to transient overvoltage caused by lightening. With this nanocomposite kraft paper, smaller power transformer can be designed to withstand more electric field stress.*

#### **6.4 Chapter Conclusion**

This chapter presented the dielectric properties of the fabricated kraft paper insulation. The dielectric dissipation factor of the kraft paper were measured to study the impact of moisture on the kraft paper specimens. The outcome shows that the samples reinforced with surface-modified rutile-TiO<sub>2</sub> NPs had a lower tan delta value indicating higher hydrophobic characteristics than the control and kraft paper reinforced with unmodified nanofillers after modification. The electrical breakdown voltage of kraft paper reinforced with nanoparticles increased. The following chapter presents the conclusion and recommendation for this thesis.

## **Chapter 7: Conclusion and Future Research Work**

### **7.1 Introduction**

The research work presented in this thesis is an effort to fabricate a novel nanocomposite kraft paper insulation. This is to produce kraft paper insulation with improved hydrophobic properties and for application in power transformer insulation. This was achieved by surface-modifying the nanofiller (rutile-TiO<sub>2</sub> NPs) with surfactants (sizing chemicals). The surfactants reduced the surface energy of the modified rutile-TiO<sub>2</sub> NPs thereby producing an hydrophobic nanofiller. Kraft paper samples were then fabricated and filled with unmodified nanoparticles in one hand, and with the surface-modified nanoparticles in the other hand for the experimental investigation.

The following section of this chapter recaps the major findings of the research work. The contributions and limitations of the research are presented in the second section. Lastly, the possible areas for further research were presented.

### **7.2 Summary of Major Findings and Knowledge Contribution**

The nanocomposite kraft paper insulation was fabricated through the reinforcement of the nanoparticles into the kraft pulp. The nanoparticles were synthesized using the sol-gel method. Temperature and time manipulation during the period of annealing produced the required size of 19 nm of rutile-TiO<sub>2</sub> nanoparticles.

The modification process of the obtained rutile-TiO<sub>2</sub> NPs produced a nanoparticle that has its surface conditioned for protection against moisture absorption. The nanoparticles surface-modification was done with two different sizing agents (surfactants); Alkyl ketene dimer (AKD) and alkenyl succinic anhydride (ASA). The percentage loading of the sizing agents was varied to investigate the optimal composition. Nanoparticles modified with the sizing chemical were less hydrophilic and had better thermal stability than the unmodified nanoparticles. The characteristics of the sizing chemicals results in modifying the surface of the rutile-TiO<sub>2</sub> NPs to be less vulnerable to the surrounding moisture, while the thermal

stability of the surface-modified rutile-TiO<sub>2</sub> NPs is attributed to improved heat resistance as a result of the long-chain organic compounds from the surfactants.

The fibre characteristics of the fabricated kraft paper insulation were examined, and it was observed that all the sample papers fall within the fibre length of softwood fibre; 1.8 to 4 millimetres. At least 50% of the nanofillers were retained within the composite kraft paper, with some traces of agglomeration being observed. The retention of the nanofillers is attributed to the retention aid added. The investigation on the resultant properties of the fabricated nanocomposite kraft paper compared with the unfilled kraft paper is presented in Table 7.1.

**Table 7.1:** Resultant properties of the fabricated kraft paper and implication on insulation design for power transformer.

	Hydrophilic properties			Thermal stability	Tensile index	Tan delta	Dielectric strength
	Moisture absorption	WVTR	Contact angle				
Percentage (%) improvement compared to unfilled kraft paper	74%	30%	12%	5.4%	9%	40%	14.81%
Possible extrapolated implications on insulation design in power transformer	The percentage of moisture to failure of insulation as well as the transformer will reduce. The nanocomposite kraft paper technology in this thesis therefore presented a more reliable technique.	The percentage of moisture to failure of insulation as well as the transformer will reduce. The nanocomposite kraft paper technology in this thesis therefore presented a more reliable technique.	The percentage of moisture to failure of insulation as well as the transformer will reduce. The nanocomposite kraft paper technology in this thesis therefore presented a more reliable technique.	Thermal endurance of the winding insulation will increase thereby paving way to increase the loading of a power transformer of the same capacity.	The hydrophobic, thermal and electrical properties of the fabricated nanocomposite kraft paper will reduce the impact the decrease in tensile strength will have on the insulation degradation.	The conductivity caused due to the presence of moisture in the kraft paper will decrease.	The increase in the electrical field strength of the nanocomposite entails that smaller transformers can be designed to withstand higher voltage. And also failure due to lightning and surges on the winding insulation will reduce.

In summary, the nanocomposite kraft paper insulation modified with rutile-TiO<sub>2</sub> NPs/5% ASA possessed better hydrophobic properties than the other kraft paper samples. However, at a higher temperature, the nanocomposite kraft paper insulation modified with rutile-TiO<sub>2</sub> NPs/5% AKD shows superior effectiveness.

## 7.3 Contributions and Limitations

### 7.3.1 Contributions

- An optimal procedure of synthesis rutile-TiO<sub>2</sub> NPs via sol-gel to arrive at 19.72 nm has been devised in the research work. The approach can be used to synthesise rutile-TiO<sub>2</sub> NPs to serve other application purposes.
- The surface modification of rutile-TiO<sub>2</sub> NPs using the sizing chemicals (surfactants) in this research is a novel attempt to mitigate the hydrophilic characteristic associated with nanoparticle used for kraft paper insulation. This can be used to address similar shortfalls associated with polymer or polymer nanocomposites.
- The application of surface-modified rutile-TiO<sub>2</sub> nanoparticles in kraft paper in this research work is a novel attempt to reduce the hydrophilic characteristics of kraft paper insulation for transformer application. The combination of ASA sizing chemical, rutile-TiO<sub>2</sub> NPs and kraft pulp to produce a kraft paper insulation is unique to this research work.
- Interm of kraft paper technology, this thesis has fabricated a transformer winding insulation that can reduce the transformer failures attributed to moisture absorption, overvoltage (due to lightning), overloading (causing thermal stress) as well as insulation failure (due to oxidation, pyrolysis, hydrolysis).

### 7.3.2 Limitations

The rutile-TiO<sub>2</sub> NPs were synthesized in small volumes for the purpose of the research work; therefore, for applications that needs large volumes of rutile-TiO<sub>2</sub>, the temperature and time combination during annealing will not be helpful.

The nanocomposite kraft paper was fabricated in a laboratory using a handsheet maker for the purpose of this research work. The procedure and mixing technique will defer for industrial application, thereby influencing the resultant properties of the insulation. Also, the rate of dispersion and agglomeration by the constraints of the laboratory equipment influenced the final properties of the fabricated kraft paper insulation.

The ageing test for the suitability of the modified kraft paper insulation was not performed due to the time limit.

#### 7.4 Recommendations for Future Work

The focus of the research work presented in this thesis is the possibility of reducing water absorption characteristics of kraft paper insulation for power transformer applications. This was achieved by reinforcing surface-modified rutile-TiO<sub>2</sub> NPs into a kraft pulp to fabricate a nanocomposite of kraft paper insulation. The outcome of this research work appears promising; however, perfection cannot be assumed to have been attained; therefore, further work is necessary to establish its applicability. The areas recommended for further research are given below;

1. The nanofiller retention, dispersion and agglomeration are significant factors influencing the final properties of the fabricated nanocomposite kraft paper insulation. In this regard, there is a need for interdisciplinary research collaboration to control these factors for the desired outcome.
2. The sizing chemicals used in this research work could be affected by sizing reversion over time, thereby comprising the effort. It is recommended that further work should focus on alternative sizing chemicals or adhering chemicals to extend the time of regression.
3. In this research work, rutile-TiO<sub>2</sub> NPs were surface condition with a sizing chemical and was then reinforced in the kraft pulp to reduce the water absorption characteristics of the composite kraft paper insulation. The efficiency of this sizing depends on the uniformity of the dispersed nanofiller within the host polymer. Given this, further research on alternative means of sizing the nanocomposite kraft paper should be explored.
4. Nanocomposites of kraft paper insulation are attracting more attention; however, the ageing characteristics and likely byproducts of these composites and dielectric properties are areas that need to be investigated.

In conclusion, the end goal of this research work was achieved by fabricating a nanocomposite kraft paper with improve hydrophobic property. The investigation of moisture/water absorption characteristics and dielectric properties of the fabricated nanocomposite kraft paper suggests that the inherent hydrophilic nature of transformer solid

insulation is reduced in this research work. However, the tradeoff in the fabrication of the nanocomposite kraft paper is the decreases in its tensile strength as compared with the unmodified kraft paper insulation.

## Reference

- [1] R. Liao, C. Guo, K. Wang, L. Yang, S. Grzybowski, and H. Sun, "Investigation on thermal aging characteristics of vegetable oil-paper insulation with flowing dry air," *IEEE Transactions on Dielectrics and Electrical Insulation*, vol. 20, no. 5, pp. 1649–1658, Oct. 2013, doi: 10.1109/TDEI.2013.6633695.
- [2] A. Elansezhiyan and S. Chandrasekar, "Understanding the Lightning Discharge Withstand and Breakdown Characteristics of Nano SiO<sub>2</sub> Modified Mineral Oil for Transformer Applications," *JAC*, vol. 12, no. 19, pp. 5200–5208, Dec. 2016, doi: 10.24297/jac.v12i19.5359.
- [3] S. T. Jan, R. Afzal, and A. Khan, "Transformer Failures , Causes & Impact," presented at the International Conference Data Mining, Civil and Mechanical Engineering, 2015. doi: 10.15242/iie.e0215039.
- [4] T. A. Prevost and T. V. Oommen, "Cellulose insulation in oil-filled power transformers: Part I - history and development," *IEEE Electrical Insulation Magazine*, vol. 22, no. 1, pp. 28–35, Jan. 2006, doi: 10.1109/MEI.2006.1618969.
- [5] K. Kalariya, H. Kannad, D. Vyas, and P. Gandhi, "A Review on Ageing of Power Transformer and Insulation Life Assessment," *Advanced Research in Electrical and Electronic Engineering*, vol. 2, no. 2, p. 6, 2014.
- [6] N. B. Azis, "Ageing assessment of insulation paper with consideration of in-service ageing and natural ester application," The University of Manchester, 2012.
- [7] J. E. Contreras, E. Rodríguez, and J. Taha-Tijerina, "Nanotechnology applications for electrical transformers—A review," *Electric Power Systems Research*, vol. 143, Feb. 2017, doi: 10.1016/j.epsr.2016.10.058.
- [8] V. A. Thiviyathan, P. J. Ker, Y. S. Leong, F. Abdullah, A. Ismail, and Md. Zaini Jamaludin, "Power transformer insulation system: A review on the reactions, fault detection, challenges and future prospects," *Alexandria Engineering Journal*, vol. 61, no. 10, pp. 7697–7713, Oct. 2022, doi: 10.1016/j.aej.2022.01.026.
- [9] J. Singh and S. Singh, "Transformer failure analysis: reasons and methods," *International Journal of Engineering Research*, vol. 4, no. 15, p. 5, 2016.
- [10] T. Suwanasri, E. Chaidee, and C. Adsoongnoen, "Failure statistics and power transformer condition evaluation by dissolved gas analysis technique," in *2008 International Conference on Condition Monitoring and Diagnosis*, Apr. 2008, pp. 492–496. doi: 10.1109/CMD.2008.4580333.
- [11] A. D. Bhagyashree, S. S. Panchayya, and G. T. Archana, "Analysis of transformer insulation parameters using polarization and depolarization current method and frequency domain spectroscopy," *IJSTR*, vol. 8, no. 09, p. 254, Sep. 2019.
- [12] T. K. Saha and P. Purkait, "Investigations of Temperature Effects on the Dielectric Response Measurements of Transformer Oil-Paper Insulation System," *IEEE Transactions on Power Delivery*, vol. 23, no. 1, pp. 252–260, Jan. 2008, doi: 10.1109/TPWRD.2007.911123.
- [13] Suwarno - and R. A. Prasajo, "Power transformer insulation assessment based on oil-paper measurement data using SVM-classifier," *International Journal on Electrical Engineering and Informatics*, vol. 10, 2018, doi: 10.15676/ijeei.2018.10.4.4.
- [14] D. Liu, J. Ye, X. Xu, C. G. Deng, and X. Li, "Optimization of mass fraction and particle size of TiO<sub>2</sub> additives in application of HVDC transformer insulation," in *2019 IEEE 20th International Conference on Dielectric Liquids (ICDL)*, Jun. 2019, pp. 1–4. doi: 10.1109/ICDL.2019.8796662.
- [15] N. S. Hanung, Suwarno, H. Nanang, Y. Mizutani, T. Takahashi, and T. Okamoto, "Degree of polymerization estimation of insulation papers in power transformers based on load and temperature histories in Java-Bali Region of Indonesia National Electric company," in *2012*

- IEEE International Conference on Condition Monitoring and Diagnosis*, Sep. 2012, pp. 637–642. doi: 10.1109/CMD.2012.6416226.
- [16] H. William and P. E. Bartly, “Analysis of Transformer Failure,” presented at the International Association of Engineering Insurers 36th Annual Conference, Stockholm, 2003.
- [17] M. S. A. Minhas, J. P. Reynders, and P. J. De Klerk, “Failures in power system transformers and appropriate monitoring techniques,” in *1999 Eleventh International Symposium on High Voltage Engineering*, Aug. 1999, vol. 1, pp. 94–97 vol.1. doi: 10.1049/cp:19990516.
- [18] C. Aj, M. A. Salam, Q. M. Rahman, F. Wen, S. P. Ang, and W. Voon, “Causes of transformer failures and diagnostic methods – A review,” *Renewable and Sustainable Energy Reviews*, vol. 82, pp. 1442–1456, Feb. 2018, doi: 10.1016/j.rser.2017.05.165.
- [19] I. Fofana, H. Borsi, E. Gockenbach, and M. Farzaneh, “Aging of transformer insulating materials under selective conditions,” *European Transactions on Electrical Power*, vol. 17, pp. 450–470, Sep. 2007, doi: 10.1002/etep.134.
- [20] M. Mahmood, R. Kadzutu-Sithole, N. Moloto, C. Nyamupangedengu, and C. Gomes, “Improving thermal stability and hydrophobicity of rutile-TiO<sub>2</sub> nanoparticles for oil-impregnated paper application,” *Energies*, vol. 14, p. 7964, Nov. 2021, doi: 10.3390/en14237964.
- [21] P. Jusner, E. Schwaiger, A. Potthast, and T. Rosenau, “Thermal stability of cellulose insulation in electrical power transformers – A review,” *Carbohydrate Polymers*, vol. 252, p. 117196, Jan. 2021, doi: 10.1016/j.carbpol.2020.117196.
- [22] N. Liang, R. Liao, M. Xiang, Y. Mo, and Y. Yuan, “Influence of Amine Compounds on the Thermal Stability of Paper-Oil Insulation,” *Polymers*, vol. 10, no. 8, p. 891, Aug. 2018, doi: 10.3390/polym10080891.
- [23] T. V. Oommen and T. A. Prevost, “Cellulose insulation in oil-filled power transformers: part II maintaining insulation integrity and life,” *IEEE Electrical Insulation Magazine*, vol. 22, no. 2, pp. 5–14, Mar. 2006, doi: 10.1109/MEI.2006.1618996.
- [24] M. Anglhuber, “Why is water killing power transformer insulation?,” *Transformers Magazine*, vol. 4, no. 3, pp. 106–112, Jul. 08, 2017.
- [25] K. Kulasinski, R. Guyer, D. Derome, and J. Carmeliet, “Water Adsorption in Wood Microfibril-Hemicellulose System: Role of the Crystalline–Amorphous Interface,” *Biomacromolecules*, vol. 16, no. 9, pp. 2972–2978, Sep. 2015, doi: 10.1021/acs.biomac.5b00878.
- [26] K. Kulasinski, “Effects of water adsorption in hydrophilic polymers,” in *Polym Sci Res Adv Pract Appl Educ Asp.*, Badajoz, Spain: Formatex Research Center, 2016, pp. 217–223.
- [27] J. Schneider *et al.*, “Understanding TiO<sub>2</sub> photocatalysis: mechanisms and materials,” *Chem. Rev.*, vol. 114, no. 19, pp. 9919–9986, Oct. 2014, doi: 10.1021/cr5001892.
- [28] K. Bourikas, C. Kordulis, and A. Lycourghiotis, “Titanium dioxide (anatase and rutile): surface chemistry, liquid–solid interface chemistry, and scientific synthesis of supported catalysts,” *Chem. Rev.*, vol. 114, no. 19, pp. 9754–9823, Oct. 2014, doi: 10.1021/cr300230q.
- [29] G. Liu, H. G. Yang, J. Pan, Y. Q. Yang, G. Q. (Max) Lu, and H.-M. Cheng, “Titanium dioxide crystals with tailored facets,” *Chem. Rev.*, vol. 114, no. 19, pp. 9559–9612, Oct. 2014, doi: 10.1021/cr400621z.
- [30] J. Bae, I. Samek, P. Stair, and R. Snurr, “Investigation of the hydrophobic nature of metal oxide surfaces created by atomic layer deposition,” *Langmuir*, vol. 35, Apr. 2019, doi: 10.1021/acs.langmuir.9b00577.
- [31] R. Malewski, J. Subocz, M. Szrot, J. Płowucha, and R. Zaleski, “Condition assessment of medium-power transformers using diagnostic methods: PDC, FDS, FRA to support decision to modernize or replace service-aged ...,” in *Malewski2008conditionao*.

- [32] P. Żukowski *et al.*, “Dielectric losses in the composite cellulose–mineral oil–water nanoparticles: theoretical assumptions,” *Cellulose*, vol. 23, no. 3, pp. 1609–1616, Jun. 2016, doi: 10.1007/s10570-016-0934-x.
- [33] W. Gerd, “Fibre Surface Properties of Kraft Pulp,” Karlstad University Studies, Karlstad, Sweden, 2009.
- [34] H. Karlsson, “Strength Properties of Paper produced from Softwood Kraft Pulp,” Karlstad University Studies, Karlstad, Sweden, 2010.
- [35] I. Sutan Chairul, Y. Md Thayoob, Y. Ghazali, M. S. Ahmad Khair, and S. Ab Ghani, “Formation and Effect of Moisture Contents to Kraft Paper’s Life of In-Service Power Distribution Transformer,” *Applied Mechanics and Materials*, vol. 793, pp. 114–118, Jun. 2015, doi: 10.4028/www.scientific.net/AMM.793.114.
- [36] Petri Hyvönen, *Prediction of insulation degradation of distribution power cables based on chemical analysis and electrical measurements*. Teknillinen korkeakoulu, 2008. Accessed: Nov. 28, 2019. [Online]. Available: <https://aaltodoc.aalto.fi:443/handle/123456789/4498>
- [37] G. Chinga-Carrasco, A. Miettinen, C. L. Luengo Hendriks, E. Kristofer, and M. Kataj, “Structural Characterisation of Kraft Pulp Fibres and Their Nanofibrillated Materials for Biodegradable Composite Applications,” in *Nanocomposites and Polymers with Analytical Methods*, J. Cuppoletti, Ed. InTech, 2011.
- [38] A. Johansson, “Correlations between fibre properties and paper properties,” KTH Royal Institute of Technology, Stockholm, Sweden, 2011.
- [39] P. Jusner, E. Schwaiger, A. Potthast, and T. Rosenau, “Thermal stability of cellulose insulation in electrical power transformers – A review,” *Carbohydrate Polymers*, vol. 252, p. 117196, Jan. 2021, doi: 10.1016/j.carbpol.2020.117196.
- [40] R. Hollertz, L. Wågberg, and C. Pitois, “Kraft-Pulp Based Material for Electrical Insulation,” *NORD-IS*, no. 24, Sep. 2017, doi: 10.5324/nordis.v0i24.2300.
- [41] D. Tarasov, M. Leitch, and P. Fatehi, “Lignin–carbohydrate complexes: properties, applications, analyses, and methods of extraction: a review,” *Biotechnology for Biofuels*, vol. 11, no. 1, p. 269, Sep. 2018, doi: 10.1186/s13068-018-1262-1.
- [42] R. Hollertz, “Cellulose-based electrical insulation materials: Dielectric and mechanical properties,” KTH Royal Institute of Technology, 2017. Accessed: Oct. 09, 2019. [Online]. Available: <http://urn.kb.se/resolve?urn=urn:nbn:se:kth:diva-205622>
- [43] L. Lars E. *et al.*, “Ageing of cellulose in mineral-oil insulated transformers,” Technical Brochure 323 D1.01.10, 2007.
- [44] P. Przybysz, M. Dubowik, M. A. Kucner, K. Przybysz, and K. Przybysz Buzala, “Contribution of Hydrogen Bonds to Paper Strength Properties,” *PLoS One*, vol. 11, no. 5, May 2016, doi: 10.1371/journal.pone.0155809.
- [45] P. Harmsen, W. Huijgen, L. Bermudez, and R. Bakker, *Literature Review of Physical and Chemical Pretreatment Processes for Lignocellulosic Biomass*. 2010.
- [46] V. G. Arakelian and I. Fofana, “Water in oil-filled high-voltage equipment part II: Water content as physicochemical tools for insulation condition diagnostic,” *Electrical Insulation Magazine, IEEE*, vol. 23, pp. 15–24, Oct. 01, 2007.
- [47] CIGRE Working Group A2.30 (V.Sokolov), “Moisture equilibrium and moisture migration within transformer insulation systems,” John Wiley & Sons, Ltd, 2008. doi: 10.1002/9781119239970.ch6.
- [48] D. Martin *et al.*, “Determining water in transformer paper insulation: analyzing aging transformers,” *IEEE Electrical Insulation Magazine*, vol. 31, no. 5, pp. 23–32, Sep. 2015, doi: 10.1109/MEI.2015.7214442.
- [49] D. Martin, T. Saha, C. Perkasa, N. Lelekakis, and T. Gradnik, “Fundamental concepts of using water activity probes to assess transformer insulation water content,” *IEEE Electrical Insulation Magazine*, vol. 32, no. 3, pp. 9–16, 2016, doi: 10.1109/MEI.2016.7527120.

- [50] J. Gielniak *et al.*, “Moisture in cellulose insulation of power transformers - statistics,” *IEEE Transactions on Dielectrics and Electrical Insulation*, vol. 20, no. 3, pp. 982–987, Jun. 2013, doi: 10.1109/TDEI.2013.6518968.
- [51] J. Cai and T. Zhang, “Moisture content assessment of transformer solid insulation using return voltage spectrum,” in *2009 IEEE 9th International Conference on the Properties and Applications of Dielectric Materials*, Jul. 2009, pp. 257–260. doi: 10.1109/ICPADM.2009.5252457.
- [52] Y. Cui, H. Ma, T. Saha, and C. Ekanayake, “Understanding Moisture Dynamics and Its Effect on the Dielectric Response of Transformer Insulation,” *IEEE Transactions on Power Delivery*, vol. 30, no. 5, pp. 2195–2204, Oct. 2015, doi: 10.1109/TPWRD.2015.2426199.
- [53] V. Guggenberg and P. A. (Philip Antony), “Applications of interdigital dielectrometry to moisture and double layer measurements in transformer insulation,” Thesis, Massachusetts Institute of Technology, 1993. Accessed: Oct. 22, 2019. [Online]. Available: <https://dspace.mit.edu/handle/1721.1/12735>
- [54] M. Koch, M. Krüger, S. Tenbohlen, and O. Energy, “Comparing various moisture determination methods for power transformers,” presented at the Southern Africa Regional Conference, Cigre 2009.
- [55] T. K. Saha and P. Purkait, “Understanding the impacts of moisture and thermal ageing on transformer’s insulation by dielectric response and molecular weight measurements,” *IEEE Transactions on Dielectrics and Electrical Insulation*, vol. 15, no. 2, pp. 568–582, Apr. 2008, doi: 10.1109/TDEI.2008.4483479.
- [56] A. Ciuriuc, L. M. Dumitran, P. V. Noțingher, L. V. Bădicu, R. Setnescu, and T. Setnescu, “Lifetime estimation of vegetable and mineral oil impregnated paper for power transformers,” in *2016 IEEE International Conference on Dielectrics (ICD)*, Jul. 2016, vol. 2, pp. 720–723. doi: 10.1109/ICD.2016.7547717.
- [57] L. E. Lundgaard, W. Hansen, and S. Ingebrigtsen, “Ageing of Mineral Oil Impregnated Cellulose by Acid Catalysis,” *IEEE Transactions on Dielectrics and Electrical Insulation*, vol. 15, no. 2, pp. 540–546, Apr. 2008, doi: 10.1109/TDEI.2008.4483475.
- [58] D. Martin, C. Perkasa, and N. Lelekakis, “Measuring Paper Water Content of Transformers: A New Approach Using Cellulose Isotherms in Nonequilibrium Conditions,” *Power Delivery, IEEE Transactions on*, vol. 28, pp. 1433–1439, Jul. 2013, doi: 10.1109/TPWRD.2013.2248396.
- [59] M. Koch, S. Tenbohlen, and T. Stirl, “Diagnostic Application of Moisture Equilibrium for Power Transformers,” *IEEE Transactions on Power Delivery*, vol. 25, no. 4, pp. 2574–2581, Oct. 2010, doi: 10.1109/TPWRD.2010.2048343.
- [60] M. Marković and B. Cucic, “Transformer Lifetime Management through Solid and Liquid Insulation Assessment,” presented at the Euro TechCon 2018, Dec. 2018.
- [61] K. Y. Raj, P. Das, A. Kumar, N. Haque, B. Chatterjee, and S. Dalai, “Polarization and depolarization current analysis of thermally aged oil impregnated kraft paper,” in *2017 IEEE Calcutta Conference (CALCON)*, Dec. 2017, pp. 457–460. doi: 10.1109/CALCON.2017.8280775.
- [62] Z. Mu, S. Y. Matharage, Z. D. Wang, and Q. Liu, “Effect of Low Molecular Weight Acids and Moisture on Space Charge of Oil Impregnated Paper Insulation,” in *2018 IEEE International Conference on High Voltage Engineering and Application (ICHVE)*, Sep. 2018, pp. 1–4. doi: 10.1109/ICHVE.2018.8641887.
- [63] Shengji Tee, “Ageing Assessment of Transformer Insulation through Oil Test Database Analysis,” The University of Manchester, 2016.
- [64] D. H. Shroff and A. W. Stannett, “A review of paper aging in power transformers,” *Transmission and Distribution IEE Proceedings C - Generation*, vol. 132, no. 6, pp. 312–319, Nov. 1985, doi: 10.1049/ip-c.1985.0052.

- [65] N. Lelekakis, D. Martin, and J. Wijaya, "Ageing rate of paper insulation used in power transformers Part 1: Oil/paper system with low oxygen concentration," *IEEE Transactions on Dielectrics and Electrical Insulation*, vol. 19, no. 6, pp. 1999–2008, Dec. 2012, doi: 10.1109/TDEI.2012.6396958.
- [66] N. Lelekakis, D. Martin, and J. Wijaya, "Ageing rate of paper insulation used in power transformers Part 2: Oil/paper system with medium and high oxygen concentration," *IEEE Transactions on Dielectrics and Electrical Insulation*, vol. 19, no. 6, pp. 2009–2018, Dec. 2012, doi: 10.1109/TDEI.2012.6396960.
- [67] N. Lelekakis, W. Guo, D. Martin, J. Wijaya, and D. Susa, "A field study of aging in paper-oil insulation systems," *IEEE Electrical Insulation Magazine*, vol. 28, no. 1, pp. 12–19, Jan. 2012, doi: 10.1109/MEI.2012.6130527.
- [68] E. Jazaeri and T. Tsuzuki, "Effect of pyrolysis conditions on the properties of carbonaceous nanofibers obtained from freeze-dried cellulose nanofibers," *Cellulose*, vol. 20, no. 2, pp. 707–716, Apr. 2013, doi: 10.1007/s10570-012-9858-2.
- [69] T. Tanaka and T. Imai, "Advances in nanodielectric materials over the past 50 years," *IEEE Electr. Insul. Mag.*, vol. 29, no. 1, pp. 10–23, Jan. 2013, doi: 10.1109/MEI.2013.6410535.
- [70] S. Palit and C. M. Hussain, "Engineered Nanomaterial for Industrial Use," in *Handbook of Nanomaterials for Industrial Applications*, Elsevier, 2018, pp. 3–12. doi: 10.1016/B978-0-12-813351-4.00001-8.
- [71] R. Liao, C. Lv, L. Yang, Y. Zhang, W. Wu, and C. Tang, "The insulation properties of oil-impregnated insulation paper reinforced with nano-TiO<sub>2</sub>," *J. Nanomaterials*, vol. 2013, p. 1:1-1:1, Jan. 2013, doi: 10.1155/2013/373959.
- [72] C. P. Wong and R. S. Bollampally, "Thermal conductivity, elastic modulus, and coefficient of thermal expansion of polymer composites filled with ceramic particles for electronic packaging," *Journal of Applied Polymer Science*, vol. 74, no. 14, pp. 3396–3403, 1999, doi: 10.1002/(SICI)1097-4628(19991227)74:14<3396::AID-APP13>3.0.CO;2-3.
- [73] G.-W. Lee, M. Park, J. Kim, J. I. Lee, and H. G. Yoon, "Enhanced thermal conductivity of polymer composites filled with hybrid filler," *Composites Part A: Applied Science and Manufacturing*, vol. 37, no. 5, pp. 727–734, May 2006, doi: 10.1016/j.compositesa.2005.07.006.
- [74] D. Liu *et al.*, "Suppression Mechanism of TiO<sub>2</sub> for the Partial Discharge of Oil-paper Insulation in Intensive Electric Field," in *IEEE 20th International Conference on Dielectric Liquids (ICDL)*, Jun. 2019, pp. 1–4. doi: 10.1109/ICDL.2019.8796771.
- [75] T. Andritsch, D. Fabiani, and I. Vazquez, "Nanodielectrics-examples of preparation and microstructure," *IEEE Electr. Insul. Mag.*, vol. 29, no. 6, pp. 21–28, Nov. 2013, doi: 10.1109/MEI.2013.6648750.
- [76] R.-J. Liao, C. Lv, L. Yang, Y.-Y. Zhang, and T. Liu, "Space charge behavior in oil-impregnated insulation paper reinforced with nano-TiO<sub>2</sub>," *BioResources*, vol. 8(4), Sep. 2013, doi: 10.15376/biores.8.4.5655-5665.
- [77] C. Nyamupangedengu, R. Kochetov, P. H. F. Morshuis, and J. J. Smit, "A study of electrical tree partial discharges in nanocomposite epoxy," *2012 Annual Report Conference on Electrical Insulation and Dielectric Phenomena*, 2012, doi: 10.1109/CEIDP.2012.6378928.
- [78] J. Ramsden, "Chapter 1. What is Nanotechnology?," *Nanotechnology Perceptions*, vol. 1, pp. 3–17, Mar. 2005, doi: 10.4024/N03RA05/01.01.
- [79] Yang Cao, P. C. Irwin, and K. Younsi, "The future of nanodielectrics in the electrical power industry," *IEEE Trans. Dielect. Electr. Insul.*, vol. 11, no. 5, pp. 797–807, Oct. 2004, doi: 10.1109/TDEI.2004.1349785.
- [80] M. Kus, T. Y. Alic, C. Kirbiyik, C. Baslak, K. Kara, and D. A. Kara, "Synthesis of Nanoparticles," in *Handbook of Nanomaterials for Industrial Applications*, Elsevier, 2018, pp. 392–429. doi: 10.1016/B978-0-12-813351-4.00025-0.

- [81] C. Gomes and M. Izadi, "Electrical Isolation of Two Earthing Systems under Lightning Conditions with TiO<sub>2</sub> Nano Fluid Barrier," in *2019 International Symposium on Lightning Protection (XV SIPDA)*, Sep. 2019, pp. 1–5. doi: 10.1109/SIPDA47030.2019.8951640.
- [82] N. Hamadneh, W. Khan, and W. Khan, "Polymer nanocomposites – synthesis techniques, classification and properties," in *Science and applications of Tailored Nanostructures*, 2016.
- [83] E. I. Akpan, X. Shen, B. Wetzel, and K. Friedrich, "2 - Design and Synthesis of Polymer Nanocomposites," in *Polymer Composites with Functionalized Nanoparticles*, K. Pielichowski and T. M. Majka, Eds. Elsevier, 2019, pp. 47–83. doi: 10.1016/B978-0-12-814064-2.00002-0.
- [84] D. Marquis, E. Guillaume, and C. CHIVAS-JOLY, "Properties of Nanofillers in Polymer," in *Nanocomposites and Polymers with Analytical Methods*, 2011. doi: 10.5772/21694.
- [85] E. Paparazzo, M. Fanfoni, E. Severini, and S. Priori, "Evidence of Si–OH species at the surface of aged silica," *Journal of Vacuum Science & Technology A*, vol. 10, no. 4, pp. 2892–2896, Jul. 1992, doi: 10.1116/1.577726.
- [86] P. Christian, F. von der Kammer, M. Baalousha, and T. Hofmann, "Nanoparticles: Structure, Properties, Preparation and Behaviour in Environmental Media," *Ecotoxicology (London, England)*, vol. 17, pp. 326–43, Aug. 2008, doi: 10.1007/s10646-008-0213-1.
- [87] R. Scaffaro and L. Botta, "Chapter 5 - Nanofilled Thermoplastic–Thermoplastic Polymer Blends," in *Nanostructured Polymer Blends*, S. Thomas, R. Shanks, and S. Chandrasekharakurup, Eds. Oxford: William Andrew Publishing, 2014, pp. 133–160. doi: 10.1016/B978-1-4557-3159-6.00005-5.
- [88] A. Díez-Pascual, "Nanoparticle Reinforced Polymers," *Polymers*, vol. 11, p. 625, Apr. 2019, doi: 10.3390/polym11040625.
- [89] Y. Yuan and R. Liao, "A Novel Nanomodified Cellulose Insulation Paper for Power Transformer," *Journal of Nanomaterials*, vol. 2014, pp. 1–6, 2014, doi: 10.1155/2014/510864.
- [90] R. Hollertz, D. Ariza, C. Pitois, and L. Wagberg, "Dielectric response of kraft paper from fibres modified by silica nanoparticles," in *2015 IEEE Conference on Electrical Insulation and Dielectric Phenomena (CEIDP)*, Ann Arbor, MI, USA, Oct. 2015, pp. 459–462. doi: 10.1109/CEIDP.2015.7351987.
- [91] C. Tang, X. Li, F. Yin, and J. Hao, "The performance improvement of aramid insulation paper by nano-SiO<sub>2</sub> modification," *IEEE Transactions on Dielectrics and Electrical Insulation*, vol. 24, no. 4, pp. 2400–2409, 2017, doi: 10.1109/TDEI.2017.006560.
- [92] Fei Gao, Min Xiang, Ruijin Liao, Zhengyu Xu, and Jiyu Wang, "The experimental investigation on space charge distribution of cellulose insulation paper modified with alumina nanoparticles," in *2016 International Conference on Condition Monitoring and Diagnosis (CMD)*, Sep. 2016, pp. 757–760. doi: 10.1109/CMD.2016.7757935.
- [93] C. Tang, S. Zhang, J. Xie, and C. Lv, "Molecular simulation and experimental analysis of Al<sub>2</sub>O<sub>3</sub>-nanoparticle-modified insulation paper cellulose," *IEEE Transactions on Dielectrics and Electrical Insulation*, vol. 24, no. 2, pp. 1018–1026, Apr. 2017, doi: 10.1109/TDEI.2017.006315.
- [94] D. Coetzee, M. Venkataraman, J. Militky, and M. Petru, "Influence of Nanoparticles on Thermal and Electrical Conductivity of Composites," *Polymers*, vol. 12, no. 4, p. 742, Apr. 2020, doi: 10.3390/polym12040742.
- [95] R. Liao, C. Lv, L. Yang, Y. Zhang, W. Wu, and C. Tang, "The Insulation Properties of Oil-Impregnated Insulation Paper Reinforced with Nano-TiO<sub>2</sub>," *Journal of Nanomaterials*, vol. 2013, pp. 1–7, 2013, doi: 10.1155/2013/373959.
- [96] R. Nikjoo *et al.*, "Comparison of oil-impregnated papers with SiO<sub>2</sub> and ZnO nanoparticles or high lignin content, for the effect of superimposed impulse voltage on AC surface PD," *IEEE*

- Trans. Dielect. Electr. Insul.*, vol. 24, no. 3, pp. 1726–1734, Jun. 2017, doi: 10.1109/TDEI.2017.006053.
- [97] R. Liao, F. Zhang, Y. Yuan, L. Yang, T. Liu, and C. Tang, “Preparation and Electrical Properties of Insulation Paper Composed of SiO<sub>2</sub> Hollow Spheres,” *Energies*, vol. 5, no. 8, pp. 2943–2951, Aug. 2012, doi: 10.3390/en5082943.
- [98] P. Calva, A. Cano, and H. Martinez, “Fillers in Electrical Papers for Power Transformers,” *Advanced Materials Research*, vol. 875–877, pp. 335–340, Feb. 2014, doi: 10.4028/www.scientific.net/AMR.875-877.335.
- [99] F. Morsy, S. el-sherbiny, M. Samir, and O. Fouad, “Application of nanostructured titanium dioxide pigments in paper coating: a comparison between prepared and commercially available ones,” *Journal of Coatings Technology and Research*, vol. 13, Sep. 2015, doi: 10.1007/s11998-015-9735-7.
- [100] M. T. Noman, M. A. Ashraf, and A. Ali, “Synthesis and applications of nano-TiO<sub>2</sub>: a review,” *Environ Sci Pollut Res*, vol. 26, no. 4, pp. 3262–3291, Feb. 2019, doi: 10.1007/s11356-018-3884-z.
- [101] U. Diebold, “The surface science of titanium dioxide,” *Surface Science Reports*, vol. 48, no. 5, pp. 53–229, Jan. 2003, doi: 10.1016/S0167-5729(02)00100-0.
- [102] M. Malekshahi Byranvand, A. Kharata, L. Fatholahib, and Z. Malekshahi Beiranvand, “A Review on Synthesis of Nano-TiO<sub>2</sub> via Different Methods,” *Journal of NanoStructures*, vol. 3, pp. 1–9, Jun. 2013, doi: 10.7508/jns.2013.01.001.
- [103] M. Kapilashrami, Y. Zhang, Y.-S. Liu, A. Hagfeldt, and J. Guo, “Probing the Optical Property and Electronic Structure of TiO<sub>2</sub> Nanomaterials for Renewable Energy Applications,” *Chem. Rev.*, vol. 114, no. 19, pp. 9662–9707, Oct. 2014, doi: 10.1021/cr5000893.
- [104] J. Bae, I. A. Samek, P. C. Stair, and R. Q. Snurr, “Investigation of the hydrophobic nature of metal oxide surfaces created by atomic layer deposition,” *Langmuir*, vol. 35, no. 17, pp. 5762–5769, Apr. 2019, doi: 10.1021/acs.langmuir.9b00577.
- [105] A. Vorontsov, H. Valdes, P. Smirniotis, and Y. Paz, “Recent Advancements in the Understanding of the Surface Chemistry in TiO<sub>2</sub> Photocatalysis,” *Surfaces*, vol. 3, pp. 72–92, Feb. 2020, doi: 10.3390/surfaces3010008.
- [106] J. Morales, A. Maldonado, and M. de la L. Olvera, “Synthesis and characterization of nanostructured TiO<sub>2</sub> anatase-phase powders obtained by the homogeneous precipitation method,” in *2013 10th International Conference on Electrical Engineering, Computing Science and Automatic Control (CCE)*, Sep. 2013, pp. 391–394. doi: 10.1109/ICEEE.2013.6676015.
- [107] L. J. Berberich and M. E. Bell, “The Dielectric Properties of the Rutile Form of TiO<sub>2</sub>,” *Journal of Applied Physics*, vol. 11, no. 10, pp. 681–692, Oct. 1940, doi: 10.1063/1.1712721.
- [108] S. El-Sherbiny, F. Morsy, M. Samir, and O. A. Fouad, “Synthesis, characterization and application of TiO<sub>2</sub> nanopowders as special paper coating pigment,” *Appl Nanosci*, vol. 4, no. 3, pp. 305–313, Mar. 2014, doi: 10.1007/s13204-013-0196-y.
- [109] P. Nyamukamba, O. Okoh, H. Mungondori, R. Taziwa, and S. Zinya, “Synthetic Methods for Titanium Dioxide Nanoparticles: A Review,” *Titanium Dioxide - Material for a Sustainable Environment*, Nov. 2018, doi: 10.5772/intechopen.75425.
- [110] J. E. Contreras, E. A. Rodriguez, and J. Taha-Tijerina, “Chapter 39 - Recent Trends of Nanomaterials for High-Voltage Applications,” in *Handbook of Nanomaterials for Industrial Applications*, C. Mustansar Hussain, Ed. Elsevier, 2018, pp. 724–738. doi: 10.1016/B978-0-12-813351-4.00040-7.
- [111] N. Abid *et al.*, “Synthesis of nanomaterials using various top-down and bottom-up approaches, influencing factors, advantages, and disadvantages: A review,” *Advances in Colloid and Interface Science*, vol. 300, p. 102597, Dec. 2021, doi: 10.1016/j.cis.2021.102597.

- [112] H.-S. Chen, C. Su, J.-L. Chen, T.-Y. Yang, N.-M. Hsu, and W.-R. Li, "Preparation and Characterization of Pure Rutile TiO<sub>2</sub> Nanoparticles for Photocatalytic Study and Thin Films for Dye-Sensitized Solar Cells," *Journal of Nanomaterials*, Nov. 30, 2010. <https://www.hindawi.com/journals/jnm/2011/869618/> (accessed Oct. 09, 2020).
- [113] X. Chen, "Titanium Dioxide Nanomaterials and Their Energy Applications," *Chinese Journal of Catalysis*, vol. 30, no. 8, pp. 839–851, Aug. 2009, doi: 10.1016/S1872-2067(08)60126-6.
- [114] T.-H. Wang, A. M. Navarrete-López, S. Li, D. A. Dixon, and J. L. Gole, "Hydrolysis of TiCl<sub>4</sub>: Initial Steps in the Production of TiO<sub>2</sub>," *J. Phys. Chem. A*, vol. 114, no. 28, pp. 7561–7570, Jul. 2010, doi: 10.1021/jp102020h.
- [115] N. Rab, F. K. Chong, H. I. Mohamed, and W. H. Lim, "Preparation of TiO<sub>2</sub> nanoparticles by hydrolysis of TiCl<sub>4</sub> using water and glycerol solvent system," *J. Phys.: Conf. Ser.*, vol. 1123, p. 012065, Nov. 2018, doi: 10.1088/1742-6596/1123/1/012065.
- [116] W. Li and T. Zeng, "Preparation of TiO<sub>2</sub> Anatase Nanocrystals by TiCl<sub>4</sub> Hydrolysis with Additive H<sub>2</sub>SO<sub>4</sub>," *PLOS ONE*, vol. 6, no. 6, p. e21082, Jun. 2011, doi: 10.1371/journal.pone.0021082.
- [117] L. Li *et al.*, "Sub-10 nm rutile titanium dioxide nanoparticles for efficient visible-light-driven photocatalytic hydrogen production," *Nat Commun*, vol. 6, p. 5881, Jan. 2015, doi: 10.1038/ncomms6881.
- [118] T. Phonkhokong, T. Thongtem, S. Thongtem, A. Phuruangrat, and W. Promnopas, "SYNTHESIS AND CHARACTERIZATION OF TiO<sub>2</sub> NANOPOWDERS FOR FABRICATION OF DYE SENSITIZED SOLAR CELLS," p. 10.
- [119] P. Kajitvichyanukul, J. Ananpattarachai, and S. Pongpom, "Sol-gel preparation and properties study of TiO<sub>2</sub> thin film for photocatalytic reduction of chromium(VI) in photocatalysis process," *Science and Technology of Advanced Materials*, vol. 6, no. 3–4, pp. 352–358, Jan. 2005, doi: 10.1016/j.stam.2005.02.014.
- [120] S. Bagheri, K. Shameli, and S. B. Abd Hamid, "Synthesis and Characterization of Anatase Titanium Dioxide Nanoparticles Using Egg White Solution via Sol-Gel Method," *Journal of Chemistry*, Dec. 12, 2012. <https://www.hindawi.com/journals/jchem/2013/848205/> (accessed Nov. 05, 2020).
- [121] M. H. Nateq and R. Ceccato, "Sol-Gel Synthesis of TiO<sub>2</sub> Nanocrystalline Particles with Enhanced Surface Area through the Reverse Micelle Approach," *Advances in Materials Science and Engineering*, Nov. 11, 2019. <https://www.hindawi.com/journals/amse/2019/1567824/> (accessed Jul. 27, 2020).
- [122] B. Tryba, J. Orlikowski, R. J. Wróbel, J. Przepiórski, and A. W. Morawski, "Preparation and Characterization of Rutile-Type TiO<sub>2</sub> Doped with Cu," *J. of Materi Eng and Perform*, vol. 24, no. 3, pp. 1243–1252, Mar. 2015, doi: 10.1007/s11665-015-1405-5.
- [123] M. Z. Yahaya, M. A. Azam, M. A. MatTeridi, P. K. Singh, and A. A. Mohamad, "Recent Characterisation of Sol-Gel Synthesised TiO<sub>2</sub> Nanoparticles," *Recent Applications in Sol-Gel Synthesis*, Jul. 2017, doi: 10.5772/67822.
- [124] Q. Shipeng, "Synthesis, Processing and Characterization of Nanocrystalline Titanium Dioxide," University of Central Florida, Orlando, Florida, 2006.
- [125] M. S. Anwar *et al.*, "One Step Synthesis of Rutile TiO<sub>2</sub> Nanoparticles at Low Temperature," *Journal of Nanoscience and Nanotechnology*, vol. 12, Jan. 2011, doi: 10.1166/jnn.2012.4634.
- [126] D. A. H. Hanaor and C. C. Sorrell, "Review of the anatase to rutile phase transformation," *J Mater Sci*, vol. 46, no. 4, pp. 855–874, Feb. 2011, doi: 10.1007/s10853-010-5113-0.
- [127] A. Wypych *et al.*, "Dielectric Properties and Characterisation of Titanium Dioxide Obtained by Different Chemistry Methods," *Journal of Nanomaterials*, Mar. 19, 2014. <https://www.hindawi.com/journals/jnm/2014/124814/> (accessed Jun. 12, 2020).

- [128] E. J. Ekoi, A. Gowen, R. Dorrepaal, and D. P. Dowling, "Characterisation of titanium oxide layers using Raman spectroscopy and optical profilometry: Influence of oxide properties," *Results in Physics*, vol. 12, pp. 1574–1585, Mar. 2019, doi: 10.1016/j.rinp.2019.01.054.
- [129] T. Mazza *et al.*, "Raman spectroscopy characterization of TiO<sub>2</sub> rutile nanocrystals," *Physical Review B, Condensed Matter and Materials Physics*, vol. 75, pp. 045416–1, Jan. 2007, doi: 10.1103/PhysRevB.75.045416.
- [130] L. Kernazhitsky *et al.*, "Laser-excited excitonic luminescence of nanocrystalline TiO<sub>2</sub> powder," *Ukrainian Journal of Physics*, vol. 59, pp. 246–253, Mar. 2014, doi: 10.15407/ujpe59.03.0246.
- [131] J. G. Moberly, M. T. Bernards, and K. V. Waynant, "Key features and updates for Origin 2018," *Journal of Cheminformatics*, vol. 10, no. 1, p. 5, Feb. 2018, doi: 10.1186/s13321-018-0259-x.
- [132] M. Hubbe, "Paper's resistance to wetting - A review of internal sizing chemicals and their effects," *BioResources*, vol. 2, Feb. 2007.
- [133] S. Porkert, "Physico-Chemical Processes during Reactive Paper Sizing with Alkenyl Succinic Anhydride (ASA)," Technische Universität Dresden, Germany, 2016. Accessed: Nov. 10, 2019. [Online]. Available: <http://rgdoi.net/10.13140/RG.2.2.18268.39045>
- [134] E. Martorana, J. Belle, and S. Kleemann, "ASA Optimisation - Control of Particle Size, Stability and Hydrolysis," presented at the International Munich Paper Symposium, Apr. 2008.
- [135] A. Kumar, N. K. Bhardwaj, and S. P. Singh, "Sizing performance of alkenyl succinic anhydride (ASA) emulsion stabilized by polyvinylamine macromolecules," *Colloids and Surfaces A: Physicochemical and Engineering Aspects*, vol. 539, pp. 132–139, Feb. 2018, doi: 10.1016/j.colsurfa.2017.12.014.
- [136] H. Chen *et al.*, "Effects of AKD sizing on the morphology and pore distribution properties of OCC fibers," *Journal of Nanomaterials*, 2019. <https://www.hindawi.com/journals/jnm/2019/9490602/> (accessed Feb. 26, 2020).
- [137] A. Karademir, "Quantitative determination of alkyl ketene dimer (AKD) retention in paper made on a pilot paper machine," *Turk J Agric For*, vol. 26, no. 5, pp. 253–260, Sep. 2002.
- [138] Y. Xie, C. Hill, Z. Xiao, H. Militz, and C. Mai, "Silane coupling agents used for natural fiber/polymer composites: A review," *Composites Part A: Applied Science and Manufacturing*, vol. 41, pp. 806–819, Jul. 2010, doi: 10.1016/j.compositesa.2010.03.005.
- [139] B. Xiang, G. Jiang, and J. Zhang, "Surface modification of TiO<sub>2</sub> nanoparticles with silane coupling agent for nanocomposite with poly(butyl acrylate)," *Plastics, Rubber and Composites*, vol. 44, no. 4, pp. 148–154, May 2015, doi: 10.1179/1743289815Y.0000000007.
- [140] J. Zhao, M. Milanova, M. M. C. G. Warmoeskerken, and V. Dutschk, "Surface modification of TiO<sub>2</sub> nanoparticles with silane coupling agents," *Colloids and Surfaces A: Physicochemical and Engineering Aspects*, vol. 413, pp. 273–279, Nov. 2012, doi: 10.1016/j.colsurfa.2011.11.033.
- [141] W.-S. Seo and S. Ohga, "Possibility of Hydrogen Bonding between AKD and Cellulose Molecules during AKD Sizing," *Journal of the Faculty of Agriculture, Kyushu University*, vol. 53, no. 2, pp. 405–410, Oct. 2008, doi: 10.5109/12849.
- [142] Q. Zhang, X. Han, and J. Pu, "In situ chemosynthesis of TiO<sub>2</sub> nanoparticles to endow paper with high water-resistance and retention rate properties," *Appl. Phys. A*, vol. 124, no. 8, p. 571, Jul. 2018, doi: 10.1007/s00339-018-1979-5.
- [143] T. N. Pliev, O. N. Karpov, O. L. Glavati, and T. D. Popovich, "Infrared spectroscopic analysis of high-molecular alkenylsuccinic anhydrides for succinic anhydride groupings," *J Appl Spectrosc*, vol. 18, no. 1, pp. 71–75, Jan. 1973, doi: 10.1007/BF00939110.

- [144] M. Nishiyama, A. Isogai, and F. Onabe, "Structures of Alkenyl Succinic Anhydride(ASA) Components in ASA-Sized Papersheet.," *Sen'i Gakkaishi*, vol. 52, no. 4, pp. 180–188, 1996, doi: 10.2115/fiber.52.180.
- [145] L. Candy, C. Vaca-Garcia, and E. Borredon, "Synthesis and characterization of oleic succinic anhydrides: Structure-property relations," *Journal of The American Oil Chemists Society - J AMER OIL CHEM SOC*, vol. 82, pp. 271–277, Apr. 2005, doi: 10.1007/s11746-005-1066-5.
- [146] P. Huang, Y. Zhao, S. Kuga, M. Wu, and Y. Huang, "A versatile method for producing functionalized cellulose nanofibers and their application," *Nanoscale*, vol. 8, no. 6, pp. 3753–3759, Feb. 2016, doi: 10.1039/C5NR08179C.
- [147] A. Biswas, H. N. Cheng, S. Kim, C. R. Alves, and R. F. Furtado, "Hydrophobic Modification of Cashew Gum with Alkenyl Succinic Anhydride," *Polymers*, vol. 12, no. 3, p. 514, Mar. 2020, doi: 10.3390/polym12030514.
- [148] M. M. Ba-Abbad, A. A. H. Kadhum, A. B. Mohamad, M. S. Takriff, and K. Sopian, "Synthesis and Catalytic Activity of TiO<sub>2</sub> Nanoparticles for Photochemical Oxidation of Concentrated Chlorophenols under Direct Solar Radiation," *Int. J. Electrochem. Sci.*, vol. 7, p. 18, 2012.
- [149] L.-V. A and E. A, "Amine Responsive Poly(lactic acid) (PLA) and Succinic Anhydride (SAh) Graft-Polymer: Synthesis and Characterization.," *Polymers (Basel)*, vol. 11, no. 9, Sep. 2019, doi: 10.3390/polym11091466.
- [150] X. Song, F. Chen, and F. Liu, "Preparation and characterization of alkyl ketene dimer (AKD) modified cellulose composite membrane," *Carbohydrate Polymers*, vol. 88, no. 2, pp. 417–421, Apr. 2012, doi: 10.1016/j.carbpol.2011.10.062.
- [151] A. Tavares, A. Xavier, and D. Evtuguin, "Biotechnology Applications in Pulp and Paper Industry," in *Bioprocess Engineering*, vol. Biotechnology Vol. 12, Studium Press LLC, USA, 2014, pp. 561–581.
- [152] B. Mirkovic, "Recycling of the Waste Paper and the Handsheets Forming," in *Proceedings of the 22nd International DAAAM Symposium*, 2011, vol. Volume 22, p. 2.
- [153] "TAPPI T 205:Forming handsheets for physical tests of pulp." Technical Association of the Pulp & Paper Industry, Revision 2012.
- [154] P. Roman, *Physical Testing of Paper*. Shrewsbury, Shropshire, SY4 4NR, UK: Smithers Group Company, 2017.
- [155] H. Dard, *PAPERMAKING: The History and Technique of an Ancient Craft*. 180 Varick Street, New York: Dover Publication, Inc., 1978.
- [156] S. Gary, *Handbook for Pulp and Paper Technologists*, 3rd Edition. 4543, West 11th Avenue, Vancouver: Angus Wilde Publications, Inc., 2002.
- [157] Seo, Won-Sung, E. International, Cho, Nam-seok, and Wood, "Possibility of Hydrogen Bonding between AKD and Cellulose Molecules during AKD Sizing."
- [158] T. Kondo, "Hydrogen bonds in regioselectively substituted cellulose derivatives," *Journal of Polymer Science Part B: Polymer Physics*, vol. 32, no. 7, pp. 1229–1236, 1994, doi: 10.1002/polb.1994.090320710.
- [159] S. Pérez and D. Samain, "Structure and Engineering of Celluloses," in *Advances in Carbohydrate Chemistry and Biochemistry*, vol. 64, D. Horton, Ed. Academic Press, 2010, pp. 25–116. doi: 10.1016/S0065-2318(10)64003-6.
- [160] A. Tayeb, E. Amini, S. Ghasemi, and M. Tajvidi, "Cellulose Nanomaterials—Binding Properties and Applications: A Review," *Molecules*, vol. 23, p. 2684, Oct. 2018, doi: 10.3390/molecules23102684.
- [161] M. H. Schneider and K. I. Brebner, "Wood-polymer combinations: The chemical modification of wood by alkoxysilane coupling agents," *Wood Sci. Technol.*, vol. 19, no. 1, pp. 67–73, Mar. 1985, doi: 10.1007/BF00354754.

- [162] M.-C. B. Salon, G. Gerbaud, M. Abdelmouleh, C. Bruzzese, S. Boufi, and M. N. Belgacem, “Studies of interactions between silane coupling agents and cellulose fibers with liquid and solid-state NMR,” *Magn Reson Chem*, vol. 45, no. 6, pp. 473–483, Jun. 2007, doi: 10.1002/mrc.1994.
- [163] A. A. Ogunwusi and H. D. Ibrahim, “Advances in Pulp and Paper Technology and the Implication for the Paper Industry in Nigeria,” *Industrial Engineering Letters*, vol. 4, no. 10, p. 3, 2014.
- [164] J. Huang, Y. Zhou, L. Dong, Z. Zhou, and R. Liu, “Enhancing mechanical strength and breakdown behavior of insulating presspaper by introduction of nanofibrillated cellulose,” in *2016 IEEE International Conference on High Voltage Engineering and Application (ICHVE)*, Chengdu, China, Sep. 2016, pp. 1–4. doi: 10.1109/ICHVE.2016.7800608.
- [165] H. Kari, “Image-based quantitative infrared analysis and microparticle characterisation for pulp and paper applications,” KTH Royal Institute of Technology, 2016.
- [166] N. Španić, I. Plazonić, V. Jambrečković, and Ž. Barbarić-Mikočević, “Wood and nonwood fibres length as main factor affecting their suitability as raw materials for papermaking industry,” in *@inproceedings pani2018WoodAN*, 2018.
- [167] M. Fiserova, J. Gigac, and J. Balberčák, “Relationship between fibre characteristics and tensile strength of hardwood and softwood kraft pulps,” *Cellulose Chemistry and Technology*, vol. 44, pp. 249–253, Jul. 2010.
- [168] R. P. Kibblewhite and D. Brookes, “Fibre, beating and papermaking properties of kraft pulps from New Zealand beech species,” *New Zealand Journal of Forestry Science*, vol. 7 (3), pp. 425–444, 1977.
- [169] H. R. Motamedian, A. E. Halilovic, and A. Kulachenko, “Mechanisms of strength and stiffness improvement of paper after PFI refining with a focus on the effect of fines,” *Cellulose*, vol. 26, no. 6, pp. 4099–4124, Apr. 2019, doi: 10.1007/s10570-019-02349-5.
- [170] N. Odabas, U. Henniges, A. Potthast, and T. Rosenau, “Cellulosic Fines: Properties and Effects,” *Progress in Materials Science*, vol. 83, Jul. 2016, doi: 10.1016/j.pmatsci.2016.07.006.
- [171] W. Fischer *et al.*, “Pulp Fines—Characterization, Sheet Formation, and Comparison to Microfibrillated Cellulose,” *Polymers*, vol. 9, Aug. 2017, doi: 10.3390/polym9080366.
- [172] J. Meyers and H. Nanko, “Effects of Fines on the Fiber Length and Coarseness Values Measured by the Fiber Quality Analyzer (FQA),” presented at the TAPPI practical paper conference, Milwaukee WI, USA, Jan. 2005, vol. 20.
- [173] R. A. Horn, “Morphology of pulp fiber from hardwoods and influence on paper strength,” Forest Products Laboratory, U.S Department of Agriculture, Madison, Wisconsin, Research Paper, 1978.
- [174] O. Joutsimo and S. Asikainen, “Effect of Fiber Wall Pore Structure on Pulp Sheet Density of Softwood Kraft Pulp Fibers,” *Bioresources*, vol. 8, Apr. 2013, doi: 10.15376/biores.8.2.2719-2737.
- [175] D. Mandlez, L. Zangl-Jagiello, R. Eckhart, and W. Bauer, “Softwood kraft pulp fines: application and impact on specific refining energy and strength properties,” *Cellulose*, vol. 27, no. 17, pp. 10359–10367, Nov. 2020, doi: 10.1007/s10570-020-03467-1.
- [176] R. S. Seth, “Fibre Quality Factors in Papermaking — II The Importance of Fibre Coarseness,” *MRS Online Proceedings Library (OPL)*, vol. 197, 1990, doi: 10.1557/PROC-197-143.
- [177] B. Nordström and L. Hermansson, “Effect of softwood kraft fiber coarseness on formation and strength efficiency in twin-wire roll forming,” *Nordic Pulp & Paper Research Journal*, vol. 33, no. 2, pp. 237–245, Jul. 2018, doi: 10.1515/npprj-2018-3029.
- [178] R. Horn, “Morphology of Wood Pulp Fiber from Softwoods and Influence on Paper Strength,” Forest Products Laboratory, U.S Department of Agriculture, Madison, Wisconsin, 1974.

- [179] I. Pulkkinen, V. Alopaeus, J. Fiskari, O. Ab, and O. Joutsimo, “The use of fibre wall thickness data to predict handsheet properties of eucalypt pulp fibres,” *O Papel (Brazil)*, vol. 69, Oct. 2008.
- [180] M. Hubbe and R. Gill, “Fillers for papermaking: a review of their properties, usage practices, and their mechanistic role,” *BioResources*, vol. 11, Feb. 2016, doi: 10.15376/biores.11.1.2886-2963.
- [181] “ISO 2144 standards: Determination of residue (ash) on ignition at 900 °C.” 1997.
- [182] “ISO 1924-2 standards: Paper and board — Determination of tensile properties.” 2008.
- [183] H. El Omari, A. Zyane, A. Belfkira, M. Taourirte, and F. Brouillette, “Dielectric properties of paper made from pulps loaded with ferroelectric particles,” *Journal of Nanomaterials*, vol. 2016, p. e3982572, May 2016, doi: 10.1155/2016/3982572.
- [184] M. M. Katun, A. Smith, R. Kadzutu-Sithole, C. Gomes, C. Nynamupangedengu, and N. Moloto, “Impact of fibres and reinforced nanoparticles on tensile strength of transformer oil-impregnated paper,” in *2022 30th Southern African Universities Power Engineering Conference (SAUPEC)*, Jan. 2022, pp. 1–6. doi: 10.1109/SAUPEC55179.2022.9730720.
- [185] J. Kim, W. Kim, H.-S. Park, and J.-W. Kang, “Lifetime Assessment for Oil-Paper Insulation using Thermal and Electrical Multiple Degradation,” *Journal of Electrical Engineering and Technology*, vol. 12, no. 2, pp. 840–845, Mar. 2017, doi: 10.5370/JEET.2017.12.2.840.
- [186] N. Zhuravleva, A. Reznik, D. Kiesewetter, and D. Tashlanov, “The impact of the degree of polymerisation of the cellulose molecules on the electrical and mechanical properties of insulating paper,” in *2017 IEEE Conference of Russian Young Researchers in Electrical and Electronic Engineering (EIConRus)*, Feb. 2017, pp. 1220–1223. doi: 10.1109/EIConRus.2017.7910781.
- [187] Y. S. Ryu, J. H. Lee, and S. H. Kim, “Efficacy of alkyl ketene dimer modified microcrystalline cellulose in polypropylene matrix,” *Polymer*, vol. 196, p. 122463, May 2020, doi: 10.1016/j.polymer.2020.122463.
- [188] X. Wang, M. Sternberg, F. T. U. Kohler, B. U. Melcher, P. Wasserscheid, and K. Meyer, “Long-alkyl-chain-derivatized imidazolium salts and ionic liquid crystals with tailor-made properties,” *RSC Advances*, vol. 4, no. 24, pp. 12476–12481, 2014, doi: 10.1039/C3RA47250G.
- [189] Dr. T. Mitra, G. Sailakshmi, A. Gnanamani, and A. Mandal, “Studies on Cross-linking of Succinic Acid with Chitosan/Collagen,” *Materials Research*, vol. 16, pp. 755–765, Aug. 2013, doi: 10.1590/S1516-14392013005000059.
- [190] G. Liu, H. G. Yang, J. Pan, Y. Q. Yang, G. Q. (Max) Lu, and H.-M. Cheng, “Titanium dioxide crystals with tailored facets,” *Chem. Rev.*, vol. 114, no. 19, pp. 9559–9612, Oct. 2014, doi: 10.1021/cr400621z.
- [191] H. Gasser, C. Krause, and T. Prevost, “Water absorption of cellulosic insulating materials used in power transformers,” in *2007 IEEE International Conference on Solid Dielectrics*, Jul. 2007, pp. 289–293. doi: 10.1109/ICSD.2007.4290809.
- [192] M. Koch, “Reliable Moisture Determination in Power Transformers,” Ph.D Thesis, Institut für Energieübertragung und Hochspannungstechnik der Universität Stuttgart, 2008.
- [193] “ISO 2528 standards: Determination of water vapour transmission rate (WVTR) — Gravimetric (dish) method.” 2017.
- [194] “ISO 187 Standards: Paper, board and pulps — Standard atmosphere for conditioning and testing and procedure for monitoring the atmosphere and conditioning of samples.” 1990.
- [195] R. Seppänen, “Durability of the sizing degree of AKD and ASA sized papers investigated by contact angle measurements and ToF-SIMS,” *Journal of Dispersion Science and Technology*, vol. 30, no. 6, pp. 937–948, May 2009, doi: 10.1080/01932690802646330.

- [196] Dr. A. Kumar, S. Kakkar, V. Chauhan, S. Chakrabarti, and R. Varadhan, "Efficacy of ASA sizing with agro-residue and recycled pulps using different fillers," *IPPTA: Quarterly Journal of Indian Pulp and Paper Technical Association*, vol. 24, p. 93, Jul. 2012.
- [197] A. Isogai, M. Nishiyama, and F. Onabe, "Mechanism of retention of alkenyl succinic anhydride (ASA) on pulp fibers at wet-end of papermaking," *Sen'i Gakkaishi*, vol. 52, no. 4, pp. 195–201, 1996, doi: 10.2115/fiber.52.195.
- [198] "ISO 535 standards: Paper and board - Determination of water absorptiveness - Cobb method." 2014.
- [199] A. varshoei, E. Javid, M. Rahmaninia, and F. Rahmany, "The Performance of Alkylketene Dimer (AKD) for the Internal Sizing of Recycled OCC Pulp," *Lignocellulose*, vol. 2, pp. 316–326, Sep. 2013.
- [200] R. PremNarayanSingh, "Strengthening of corrugated boards by chemical impregnation," M.S. Thesis, Western Michigan University, Kalamazoo, Michigan, 2004.
- [201] J.-P. Merisalo, "Optimization of ASA emulsification in internal sizing of paper and board," Faculty of Chemistry and Materials Sciences, Helsinki University of Technology, Finland, 2009.
- [202] R. Seppänen, "On the Internal Sizing Mechanisms of Paper with AKD and ASA Related to Surface Chemistry, Wettability and Friction," 2007, Accessed: Oct. 07, 2019. [Online]. Available: <http://urn.kb.se/resolve?urn=urn:nbn:se:kth:diva-4537>
- [203] T. A. Prevost, "Thermally upgraded insulation in transformers," in *Electrical Insulation Conference and Electrical Manufacturing Expo, 2005*, Nov. 2005, pp. 120–125. doi: 10.1109/EEIC.2005.1566272.
- [204] H. Yong, X. Shupe, W. Jianjian, and F. Hui, "Influence of multiple factors on the wettability and surface free energy of leaf surface," *Applied Sciences*, vol. 9, p. 593, 2019, doi: 10.3390/app9030593.
- [205] "TAPPI T 558: Surface wettability and absorbency of sheeted materials using an automated contact angle tester (Five-year review of Official Method T 558 om-15)." Technical Association of the Pulp & Paper Industry, 2020.
- [206] I. Kolcunova, M. Pavlik, and L. Lison, "Assessment of Long Thermal Ageing on the Oil-Paper Insulation," *Advances in Electrical and Electronic Engineering*, vol. 14, Dec. 2016, doi: 10.15598/aeer.v14i5.1836.
- [207] A. Betie, F. Meghnefi, I. Fofana, and Z. YEO, "On the Impacts of Ageing and Moisture on Dielectric Response of Oil Impregnated Paper Insulation Systems," presented at the 2012 IEEE Annual Conference on Electrical Insulation and Dielectric Phenomena (CEIDP), Oct. 2012. doi: 10.1109/CEIDP.2012.6378760.
- [208] M. Koch, S. Tenbohlen, M. Krüger, and A. Kraetge, "Improved Moisture Analysis of Power Transformers using Dielectric Response Methods," in *MatPost07-3rd European Conference on HV & MV Substation Equipment*, 2008, p. 6.
- [209] "IEC 60243, 'Electric strength of insulating materials'."
- [210] T. Tanaka, M. Kozako, N. Fuse, and Y. Ohki, "Proposal of a multi-core model for polymer nanocomposite dielectrics," *IEEE Transactions on Dielectrics and Electrical Insulation*, vol. 12, no. 4, pp. 669–681, Aug. 2005, doi: 10.1109/TDEI.2005.1511092.
- [211] T. Tanaka, "Dielectric nanocomposites with insulating properties," *IEEE Trans. Dielect. Electr. Insul.*, vol. 12, no. 5, pp. 914–928, Oct. 2005, doi: 10.1109/TDEI.2005.1522186.
- [212] S. Li, G. Yin, S. Bai, and J. Li, "A new potential barrier model in epoxy resin nanodielectrics," *IEEE Transactions on Dielectrics and Electrical Insulation*, vol. 18, no. 5, pp. 1535–1543, Oct. 2011, doi: 10.1109/TDEI.2011.6032822.

## APPENDIX A:

Detailed calculation and experimental procedure for the fabrication of the kraft paper

### 1. Fabricating the control sample:

The screen of the handsheet maker (Rapid Kother at Sappi) has an area of 0.0314 m<sup>2</sup>. The dry pulp required to fabricate 120g/m<sup>2</sup> of paper sheet therefore is;

$$\begin{aligned} \text{Dry pulp (g)} &= \text{Area (m}^2\text{)} \times 120 \text{ (g/m}^2\text{)} \\ &= 0.0314 \times 120 = 3.768\text{g weight of dry pulp} \end{aligned}$$

A pilot sheet was first produced to get the amount of wet pulp needed to fabricate a 120 g/m<sup>2</sup> sheet. Wet pulp was weighed with an initial mass recorded as 146.61g. Water was added, and the pulp was disintegrated at 2500 rpm to disperse the fibre bundles for 8 minutes (20,000 revolutions). The filtration unit wires were carefully cleaned to remove tiny fibres hanging on the surface. The pulp was then carefully poured into the filtration unit of the handsheet machine, and the unit was half full with water; the start button was on to drain the water through the mesh. The sheet was then placed between clean blotting paper with a couch plate; it was rollover with five passes of a couch roller to remove the residual water in the sheet within 10 seconds. The pilot sheet made was labelled using an indelible pencil, pressed for 2 minutes at 4 bar pressure and dried at 92 °C for 8 minutes, and the final mass after drying was 5.58g.

The dry matter weight (consistency) of the sheet was calculated as follows;

$$\begin{aligned} \text{Dry matter weight (const.)} &= \frac{\text{mass of the dry pilot sheet made}}{\text{mass of wet pulp (g)}} \times 100 \\ &= \frac{5.58}{146.61} = 3.81\% \end{aligned}$$

Therefore 3.81% makes the dry matter (fibre) from the wet pulp of 146.61g used in producing 5.58g of the pilot paper sheet.

The amount of wet pulp required, therefore, to produce a 120 g/m<sup>2</sup> sheet is;

$$= \frac{146.61 \times 3.768}{5.58} = 99.001g \text{ of wet pulp.}$$

$$\text{Or } \frac{120 \times 0.0314}{\frac{3.81}{100}} = 98.897g \text{ of wet pulp}$$

Therefore, to fabricate the control sample (reference), 99.001 g of wet pulp was used. The exact steps for fabricating the pilot sheet were repeated for the reference sheets. For each sample produced, the sheet's mass was weighed and divided by the area of the sheet (mesh screen) by 0.0314 m<sup>2</sup> to get the grammage. The mass of the sheets produced was between 3.77g and 3.76g.

## 2. Making paper sheet with nanofiller:

To add 3 wt% of nanofiller to each sheet, the following was calculated;

3wt% of dry pulp = 3 wt% of 3.768 mass of dry pulp required to produce 120g/m<sup>2</sup> = 0.11304g of nanofiller added to the dry pulp.

The amount of dry pulp to fabricate the 120g/m<sup>2</sup> hence is 3.768-0.11403g = 3.6549g of dry pulp. The mixing ratio of the nanofiller to distilled water is 1:100. Therefore, each 100g of solution contains 1g of nanofiller. The wet content of the nanofiller is calculated thus;

$$\frac{0.11304}{1\%} = 11.3 g \text{ wet of nanofiller}$$

The wet pulp required for the modified sheets is;

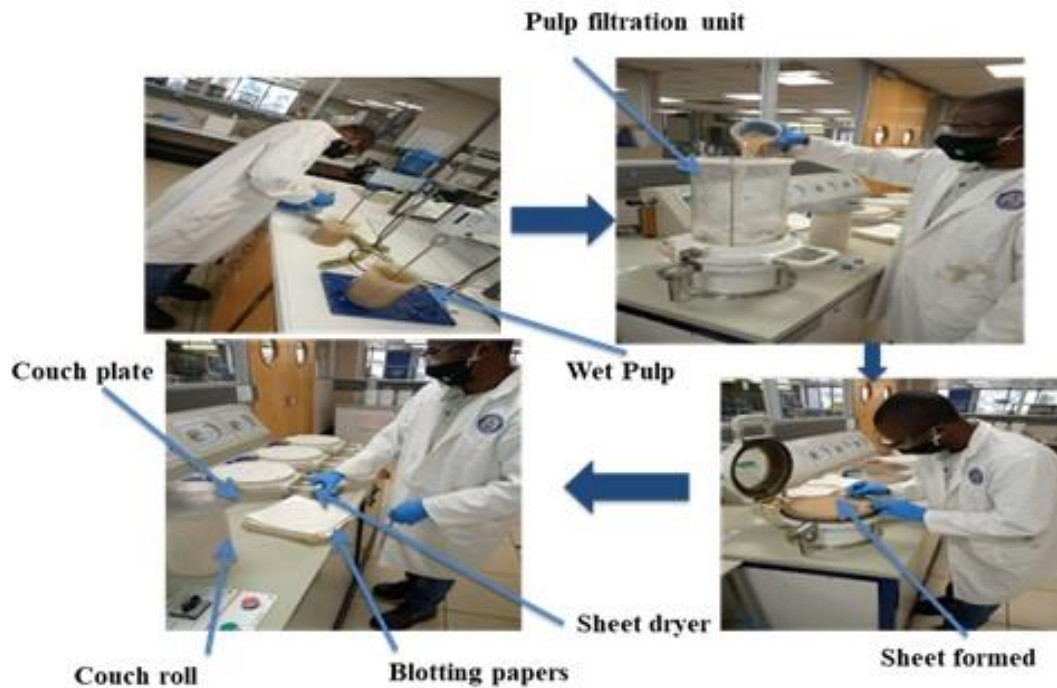
Wet pulp of control sample – wet solution of the nanofiller

$$= 99.001 - 11.3 g = 87.701 g \text{ of wet pulp.}$$

*Preparation of the retention aid:*

The retention aid captures the nanofiller, fines and fiber branches to keep them together. Perform PC8719 CPAM was used. 2 g of PC8719 was weighed, and a solution of 1:100 was prepared. For each sheet made, 10 ml of retention aid was added.

Following the same procedure of fabricating the control samples, the sample modified with reinforced nanofiller were prepared. Thus under stirring at 2500 rpm, 11.3 g of nanofiller was added to the pulp slurry containing 87.701 g of pulp. The mixture was stirred for 8 minutes, then 10 ml of retention aid was added and allowed to stir for another 4 minutes (total of 35,000). The filtration unit wires were carefully cleaned to remove tiny fibres hanging on the surface. The pulp was then carefully poured into the filtration unit of the handsheet machine, and the unit was half full with water; the start button was on to drain the water through the mesh. The sheet was then placed between clean blotting paper with a couch plate; it was rollover with five passes of a couch roller to remove the residual water in the sheet within 10 seconds. The sheet made was labelled using an indelible pencil, pressed for 2 minutes at 4 bar pressure and dried at 92 °C for 8 minutes, and the final mass after drying was weighed. For each sample of the reinforced sheets, this procedure was repeated.



**Figure A:** Images taken at some stages of fabricating the kraft paper insulation.

## APPENDIX B:

The procedures involved in sample preparation and analysis using the L&W FT (Code 912+)

### Sample Preparation:

To analyse a pulp sample using the L&W FT+ fibre tester, 1 g of the fabricated kraft paper was added to 1 L of water, and the pulp was transferred into a 1 L beaker. A 300 ml of water was added, and a handheld blender was used to break up and mix the pulp. The pulp suspension was transferred into a 1 L measuring cylinder, and then 700 ml of water was added to the 1 L mark. The pulp was transferred back to the 1 L beaker, and three 100 g samples were weighed off in 500 ml glass beakers to obtain three repeats containing 0.1 g of oven-dry pulp each. These steps are repeated for each test sample.

### Sample analysis:

The L&W FT+ PC was switched on, and the L&W FT+ software on the desktop of the PC was started. The water valves were open, and the compressed air switch was on. 110 ml of water in a glass beaker was placed on the sample-changer carousel, and the three 0.1 g pulp suspensions on the sample-changer carousel. The sample names were entered in the various carousel positions in the sample-changer window, and for fibre and fines analysis, the Pulp with Crill method was chosen from the drop-down list for each sample, and the sample weight was entered. The analysis starts by clicking the start button for each individual sample test. Table B shows the fibre characteristic.

**Table B:** Fibre characteristics obtained from the L&W Fiber Analyzer.

Fibre characteristics	Control	KP/T- Pure	KP/T- AKD 1 %	KP/T- AKD 3%	KP/T- AKD 5 %	KP/T- ASA 1%	KP/T- ASA 3 %	KP/T- ASA 5 %
Mean length-weighted fibre length ( $\mu\text{m}$ )	2029	2000	2052	1994	2016	2000	2001	1997
Primary (coarse ) fines (%)	10.333	10.700	10.100	10.567	10.567	10.700	10.367	11.000
Secondary (fine) fines (%)	19.633	25.267	21.700	25.967	24.967	25.500	24.700	24.433
Mean fines content %	30.000	35.933	31.800	36.600	35.567	36.200	35.067	35.367
Coarseness (mg/m)	0.213	0.238	0.235	0.215	0.216	0.231	0.221	0.221
Fibre content ( $10^6/\text{g}$ pulp)	2.620	2.234	2.314	2.450	2.465	2.299	2.437	2.443
Fiber Wall Thickness ( $\mu\text{m}$ )	3.500	3.967	3.900	3.567	3.600	3.933	3.667	3.700

## **APPENDIX C:**

The steps involved in sample preparation, visualization with optical/electron microscope of the kraft paper specimen using the Phenom ProX SEM

### **Sample Preparation:**

A test sample was cut into 25 mm in diameter and 30mm in height. Then a bare metal stub was placed onto a sample tray, and a double-sided carbon adhesive pad was used to cement the sample down to the sample stub. The sample was then placed on top of the exposed adhesive surface with tweezers, and the material was distributed across the area for clear visualisation. To remove any loose particles from the sample stub, the sample was gripped with the stub-holding tweezers, and the stub was forcibly tapped on the side against the work surface. The surface was sprayed with compressed air to remove any remaining loose particles. The sample was then placed in the microscope, and the sample holder was inserted into the microscope. The sample moved automatically to the optical imaging position after the door of the microscope was closed.

### **Sample Visualization with Optical Microscope:**

The optical camera displayed an image of the loaded sample in the main viewing window of the image screen. The focus icon was clicked to activate focus adjustment then the brightness/contrast was used to activate the brightness and contrast adjustment. The magnification was adjusted and image was rotated in a desired direction. The area of interest from the image was moved and centred on the main viewing window. In each position the image is captured and shown in the optical overview window to produce an optical overview of the entire holder content.

### **Sample Visualisation with Electron Microscope**

After the area of interest had been centred in the optical overview window, the sample was transferred to the electron imaging chamber for visualisation with the electron microscope. It was displayed in the main viewing window at the lowest possible magnification. The image was focused, and brightness/contrast was activated and adjusted. The sample was rotated, and

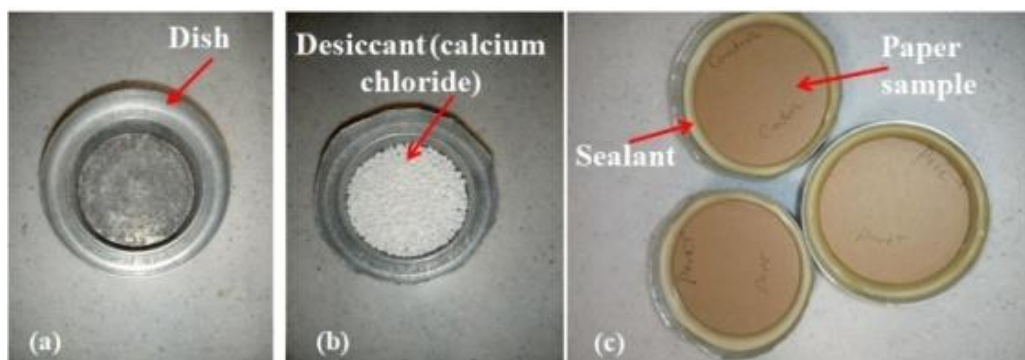
the area of interest was moved to the centre. Images were captured using the electron overview window's camera icon and stored on the Phenom USB flash drive.

## APPENDIX D:

### Water vapour transmission rate and water Cobb experimental procedure

#### 1. Experiment procedure on Water Vapour Transmission Rate (WVTR):

This experiment involved using a metal dish to determine the moisture penetration rate under the influence of desiccant (calcium chloride anhydrous) when covered by the paper sheet. An aluminium dish with a groove at the top as in Figure D(a) was used. The samples were cut in to circular shapes using a cutting template to fit into the dish rim. Calcium chloride was put into the different dish, and covered with the sample paper sheets. The sample was sealed at the edges with hot wax; sealant (wax) was melted and distributed around the rims. Three replications were prepared from each paper sheet. The sample was weighed and recorded using the weighing balance. Figure D shows the experimental setup. The final mass of each sample was weighed and recorded.



**Figure D:** (a) Empty dish, (b) Dish containing desiccant and (c) Sample papers fitted into the rim of the dishes.

**Table D:** Water vapour transmission rate.

Sample	MVTR (g/m <sup>2</sup> /24Hrs)
Control	730 ±29
Kraft paper/T-Pure	734 ±39
Kraft paper/T-ASA 5%	561 ±12
Kraft paper/T-ASA 3%	684 ±29
Kraft paper/T-ASA 1%	728 ±26
Kraft paper/T-AKD 5%	576 ±11
Kraft paper/T-AKD 3%	697 ±21
Kraft paper/T-AKD 1%	719 ±32

2. Experiment procedure on water Cobb test:

The sample sheets were cut into a circular shape using the cutting template (10x10cm) and were weighed. A sample was laid on a rubber mat, and a steel O-ring was placed on the test sample. The ring was fastened firmly to avoid leakage between the test sample and the ring. 25 ml of distilled water was carefully but rapidly poured into the ring. The stopwatch was started immediately and ran for 45s. The water was quickly taken out of the ring, and the wing nuts were loosened to remove the ring. The wet test specimen was placed between blotting paper and was subjected to two passes of a 20 kg metal roller before weighing.

## APPENDIX E:

### Data results from DIRANA

Table E shows the tan delta values immediately after curing and the values after 72 hours recorded at the nominal frequency of 50 Hz. The tan delta values recorded indicate that AKD is more effective at a higher temperature than ASA.

Table E: Tan delta measured values with DIRANA.

Sample	The absolute value of Tan <sup>δ</sup> after oven-dry	Tan <sup>δ</sup> after oven-dry (%)	Absolute Tan <sup>δ</sup> after 72 hours	Tan <sup>δ</sup> after 72 hours (%)
Control	0.003156	0.3156	0.104452	10.4452
Kraft paper/ Pure TiO <sub>2</sub> NP	0.004468	0.4468	0.112502	11.2502
Kraft paper/ TiO <sub>2</sub> NP/AKD 1%	0.003033	0.3033	0.093711	9.3711
Kraft paper/ TiO <sub>2</sub> NP/AKD 3%	0.002825	0.2825	0.077428	7.7428
Kraft paper/ TiO <sub>2</sub> NP/AKD 5%	0.001925	0.1925	0.069851	6.9851
Kraft paper/ TiO <sub>2</sub> NP/ASA 1%	0.003459	0.3459	0.090666	9.0666
Kraft paper/ TiO <sub>2</sub> NP/ASA 3%	0.003850	0.3850	0.066292	6.6292
Kraft paper/ TiO <sub>2</sub> NP/ASA 5%	0.002848	0.2848	0.058736	5.8736